# FABRICATION OF SYNTHETIC NANOPORES IN THIN FILMS FOR STUDIES OF ANALYTICAL APPLICATIONS

By

PU JIN

A DISSERTATION PRESENTED TO THE GRADUATE SCHOOL
OF THE UNIVERSITY OF FLORIDA IN PARTIAL FULFILLMENT
OF THE REQUIREMENTS FOR THE DEGREE OF
DOCTOR OF PHILOSOPHY

UNIVERSITY OF FLORIDA

2009

To my loved parents

# ACKNOWLEDGMENTS

In the past five years of my graduate study and pursuing the truth of science, I have always been supported, advised and encouraged by many individuals around me. They are behind every progress that I made to achieve more success in my research.

First of all, I would like to thank my research advisor, Dr. Charles R. Martin for his great guidance and support, especially his encouragement through my doctorate research. I am grateful to have an advisor who allows independent thinking and scientific creativity. His serious attitude about scientific research really impressed me and made me a professional scientist throughout my future career.

I also acknowledge the entire martin group and every member in the past five years. I would thank Dr. Lane A. Baker, who gave me the insight of my first research project and guided me with his experience. I also thank Dr. Hitomi Mukaibo for teaching me a lot about electrochemical experiments. I would thank my great colleagues, Lloyd Horne, Jiahai Wang, Lindsay Sexton, Gregory Bishop, Peng Guo, Kaan Kececi, Dooho Park, Fan Xu for their supports and sharing their wisdom and experience with me. I truly appreciate the chances and time to work with these great people.

I also give special thanks to the scientists at Major Analytical Instrumentation Center in Department of Material Science and Engineering at UF. They provided me the great help in instrumentation training and then allowed me to access the instrument by myself.

I would appreciate my parents for caring and supporting me in study and personal life. I also thank all my friends in Gainesville, and I did have a great, pleasing time in this peaceful town.

TABLE OF CONTENTS

page

LIST OF TABLES

LIST OF FIGURES

Abstract of Dissertation Presented to the Graduate School
of the University of Florida in Partial Fulfillment of the
Requirements for the Degree of Doctor of Philosophy

# FABRICATION OF SYNTHETIC NANOPORES IN THIN FILMS FOR STUDIES OF ANALYTICAL APPLICATIONS

By

Pu Jin

December 2009

Chair: Charles R. Martin
Major: Chemistry

The goal of this research is to develop nanoporous membrane devices for resistive-pulse sensing or separation applications. The first part of the research involves the fabrication of single conical nanopore in poly(ethylene terephthalate) (PET) membranes. A model analyte poly(styrene sulfonate) (PSS) was driven electrophoretically through the nanopore and the corresponding ion current pulses were observed. The effects of the supporting electrolyte pH, transmembrane potential and concentration of polyelectrolyte on pulse frequency were studied.

The second part of the research involves developing a multi cycle chemical etch method for fabrication of a single or multiple pyramidally shaped nanopore in muscovite mica membrane. The effects of the etchant concentration, applied transmembrane potential and number of etch cycles on nanopore opening sizes and geometry were studied in detail. A significant ion current rectification was observed in such a single pyramidally shaped nanopore embedded mica membrane.

In the third part, a new mechanism for improving the resistive pulse signal intensity was investigated by using single pyramidal nanopore in mica. The experimental results were the same as what we predicted based on this hypothesized mechanism, the pulse signals were current drops when the particles transported from tip to base and the pulses were current enhancement

when the particles transported from base to tip in the nanopore. The effect of the nanopore geometry on resistive pulse detection was studied as a control experiment to test this hypothesized mechanism.

In the last part of this work, electroosmosis in pyramidally shaped multi-pore mica membrane was studied. The asymmetric nanopores in these mica membranes demonstrate the ability to rectify the ion current flowing through the nanopore. As a result, the solution resistivity in the pore changes depending on the polarity of the applied electric field. If a constant current was applied to flowing through the nanopore membrane from the opposite directions, a rectified electroosmotic flow was observed. It was found that this rectified electroosmotic flow was the inherent result of ion current rectification in these asymmetric nanopores.

# CHAPTER 1
# INTRODUCTION AND BACKGROUND

## Introduction

At the nanometer scale, the physical properties of the macroscale world no longer hold.[1] Due to this phenomenon, the physical and chemical properties of a nanoscale material may be different from the macroscale material composed of the same substance. These materials usually have special properties which have potential applications in a wide variety of sectors, including electronics, energy, biotechnology and environmental monitoring et. al.[1]

There is an increasing interest in the research of the nanostructures in thin film in recent years. Nanoporous membrane can be used for diverse nanotechnology applications, including template synthesis[2-8], bio-separation[3, 9-13] and bio-sensing paradigm[14-17]. These membranes are attractive platforms for nanotechnology due to the simple, yet effective methods in which they can be used. Membranes offer a convenient way to handle and manipulate nanostructures or nanomaterials without the use of a specialized instrument. Furthermore, homogenous pores ensure homogeneous nanomaterials, a characteristic that is not easily achieved at these small scales. Appropriate membranes can be commercially available, or can be fabricated and relatively simple techniques can be used to chemically or physically modify the membrane properties.

There is a great deal of interest in developing the synthetic nanopores as analogues of biological protein channels for biosensing applications.[18-20] Such artificial nanopores have been fabricated in various materials by using different techniques.[21-26] In the Martin research group, we have been exploring fabrication of conically shaped nanopores polymeric and inorganic membranes by using the track-etch method.[27-29] These membranes have been used to study mass

transfer properties,[28, 30-33] biosensing applications[10, 34-37] and as template for two-dimensional nanomaterials synthesis.[2, 38-40]

This research focused on the fabrication of asymmetrically shaped nanopores in muscovite mica membrane. It was shown that the pyramidal shaped nanopores in such material highly rectified the ion current flowing through the nanopore. Correspondingly, an interesting electro-kinetic phenomenon, rectified electroosmotic flow was also observed in these nanopores. Based on the strong ion current rectification in these pyramidally shaped nanopores, a new resistive-pulse detection mechanism was proposed to enhance the current pulse signal intensity.

## Fabrication of Conical Nanopores in Thin Film Materials

### Track-Etch Method

The track-etch method entails the chemical etch of the latent damage tracks that formed during the irradiation of thin film materials with a high energy, heavy ion beam (Figure 1). This method allows uniform pore size with adjustable pore diameter. The nanopore orientation could also be controlled by the heavy ion trajectory. In industry, this method has been utilized to prepare various types of nanoporous polymer membranes for filtration applications. The membrane materials containing nanopore are also good templates for two-dimensional structure synthesis.

A variety of dielectric membrane materials (crystals, glasses, and polymers) are compatible with this technique, yielding diverse pores with different shapes.[41] Polymer membrane[1], such as porous poly(carbonate) (PC)[42, 43], poly(ethylene terephthalate) (PET)[44, 45] and poly(imide) (Kapton)[46-48] membranes are all commonly used to prepare nanopores via this technique.

### Formation of Latent Ion Tracks

Damage tracks are usually prepared by bombarding the membrane materials with high energy particles or ions.[49, 50] A very convenient way to obtain energetic heavy particles of about

1 MeV/nucleon specific energy is spontaneous fission from artificial nuclides.[41] Such high energy particles can usually leave damage tracks in the solids on the order of 10 μm in thickness. Nuclear reactors provide improved beam intensity and collimation so that larger scale application like the commercial production of nuclear track filters with track density at $10^{10}$ per $cm^2$ becomes realistic.[41] The third, rather exclusive way to irradiate track with excellent control is to use a heavy-ion accelerator. Such an accelerator can provide highly parallel ion beams leading to damage trails in the form of latent tracks.[41]

For crystal materials, the penetrating ion creates a positive ion cloud around its path, which "explodes" by electrostatic repulsion. This leads to atomic displacements (defects), a highly disordered zone, with a core of decreased density surrounded by a sheath of increased density (Figure 1-2A).[41, 49] In organic polymer materials, the track core consists of a zone of drastically reduced molecular weight, corresponding to broken molecular bonds close to the track (Figure 1-2B).[41, 49, 51]

Latent tracks consist of metastable or permanently changed zones with increased chemical reactivity. The etching transforms the latent track into an inerasable structure by supplying the required amount of energy for the enlargement process.[41]

Gesellschaft fuer Schwerionenforschung (GSI, Darmstadt, Germany) has developed a technique to control that there is only one single track prepared in each membrane.[52] Single heavy ion irradiation is achieved by placing a shutter between the ion beam and the membrane and an ion detector behind the membrane. The shutter is closed when the ion detector senses that a single ion traverse the membrane to prevent further exposure of the membrane to ion beam. Such technique provides promising applications for these nanopore membranes that were

fabricated from the ion-tracked films, especially those with only single pore, as a paradigm for sensing devices.[16, 42, 48]

**Ion Track Chemical Etching**

After irradiation, the latent damage tracks can then be chemical etched to create pores. A variety of membrane materials were fabricated with nanopores by using the ion track etch method.[16, 42, 48, 53] Depends on the chemical structure and composition of each material, the chemical reagents and etch condition vary in detail, especially for accurate controlling the nanopore dimensions and geometry.

In the case of preparing the nanopore membranes that were used as filters, cylindrical shaped nanopores are preferentially fabricated.[10, 13, 54, 55] For example, the commercial available nanoporous membranes, the ion-tracked membranes are simply immersed into the etching solution for a certain time and the damage tracks are etched from both sides of the membranes. This leaves straight, usually cylindrical shaped nanopore through the membranes. The nanopore opening sizes could be controlled by carefully choosing the types of etchant, etchant concentration and etch time.

Conically shaped multipore membranes were also prepared when the high flux is preferred and the narrowest part of the nanopore still need to be small.[28] There is an increasing interest in developing conically shaped nanopore in polymer membranes because of their novel characteristics[56, 57] and the potential application as a paradigm for sensing.[16, 58]

To fabricate asymmetric nanopore, an ion-track membrane is mounted between two halve of electrochemical cell as shown in Figure 1-3.[53] An etching solution that reacts with the polymer along the ion tracks is added to one side of the membrane. A stopping solution that does not react with the membrane is placed to the other side. The latent damage tracks are preferentially etched along the direction of the tracks from the surface of membrane where in contact with the etchant.

When the etchant breakthrough the latent damage tracks, it is neutralized or reacted with the stopping solution. This results in asymmetrically shaped nanopores with larger opening (base) facing the etching solution and small opening (tip) facing the stopping solution.[53] The reaction between the etchant and stopping solution is the key for fabrication of asymmetrically shaped nanopore and this effect is referred as chemical stopping.

Another important effect favorite the fabrication of conically shaped nanopore is electrical stopping.[56] During the chemical etching, a Pt electrode is placed in the solution on either side of the membrane and a constant transmembrane potential is applied. After the nanopore breakthrough, in the case of essential etch species is charged, the electrical field drives the charged species close to or far away from the membrane to affect the nanopore etch.

For example, PET membranes with only single conical nanopore were successfully prepared by Apel et al.[47] After the PET membranes were irradiated with heavy ions and latent tracks were left in the center of the membrane. An etch solution of 9 M NaOH was placed on one side of the membrane and a stopping solution of 1 M formic acid with 1 M KCl was on the other side. A Pt electrode was placed in each solution and a transmembrane potential of 1 V was applied with the anode on the etchant side. These fabricated nanopores have large openings (base) facing the NaOH and small openings (tip) facing the formic acid. After the nanopore broke through, the electrical field drove the $OH^-$ etchant electrophoretical moving far away from the nanopore small openings. At the same time, formic acid neutralized the $OH^-$ etchant and decreased the chemical etch rate at the tip region. This usually resulted in conical nanopores with small tip diameter (<10nm).

The etchant etch the polymer in both the directions- parallel (track etch) and perpendicular (radial etch) to the damage tracks (Figure 1-4). Usually the track etch rate $v_T$ is much faster than

the bulk materials etch rate (bulk etch, $v_B$). Both of the $v_T$ and $v_B$ determine the shape of track-etch pores as well. The geometry of the conical nanopore is usually described by using the cone half-angle (Figure 1-4), α, defined as the ratio of $v_B/v_T$ at high track etch case. The track-etching rate is influenced by the sensitivity of the materials to tracking, UV irradiation condition[59], post irradiation storage and etching conditions.[59-62] For materials with a very high track-bulk etch ratio, the etched pores usually have straight shape with constant cross section.[63]

To explore the potential application as a resistive-pulse sensing device, the reproducibility of the signals that were obtained from different membranes is important. Therefore the reproducibility of the conical nanopore tip, base and corresponding geometry become the key issues of these nanopore fabrications. The method which Apel et cl had developed could control the nanopore base openings pretty well, however, has less control about the nanopore tip size. The Martin group has modified this method based on their approach and developed a two-step chemical etch method to fine control both base and tip of the conical nanopore with excellent reproducibility.[53]

**Fabrication of single conical nanopore in poly(ethylene terephthalate) with two-step etch method**

The two-step chemical etch method involves an anisotropic etch step for controlling the nanopore base opening size and an isotropic etch step for precise controlling the nanopore tip opening size. The first step – anisotropic etch is to control the conical nanopore base opening size while still maintain a small tip. The membrane that is used for etch need to be irradiated under UV at wavelength λ~320 nm for 12 hours for fully sensitize the track etching process.[59, 64] It is important to ensure the nanopore breakthrough so that both ends of the nanopore are open when chemical etch is terminated at the predetermined amount of time. The first step etch is quite similar to the procedure that was developed by Apel.[47] The PET membrane is etched with 9

M NaOH and stopped with 1 M formic acid solution at room temperature and a transmembrane potential of 1 V is applied with anode in the NaOH solution (Figure 1-5A). The NaOH hydrolyze the ester bonds in PET resulting in the formation of carboxylate groups and hydroxyl groups on the surface of nanopore wall and membrane face.[65]

Before the etchant breaks through the membrane, the ion current flowing though the membrane is essential zero. A sudden current increase is usually observed when the nanopore breaks through as shown in Figure 1-5B. Such a current jump only indicates the nanopore formation; however, the nanopore may not have the dimension or geometry desired for resistive-pulse sensing. The membrane is usually etched for the predetermined time, about two hours in most of the cases. It was determined that the nanopore base openings etched under this condition have a average diameter of 520±45 nm.[53] To explore the reproducibility of nanopore base openings, several multi-track membranes were etched and the above average nanopore size was determined by using scanning electron microscopy (SEM).

But it has been found that the tip size of single conical nanopores with similar size of base opening vary from membrane to membrane. The complicated acid-base neutralization make it hard to control the chemical etch at the tip region. It is also difficult to monitor the current accurately so that anisotropic etch cannot be stopped in time before the tip becomes too large. However, a second isotropic etching step was developed to fine tune the nanopore tip opening.[53] The second step-isotropic etch is similar to the anisotropic etch. The only difference is that both halves of the chemical cell are filled with the etch solution of 1 M NaOH (Figure 1-6A). As known, the conductance of nanopore increases when the pore size increases and the rate of such an increase depends on the bulk etching rate.[51, 66]

There is an assumption that is the etch rate is the same at every position along the axis of the nanopore during the isotropic etch, in other words, both the nanopore tip and base increase the same amount of value during this step etch.[53] The observed ion current increasing demonstrates the nanopore is increasing at the same time. Instead of being stopped at a predetermined time, the isotropic etch step is ended at a predetermined current value. As shown in Figure 1-6B, the isotropic etches of three individual membrane were terminated when the ion current value reached ~40 nA. The real-time current monitoring allows the termination of isotropic etch in time. Besides, a low concentration of etchant etches the nanopore very slowly, and it can be easily neutralized to terminate the isotropic etch. Therefore, highly reproducible tips with accurately controlled diameter were obtained by stopping the isotropic etch process at a pre-determined current value,

**Fabrication of asymmetrically shaped nanopores in other membrane materials**

A variety of membrane materials were utilized for track-etch technique. Polymer membranes have the greatest use due to their chemical and mechanical robustness. A number of polymer materials are suitable for preparing ion track-etched conical nanopores, including poly(carbonate) (PC),[42] poly(ethylene terephthalate) (PET),[47] Poly(imide) (Kapton),[47] poly(propylene) (PP).[67] The chemical structures of the three commonly used polymer membranes (PC, PET and Kapton) are shown in Figure 1-7. Besides, asymmetrically shaped nanopores were also fabricated in inorganic materials, such as glass.[41, 68] The Martin research lab recently started exploring the fabrication of asymmetric pores in crystal materials, such as muscovite mica.[69] According to the materials composition, the etchant, stop-etching solution, etch temperature differ from one to another; correspondingly, nanopore opening dimensions and geometries vary a lot.

The fabrication of conical nanopore in poly(carbonate) is similar to that of PET. A 9 M NaOH is used as etchant and a solution containing 1 M formic acid and 1 M KCl is the stopping solution. Chemical etch is performed at room temperature with a transmembrane potential of 1 V applied on the anode in the NaOH solution.[62] It is also demonstrated that the cone angle increase by using higher transmembrane potential.[62]

The ion tracks in poly(imide) (Kapton) are etched by using a NaOCl solution with an active chlorine content of 13%. A 1 M KI solution is used as the stopping reagent.[70] The chemical etch is usually performed at 50°C to make the nanopore breakthrough quickly. When the etchant NaOCl breakthrough to the other side of the membrane, the iodide ions reduce the hypochlorite ions to produce chloride ions, as a result, the chemical etch is stopped. Etching of Kapton results in the formation of carboxylate groups via hydrolysis of imide bonds.[46]

Conical shaped nanopores were fabricated not only in polymeric membrane, but also in inorganic thin films, such as glass.[41] Ion tracks in glass are usually etched with hydrofluoric acid. These cheap material offers a low but highly reproducible etch ratio.[41] Another promising candidate for a technological application is the very homogeneous and isotropic phosphate glass. For highly ionizing heavy ions, phosphate glass has an etch ratio $v_T/v_B$ of the order of ~10. This allows prolonger etch breakthrough time and the tracks can be easily etched to spherical sections of relatively large diameter (>200 μm).[41]

Compare with glass, it is a great challenge to fabrication asymmetrically shaped nanopore in crystal materials, such as muscovite mica. Mica has a very high relative track-bulk etch ratio in hydrofluoric acid ($V_T/V_B >> 10^3$).[71] Because of such a high track-etch rate, etchant HF breakthrough to the other side too fast to etch in the radial direction larger enough. Unlike using polymer membrane, it is not easy to fabricate asymmetric nanopore in mica.

Martin group started to explore the fabrication of asymmetric pore in mica.[69] One approach is to first etch straight nanopores, followed by replacing the pore with a material that is more controllably etched, for instance metal nanowires. Then a mixture of HF and $HNO_3$ was used with $HNO_3$ etched the nanowires and HF etched the bulk mica around the metal. Asymmetric nanopores were prepared this way, but it has less control over the etch process so that it is difficult to maintain the nanopore tip small enough for resistive-pulse sensing.

## Characterization of Conical Nanopores and Properties

The dimension and geometry of nanopores are critical important regarding their applications in resistive-pulse sensing[53] and separation[9]. Scanning electron microscopy was used for imaging and measuring both the base and tip openings of nanopores in multi-pore membrane. However, it is challenging to obtain such images for nanopore in single pore membranes. This is especially true of the tip opening because they are so small and there is only one per sample. An alternative method, electrochemical measurement, is used for measure the conductance of nanopore filled with electrolyte solution and calculate nanopore tip opening.

### Electron Microscopy

Both the tip and base openings on multi-pore membrane surface were measured with field-emission scanning electron microscopy (FESEM). The base diameter, $d_{base}$, of conical nanopore in PET membranes obtained after the anisotropic etch was used to determine the bulk etch rate $v_B$ of PET in 9 M NaOH at room temperature. SEM images were obtained from different individual membranes and an average etch rate was obtained. The PET bulk-etch rate $v_B$ using 9 m NaOH is ~2.17 nm $min^{-1}$.[72] Therefore, it is possible to calculate the nanopore base size as a function of etch time if the membrane is etched under the same condition. This is especially useful to estimate the nanopore base size for single pore membrane. For example, the nanopore base is

about 520 nm in diameter after 120 minutes anisotropic etch with 9 M NaOH.[53] Figure 1-8 shows the FESEM images of conical nanopore etched in PC[73], PET, Kapton[69], glass[41] thin films.

Although the SEM images of nanopore base and tip opening clearly demonstrate the asymmetric shape of nanopore, but the exact geometry of nanopore is still unknown. To investigate this issue, an alternative method was developed to image pore geometry in multipore membrane entails depositing a material such as metal[62] or carbon[29] within the pores. For most of the nanopore polymer membranes (PC and PET), a well established electroless gold plating produced is used to deposit gold inside the empty nanopore.[16, 62] This also leaves a gold layer on both sides of the membrane. After removing the surface gold layer, the part remains is the gold replica of conical nanopores. For inorganic materials, such as mica, a chemical vapor method was used to deposit carbon inside the nanopore channel.[29] Both these methods create replicas of the pores, which can be liberated by dissolution of the template membranes and imaged by using FESEM. Figure 1-9 shows the example of gold replica from conical nanopore in PET and carbon replica from straight nanopore in mica, respectively.

**Electrochemical Measurements**

Because it is difficult to measure the base and tip opening of single conical nanopore in membrane by using SEM, a current-voltage curve measurement is helpful to determine the nanopore tip size ($d_{tip}$) based on a few assumptions.

This measurement entails mounting a membrane containing a single pore between the two half-cells (Figure 1-3). An electrolyte solution with known ionic conductivity is introduced into the cells on both sides of the membrane with a Ag/AgCl electrode on each side. A current-voltage curve is obtained via a linear scanning of transmembrane potential and measuring the resulting ion current flowing through the nanopore. The slope of the current-voltage curve represents the ionic conductance (G) of electrolyte-filled nanopore. Sometimes the ion current-

voltage curve is not complete linear in the entire range of scanned voltages, only the most linear part of the current-voltage curve (usually the part between -200 mV and +200 mV) is used to calculate the nanopore tip diameter.[53] Equation 1-1 describes the ionic conductance of the nanopore filled electrolyte solution as,

$$G = \frac{\sigma \pi d_{base} d_{tip}}{4L} \quad (1\text{-}1)$$

where σ is the specific conductivity of the electrolyte solution. L is the length of the nanopore (equal to the thickness of membrane), $d_{tip}$ and $d_{base}$ are the diameters of tip and base opening, respectively. Base opening diameter $d_{base}$ is usually calculated from the etch time and bulk-etch rate. Tip opening diameter $d_{tip}$ can be calculated using Equation 1-1 if pore conduce G can be measured experimentally. However, there are two assumptions that have to be satisfied if Equation 1-1 can be used to calculate single pore tip size. First, it is assumed that the bulk-etch of single track membrane is the same as that of multi-track membrane, which is also ~ 2.17 nm $min^{-1}$ in 9 M NaOH. The second assumption is that the nanopore is in a perfect cone shape or cylindrical shape. It need to be mentioned that the increase of base opening (Δd) need to be considered in the case of the second step etch. The diameter of base opening $d_{base}$ after the isotropic etch needs to be corrected with the original size and its increase Δd during the etch.

**Ion Current Rectification**

It has been known that the current-voltage curve of single conical nanopore is not always linear, especially when the nanopore is filled with low ionic strength solution.[57] It is usually observed as the ion current is higher at one electrode polarity and it is lower at the same absolute voltage but the opposite polarity (as shown in Figure 1-10). There are several models have been developed to explain ion current rectification in artificial nanopore or nano-capillary system.[24, 57,

[74-76] Among these models, "ratchet model"[76] and "ion accumulation and depletion model"[74] are widely accepted by researchers.

The chemical etching of the ion tracks in PET and Kapton membranes leaves carboxylate groups on the membrane surface.[47] When the pH is above the polymer's isoelectric point (~ 3 for PET, Kapton), the carboxylate groups deprotonated, which results in negative charges on the surface. It is proposed that the membrane becomes cations permselective when the nanopore size is comparable to the thickness of electrical double layer (EDL) on the pore wall, which means the nanopore will preferentially transport cations and reject anions.[30] Therefore in these theories, only cations transport are considered for the surface negatively charged pore. In the model proposed by Siwy et. al., cations is electrostatic trapped in the nanopore where is close to the tip region at positive potential (anode at base side of the membrane). The electrostatic trap effectively inhibits the movement of cations and decreases the current flowing through the conical nanopore. However, at the negative potential (anode at the tip side of the membrane), the electrostatic trap is eliminated and larger current is observed.[57, 76] In the case of positively charged surface, this "ratchet" model will be reversed.

There are three requirements for the ion current rectification base on ratchet mode. Such requirements are (i) pore surface is negatively or positively charged, (ii) pore has an asymmetric shape, (iii) the dimension of tip is comparable to the thickness of electrical double layer on the pore wall. It is also demonstrated that a cylindrical nanopore with equal size openings on both sides of the membrane does not rectified the ion current.[76] It is reported that the nanopore at certain size will rectify the ion current more strongly in lower ionic strength supporting electrolyte solution.[57]

Another well accepted model, introduced by Cervera et. al. also has the requirements as pore wall surface charge and asymmetric pore shape. As shown in Figure 1-11A, when the anode is on the tip side of the nanopore, cations are transported from the tip (anode) to base (cathode). Anions are driven from the external solution on the base side into the nanopore by the electric field. However, they cannot pass through the nanopore tip because of the electrostatic repulsion from the negatively charged pore wall at tip. As a result, anions accumulate in the nanopore. To maintain electrostatic neutrality, more cations are needed in this tip region to balance the extra anions. As a result, the local salt concentration in the nanopore increases and the resistance of membrane decreases. Therefore, a higher ion current is obtained when a transmembrane potential is applied at such electrode polarity. We refer this situation to the "on state" (Figure 1-11A).

On the contrary, when the anode is placed on the base side of the nanopore, cations are transported from base to tip in the nanopore (Figure 1-11B). Anions inside the nanopore are vacated from the nanopore and into the bulk solution at the base side by electric field. However, the anions on the tip side are less likely to enter the nanopore because of the strong electrostatic repulsion from the anionic pore wall at the tip. As a result, the local salt concentration in the nanopore decreases, and the resistance of membrane increases. When a transmembrane potential is applied at such electrode polarity, a lower ion current is obtained. We refer this situation to the "off state" (Figure 11-B).

In both of Siwy or Cervera's model, one critical assumption or requirement is that the nanopore tip is cation or anion perm-selective. In general, for surface negatively charged materials, the transference number of the cations is larger than of the anions, in other words, nanopore preferentially transports cations but reject anions. This might raises a problem for

applications of these membranes in separation or bio-sensing, if the analyte is electrostatic repelled by the charges on pore wall.

**Electrical Field Focusing**

A very important feature of the conical nanopore is that the voltage drop caused by the ion current flowing through the nanopore is focused at the nanopore tip.[16, 77] Lee et. al. had simulated the electrical field distribution across a single conical nanopore embedded in a polymer membrane.[77] They demonstrated that the majority of the potential drop across the membrane occurs in proximity of the small opening of the pore. In this investigation, even the electrical potential applied across the 6 μm thick membrane is only 1 V, the electrical field strength at the nanopore tip is enormously huge (~$1\times10^6$ V/m) (Figure 1-12).[77] In the nanopore, the electrical field strength decreases dramatically at the position with larger cross section. The consequence of electrical field focusing at the tip is that the steady state current is extremely sensitive to any resistance change close to the tip. If an analyte passes through the field strength focused region and results a resistance change, such resistance change can be reflected by the ion current change.

It is known that the electrical field strength is not uniformly distributed along the nanopore (Figure 1-12B). The electric field decays to ~1% of its value at the pore base opening, equivalent to ~$1\times10^4$ V/m. Thus, an appreciable electric field exists far from the pore tip opening. It is only the part in close to the tip is sensitive to the resistance change and that region is usually called the “sensing zone”.

If we arbitrary setup a criterion that the effective length of sensing zone in the pore is that the length over which 80% of the voltage is dropped, then the sensing zone is only about 50 nm long in the case of a 10 μm long conical pore with 5 μm base and 20 nm tip.[72] Such short “sensing zone” provides some advantages of conical nanopore than straight nanopore as a

paradigm sensing devices. For example, a short sensing zone would greatly decrease the possibility that multi analyte enter the zone at the same time, therefore make single analyte molecule signaling possible. More importantly, such simulations show that the effective length of the sensing zone can be controlled by varying the cone angle of the nanopore. This demonstrates the significance of tailoring the nanopore size and geometry to allow analyte species to be detected.

## Resistive-Pulse Sensing

The resistive-pulse sensing method[14], also referred as stochastic sensing, is based on an electrochemical cell in which a small aperture separates two electrolyte solutions. An ionic current is passed through the aperture. When an analyte with dimensions comparable to the diameter of this aperture is driven through the pore by electrical field, the analyte partially occludes the pathway for ionic conduction and the ionic current flowing through the aperture decrease (Figure 1-13). Depending on the device, such change in ion current can be used to size identify and determine the concentration of the analyte species.

Current research in the field of resistive-pulse sensing is aimed at the detection and characterization of DNAs, proteins, ions, small organic molecules et.al. The developments of nanopore with molecular size in both biological and synthetic membrane make such detections possible. In particular, a great number of resistive-pulse sensing research had been accomplished by using biological nanopores.[14, 17, 78-89] It is also important to develop the synthetic nanopore because of their more adjustable size and geometry and surface properties.

### Resistive-Pulsing with Biological Nanopores

The most commonly used biological nanopore is α-hemolysin,[78] a type of protein nanopore embedded in a lipid bilayer support (Figure 1-14).[90] The nanopore is formed by either wild-

type[78] or engineered protein.[81, 86, 87] The extramembraneous domain contains a large cavity which hosts the transmembrane domain during the assembly process.

Biological nanopore have been used to detect DNAs,[83, 88] metal ions,[80] anions,[82] organic molecules,[84, 85] proteins,[89] polymers[79] and enantiomers of drug molecules.[91] There are two advantages that make biological nanopore very useful. The first one is that the excellent reproducibility of nanopore from sample to sample. The second advantage is that the powerful bioengineering technique allows such α-hemolysine pores to be modified through genetic engineering and chemical reactions, introducing a highly selective sensor platform. The large amount of work that has been done with α-hemolysine has an important influence on the development of resistive-pulse sensing.

However, the planar lipid bilayers cannot endure a wide range of pHs, temperatures, applied transmembrane potentials, or solvents, and they are sensitive to vibrations.[78] An alternative way is to using more stable bilayer with enhanced solid support[92] or artificial membrane. Another limitation of such protein channels is that their dimensions of cavity allow the translocation of small analytes only at a couple of nanometer scale. Therefore, a significant amount of research focused on the developing of synthetic nanopores as analogues of biological channels to be resistive-pulse sensing devices.

**Resistive-Pulsing Sensing with Synthetic Nanopores**

Many techniques have been explored to fabricate single nanopore in solid state materials.[93, 94] One widely used method entails using electron beam[21] or ion beam[23] to drill a single nanopore in silicon nitride and silicon oxide membranes. While monitoring the fabrication process using transmission electron microscopy (TEM), the size of such a nanopore could be controlled down to 1 nm. These types of nanopores have been used to study mainly DNA,[95-103] also some protein sensing and analyte interactions with nanopores.[104] The microfluidic channel fabricated using

soft lithograph has been used to detect cell,[105, 106] DNA,[107] the binding of antigens to primary antibody-coated colloidal particles,[108, 109] and quantitatively distinguish colloidal particles at different size.[110] A single carbon nanotube embedded in an epoxy membrane have been used as sensing device for detection of nanoparticles[111-113] and DNA translocation through such a device was observed using fluorescence microscopy.[114] A femtosecond-pulse laser based technique has been used to create single pore in glass and such nanopore is used to examine immune complexes.[115-117] A feedback electrochemical etching method has been used to fabricate nanopore in silicon.[118] In the Martin group, polymer membranes contains single conically shaped nanopore were widely used for resistive-pulse detection of different analytes.[16, 42, 45, 48, 78]

**Other Nanopore-Based Sensing Strategies**

Other sensing strategies have also been used with single conical nanopores fabricated in polymer membranes. A single conical Au nanotube in a PET membrane was used to design a new type of protein biosensor.[35] The nanotube was modified with various biochemical molecular recognition agents (MRAs) to detect analytes in solution with an on/off response. Similar to the resistive-pulse sensing method, this sensing protocol also involves passing an ion current through the single nanotube membrane. However, current-pulse translocation events were not observed in this case. Instead, as the analyte bound to the MRAs that had been attached on the pore surface, the current flowing through the nanopore was permanently shut off. Blockage of the ion current occurred because the diameter of the analyte was of comparable dimension to that of the nanotube tip. This sensor has been shown to be a highly sensitive and selective type of biosensor, and it should be possible to modify the Au nanotube surface with a wide range of MRAs to selectively detect a wide variety of analytes.

Conical nanopore sensors that use the ion current rectification phenomenon have also been developed.[58, 119] There devices consisted of a single conical nanopore in polymer membrane and

demonstrated ion current rectification when nanopore is filled with low concentration electrolyte solution. When the nanopore membrane was exposed to the analyte solution, the analyte bound on the nanopore surface and changed the local charge condition. An ion current rectification change was observed corresponding to the analyte binding. The quantitatively correlation between the analyte concentration and the ion current rectification ratio was observed.[119]

**Mass Transfer in Asymmetric Nanopores**

Single asymmetric nanopore in membrane materials were widely studied as a potential sensing device. The membrane contains multiple nanopore have been studied for filtration and separation applications. There is a increasing interest in the mass transfer in the asymmetric nanopore.[32, 120]

A widely studied phenomenon is the rectified ion transport in the nanopore[32, 67] or nanochannel[121-123] system. These studies demonstrated interesting transport phenomenon for the charged species under the effect of electrical field. It is observed that a larger current flowing through the membrane from one direction and a smaller current flowing through the membrane from the opposite direction. This means there is a higher transport rate of charged species from one direction and lower transport rate from the other direction.

It was also observed that the nanopore geometry had a effect on the diffusion.[69, 120] It has been demonstrated that the diffusion rate of analyte entered from the large opening of the membrane is higher than that of analyte entered from the small openings when the size of the analyte is comparable to the size of the nanopore small opening.

. Electroosmotic flow (EOF) is an electro-kinetic phenomenon that occurs when an ionic current is passed through a channel or porous materials that contain excess surface charge.[124-132] EOF is used to pump fluids through microfluidic[126] and capillary electrophoresis[127] columns. In addition, we and others have been exploring EOF through charged membranes that contain

straight nanopores. We are wondering whether the nanopore geometry has an effect on the electroosmosis in the nanopore. In other words, is that possible to have a rectified electroosmotic flow phenomenon in the asymmetric nanopores.

## Dissertation Overview

The goal of this research is to explore the fabrication of asymmetric nanopores in thin film materials, including polymer and crystal materials, and the corresponding potential applications in analytical chemistry. In particular, the research has been focused on the fabrication of pyramidally shaped nanopores in muscovite mica membrane and the relative studies of resistive-pulsing sensing by using this type of nanopore platform.

Chapter 1 has reviewed necessary background information for this dissertation including, track-etch method, ion current rectification in asymmetric nanopore, resistive-pulse sensing by using biological nanopores and artificial nanopores.

In Chapter 2, we prepared a single conical nanopore in PET membrane with good reproducibility. A model polymer analyte, sodium poly(styrene sulfonate) (PSS), was used for resistive-pulse method studies. The translocation of PSS through the nanopore were detected and quantitatively measured. The relationship between the transmembrane potential and the resistive pulse frequency was studied.

In Chapters 3, the fabrication of asymmetric nanopores in a crystal material, muscovite mica, was discussed in detail. The effects of etch time, transmembrane potential on nanopore sizes and geometry were studied. A chemical vapor deposition method was used to deposit carbon in the nanopores to produce the nanopore replicas for geometry studies. A highly ion current rectification was observed in these pyramidal shaped nanopore in mica. We think this highly ion current rectification is because of the high charge density on mica surface.

In Chapter 4, a new mechanism was proposed to improve the resistive-pulse detection signal intensity based on the nanopore ion current rectification characteristic. A coating molecule was introduced to modulate the nanopore local charge condition. The current pulses were studied based on the interaction of model analyte nanoparticles and such coating reagent.

In Chapter 5, we have shown for the first time that the asymmetric nanopore in mica membrane rectifies EOF. We studied the phenol transport through the membrane from different direction of the membrane. When a constant current were applied during the transport, a higher transport rate was observed from the base side to the tip side and a lower transport rate was observed from the opposite direction. We demonstrated that such rectified EOF is the direct consequence of the ion current rectification in asymmetric nanopores.

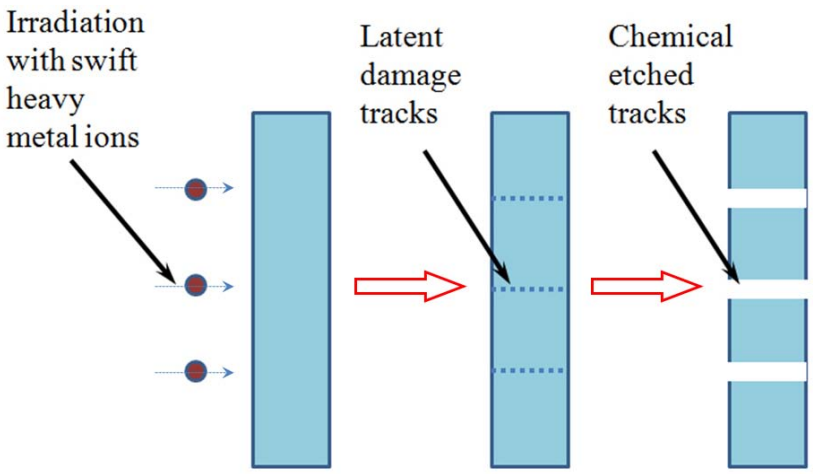


Figure 1-1. Schematic of track-etch method for the fabrication of nanopores in membranes. A) Irradiation of a thin film with swift, heavy metal ions. B) Formation of latent damage tracks along the path of ions. C) Selectively chemical etch of damage track resulting pore openings across the thin film.

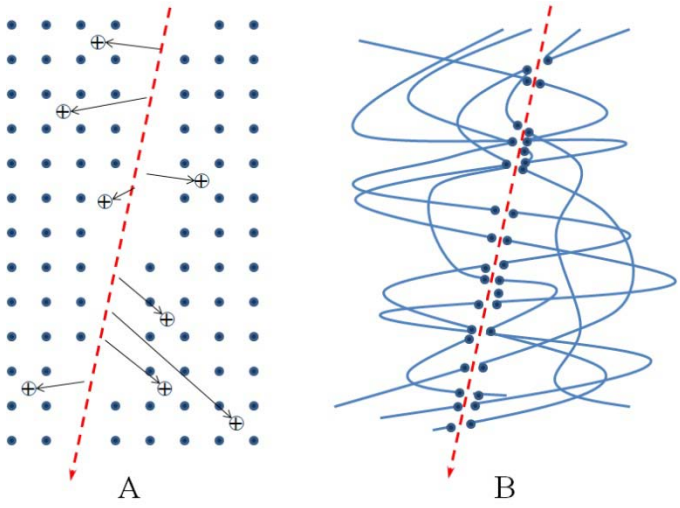


Figure 1-2. Schematic of ion track in different membrane materials. A) In crystal. B) In polymer.

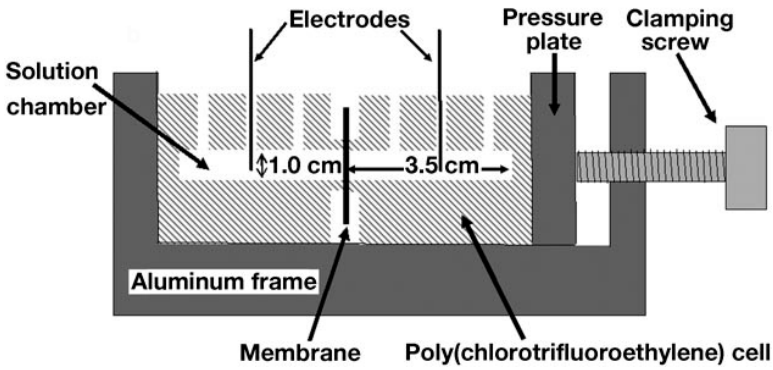


Figure 1-3. Diagram of the electrochemical cells for nanopore chemical etch and electrochemical measurement.

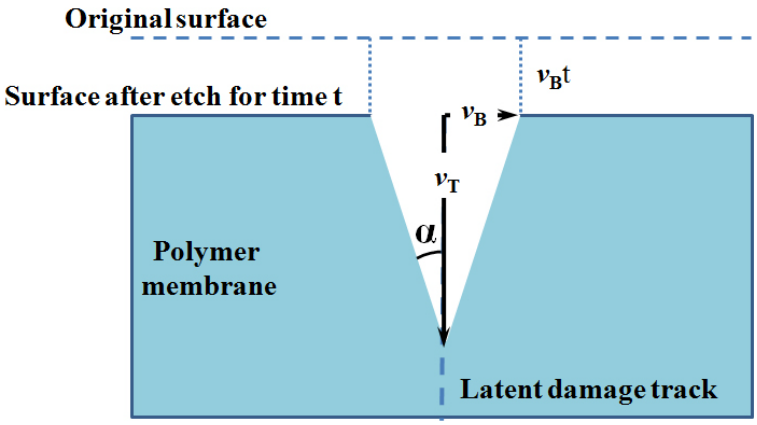


Figure 1-4. Schematic of track-etch and bulk-etch of a conical pore. Bulk-etch rate $v_B$, track-etch rate, $v_T$ and cone half angle α.

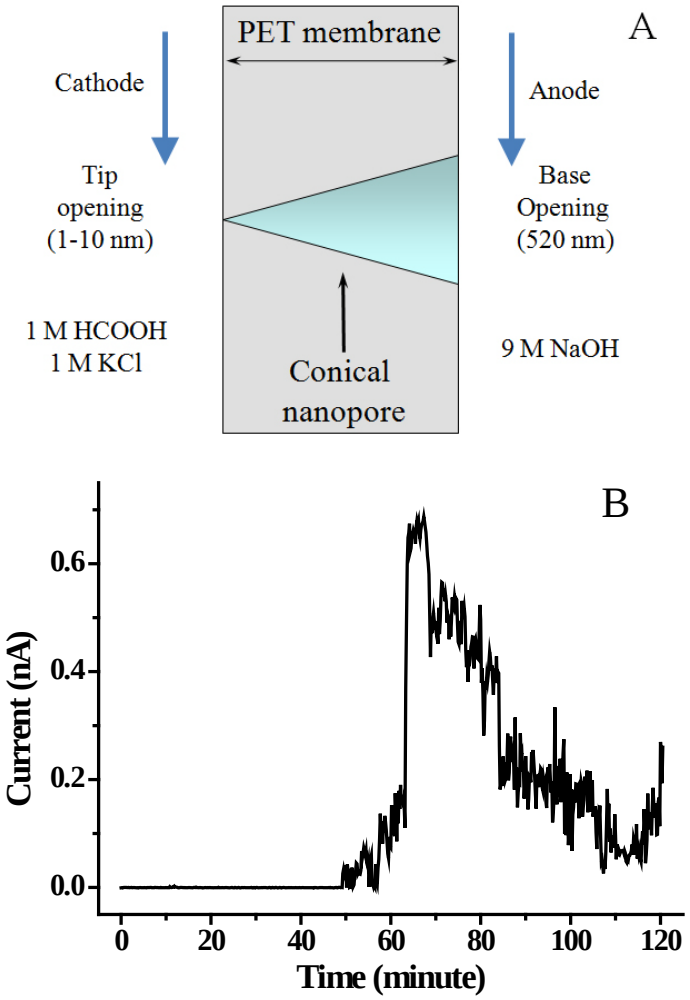


Figure 1-5. Schematic of anisotropic etch of a single conical nanopore in PET and the resulting current-time trace. A) Schematic of anisotropic etch. B) Current-time trace of single pore anisotropic etch for 120 minutes.

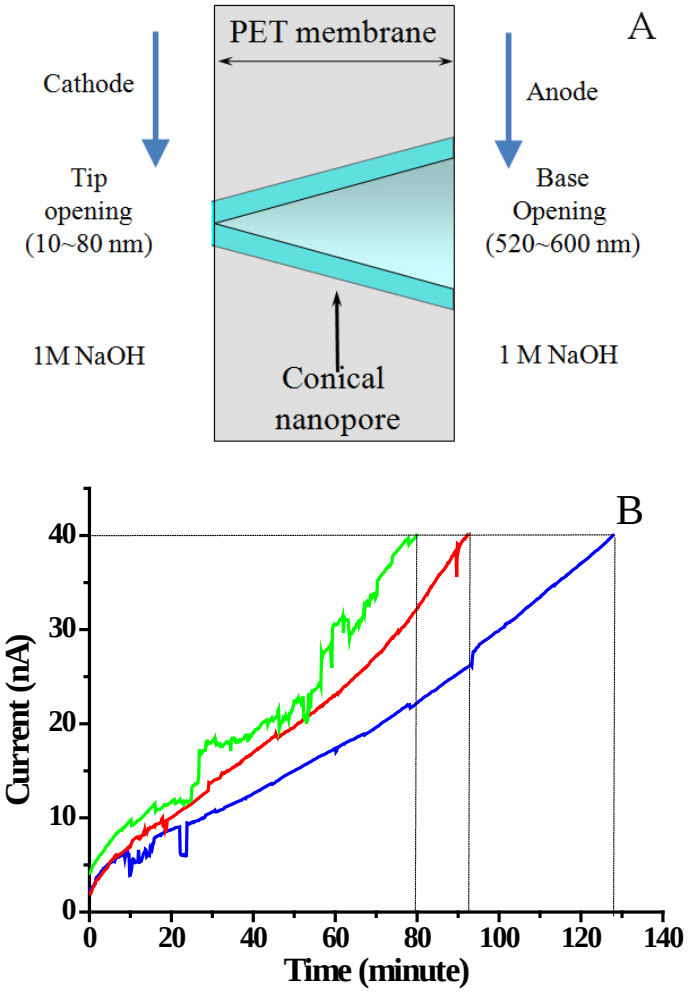


Figure 1-6. Schematic of isotropic etch of a single conical nanopore in PET and resulting current-time trace. A) Schematic of isotropic etch. B) Current-time trace of single pore isotropic etch until final current at 40 nA.

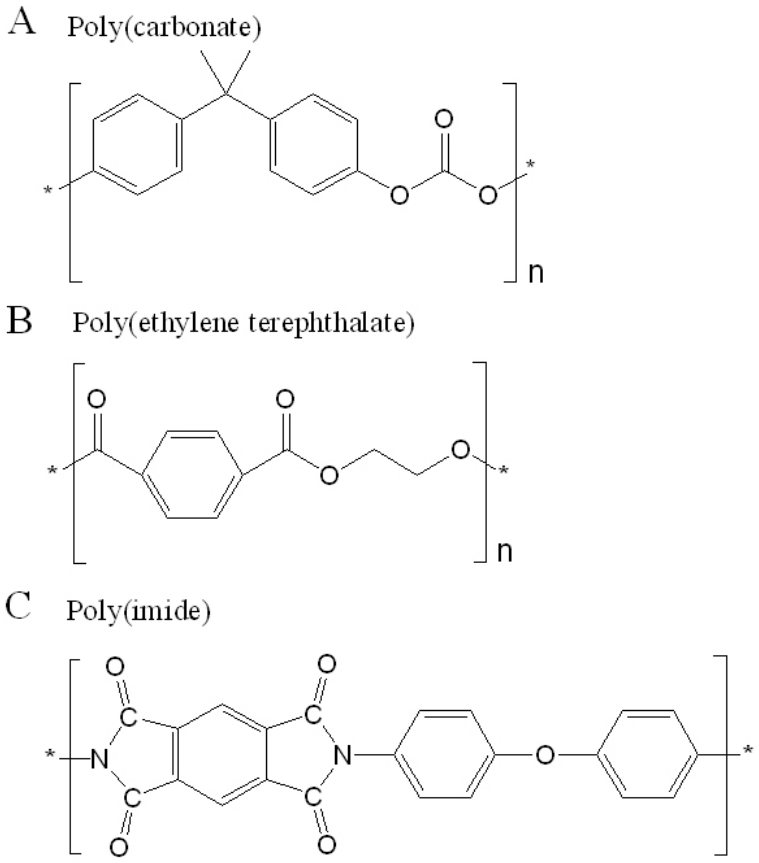


Figure 1-7. Chemical structure of polymers typically used for track-etching. A) Poly(carbonate) (PC). B) Poly(ethylene terephthalate) (PET). C) Poly(imide) (Kapton).

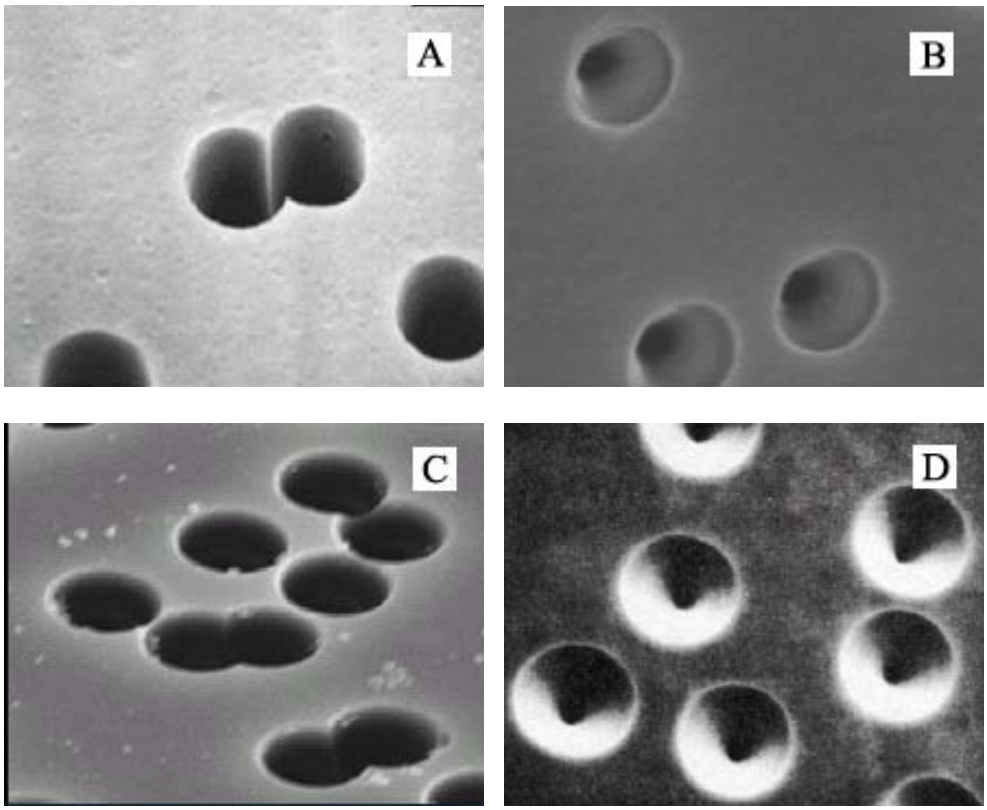


Figure 1-8. SEM images of conical nanopores in different membrane materials. A) PC[73]. B) PET. C) Kapton[72]. D) Glass[41].

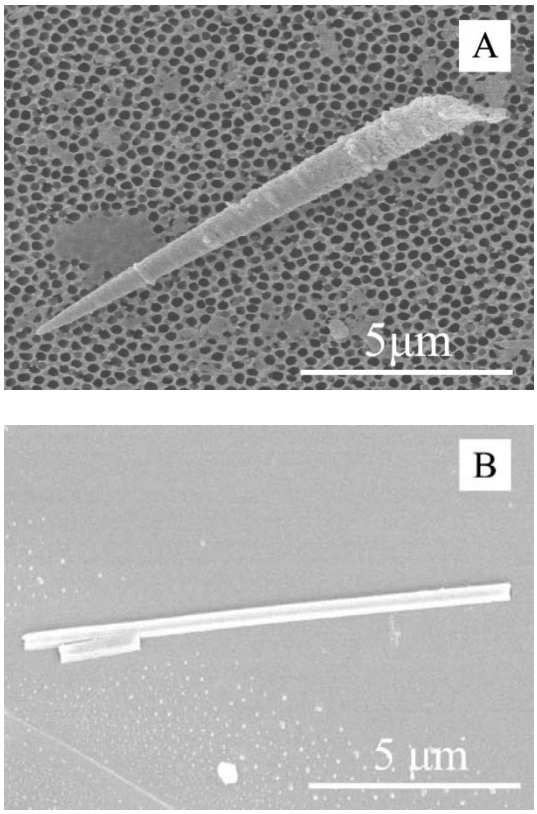


Figure 1-9. FESEM images of replicas of nanopore in different membrane materials. A) Gold replica of conical nanopore in PET membrane. B) Carbon replica of straight nanopore in mica membrane.

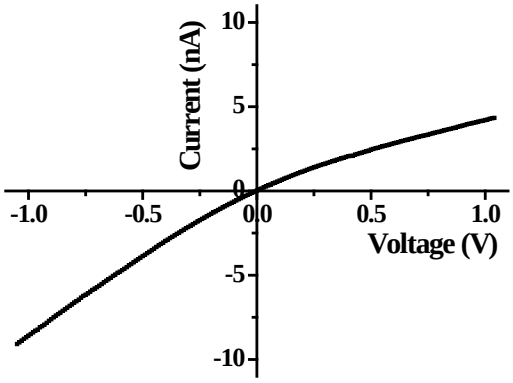


Figure 1-10. A typical current-voltage curve used to determine the single conical nanopore tip opening diameter.

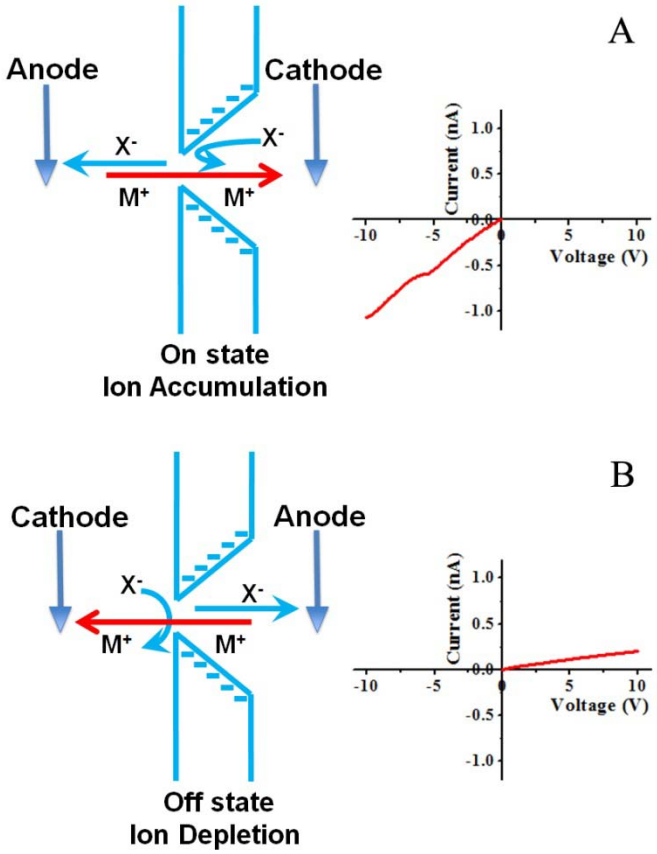


Figure 1-11. Schematic of ion current rectification model. Model proposed by Cervera *et. al.*[74] (drawing of pore not to scale).

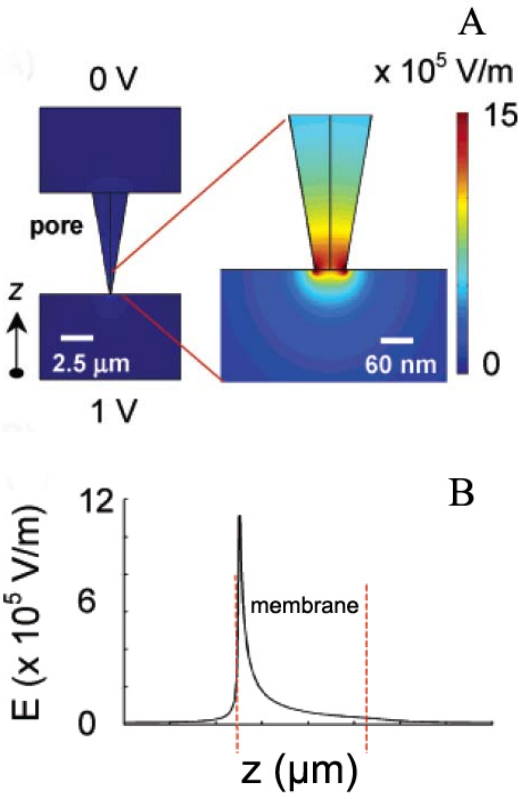


Figure 1-12. Distribution and line profile of the electric field across a conical nanopore membrane. A) Distribution of electric field across a conical shaped pore with base opening diameter of 2.5 µm, tip opening diameter of 60 nm and membrane thickness of 6 µm.[77] B) Line profiles of the electric field strength across the membrane corresponding to the centerline axis of the pore.[77]

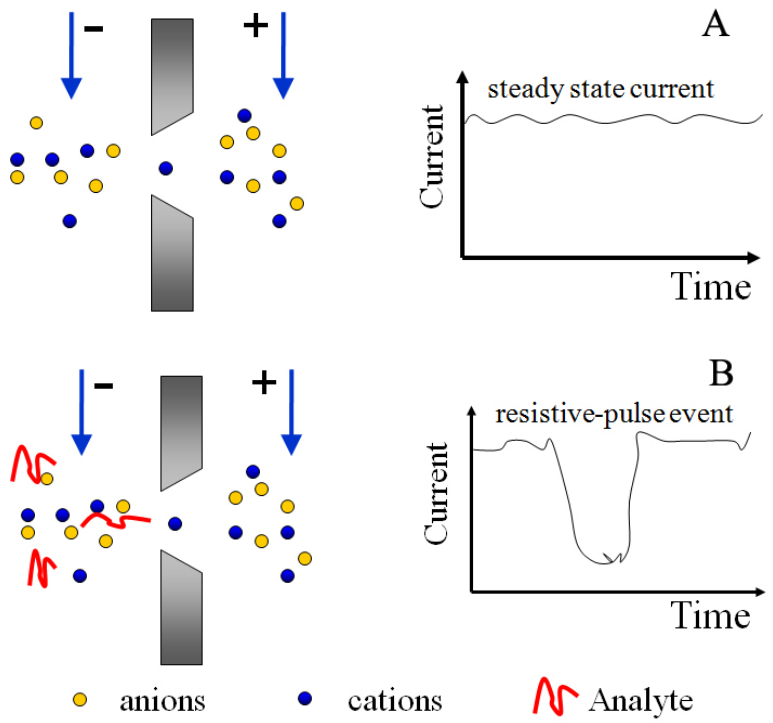


Figure 1-13. Illustration of the resistive-pulse sensing method. A) Steady state current in the absence of analyte. B) Resistive-pulse event in the presence of analyte.

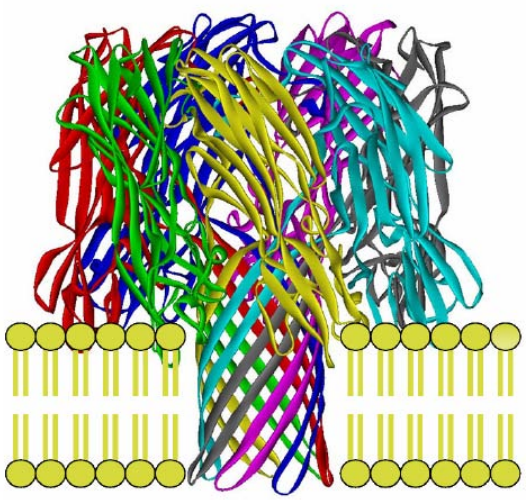

Figure 1-14. Illustration of α-Hemolysin protein embedded in a lipid bilayer support. It formed a nanopore across the support lipid bilayer.[90]

# CHAPTER 2
# RESISTIVE-PULSE DETECTION OF A MODEL POLYMER ANALYTE USING A CONICAL NANOPORE IN PET MEMBRANES

## Introduction

There is increasing interest in using nanopores in synthetic or biological membranes for resistive-pulse studies of molecular[14, 78, 80, 82] and macromolecular[35, 42, 83, 88, 96, 97, 101, 102, 108, 114, 133, 134] analytes. The resistive-pulse method entails mounting a membrane containing a nanopore that is filled with electrolyte solution and measuring the ion current flowing through the nanopore when applying a transmembrane potential. If a charged analyte is moving into the pore and blocking the nanopore, a transient current pulse signal is usually observed. The current pulse frequency is usually related the analyte concentration, and the identity of the analyte is encoded in the current-pulse signature, usually defined as the current pulse amplitude and current pulse duration.[14, 16]

A single conically shaped nanopore in PET membrane was fabricated through a two-step etch method and used for resistive-pulse detection studies. The two-step chemical etch method includes an anisotropic etch (the first step) where nanopore large opening (base) size is well controlled and an isotropic etch (the second step) where the nanopore tip opening size is accurately adjusted. The model analyte used in this study, sodium poly(styrene sulfonate), is a negatively charged linear polyelectrolyte which is stable at different pH solution. We studied the pulse frequency varied with polyelectrolyte concentration. We also investigated the effect of transmembrane potential on pulse frequency and explore a method to lower the limit of detection.

## Experimental

### Materials

Poly(ethylene terephthalate) membranes (~3 cm in diameter, ~12 μm in thickness) that had been irradiated with a heavy ion of 2.2 GeV kinetic energy to create a single damaged track through the film) were obtained from GSI Darmstadt, Germany. Sodium polystyrene sulfonate standard (Mw = 126,700 by gel permeation chromatography and molecular distribution Mw/Mn = 1.17) was obtained from Scientific Polymer Product INC. (Ontario, NY). All other chemicals were reagent grade and used as received. Purified water, obtained by passing house-distilled water through a Barnstead, E-pure water purification system, was used to prepare all solutions.

### Fabrication of Single Conical Nanopore in Ion Track PET Membrane

The ion-tracked PET membrane with a single damage track was irradiated under the UV light at wavelength ~320 nm for 15 hours before etch. To modulate the conically shaped nanopore tip size more accurately, we modified the etching procedure described in literature.[56] We refer to our method as the two-step chemical etch method.[53] The first step is an anisotropic chemical step and is used to control the size of the conically shaped nanopore large openings (base). The second step is an isotropic chemical etch step which is used to tailor the conical nanopore tip size with accuracy at the nano-meter scale.

The first step is the same as described by Apel previously.[56] A single tracked PET membrane was mounted between two half conductive cells. A ~3 mL 9 M NaOH (etching solution) was added to one half cell and 1 M formic acid (HCOOH) and 1 M KCl (stopping solution) was added to the other. A Pt wire electrode was placed in each conductive cell. A transmembrane potential +1 V was applied on the electrode placed in the etching solution during the first etch step by using Keithley 6487 picoammeter voltage source. The ion current during the etching was monitored at real time to allow us to collect the information about etch. The

anisotropic chemical etch was terminated at 120 minutes and solutions on both sides of the membrane were replaced with a fresh stopping solution (1 M HCOOH and 1 M KCl). The membrane was then rinsed with deionized water and immersed in the stopping solution for 15 minutes after rinsing. The membrane was untouched and kept in the cells and immersed in deionized water for storage.

A second step chemical etch was used for fine control the single conical nanopore tip size. At the second step chemical etch, the same etchant 1 M NaOH was placed on both sides of the membrane. A Pt wire electrode was placed in each conductive cell and a potential +1 V was applied on the anode that was placed in the etching solution. The ion current was monitored at real time and chemical etch was terminated when the desired ion current was achieved. In these studies, the isotropic etch was stopped when the ion current increased to 5.0 nA. The etchant 1 M NaOH was replaced with mixture of 1 M HCOOH and 1 M KCl and kept for 15 minutes. The membrane was then rinsed and immersed in deionized water for 1 hour.

**Current-Voltage Curves Measurement**

A membrane sample contained only single nanopore was mounted between the two half cells and a 100 mM phosphate buffer solution (pH 7.0) that was also 1 M KCl was placed on both sides of the membrane. A Ag/AgCl electrode was placed in each solution. A current-voltage was scanned from -1 V to +1 V with working electrode at the base side of the membrane. The conical nanopore tip size can be calculated via Equation 2-1,

$$G = \frac{\pi \kappa \, d_{base} \, d_{tip}}{4l} \tag{2-1}$$

where G is the conductance of nanopore filled with electrolyte solution. The conductivity of supporting electrolyte solution κ is about 118 mS $cm^{-1}$, $l$ is the length of nanopore, $d_{base}$ and $d_{tip}$ are the diameter of conical nanopore base and tip, respectively.

**Characterization of Sodium Poly(styrene sulfonate)**

Sodium poly(styrene sulfonate) (PSS) standard (Mw = 126,700 and Mw/Mn = 1.17 by gel permeation chromatography) were obtained from Scientific Polymer Products Inc (Ontario, NY). To determine the dimensions of PSS in the solution used for resistive-pulse measurements, dynamic light scattering (DLS) measurements under identical conditions were performed by using a ZetaPlus particle size analyzer (Brookhaven Instrument Corp. Holtsville, NY). A 100 μM of PSS in 100 mM phosphate buffer with 100 mM KCl at pH 7.0 was serially diluted to 20 μM and 2 μM of PSS using the same buffer solution. DLS measurements were taken for 5 minutes for samples at each concentration. Data were analyzed using ZetaPlus particle sizing software, assuming PSS adopts a wormlike coil under the conditions employed for DLS measurements.

**Resistive-Pulse Measurement of PSS**

A bare single nanopore PET membrane was mounted between the two half electrochemical cells and both cells were filled with 100 mM phosphate buffer solution (100 mM KCl pH.7.0). A constant transmembrane potential was applied on the Ag/AgCl electrodes that were inserted in each solution. The ionic current flowing through the single nanopore filled with electrolyte was measured with an Axopatch 200B current amplifier (Molecular Devices Corporation, Union City, CA) in the voltage-clamp mode with a low-pass Bessel filter at 2 kHz bandwidth. The signal was digitized using a Digidata 1233A analog-to-digital converter (Molecular Devices Corporation). Data were recorded and analyzed with pClamp 9.0 software (Molecular Devices Corporation). The ion current data was recorded every 10 μs and the time window was 1 minute. At least 5 minutes data were recorded for each experimental condition. During the analyte translocation experiment, the anode was placed in the solution facing the base opening of the conical nanopore and the cathode on the other side of the membrane was grounded. The steady-state ion current of the buffer solution without analyte was measured for half an hour before

being replaced with pre-diluted sodium polystyrene sulfonate solution that had the same ionic strength as the buffer solution.

## Results and Discussion

### Preparation and Characterization of Single Conical Nanopore

The first requirement for this research is to prepare a single conical nanopore with good reproducibility. A two-step etch procedure, including anisotropic and isotropic etch, was performed for tailoring the shape of nanopore.[53] The single ion tracked PET membrane was anisotropic etched for 120 mins. Because it is hard to locate a single nanoscale pore on the sample of 0.78 $cm^2$ under SEM, so we took the images of multipore membrane and use the mean base diameter for calculating the size of the single pore base opening.

Also according to the literature, we use the PET bulk etching rate of 2.17±0.19 nm $min^{-1}$ to calculate the base size as a function of etching time.[53] The tip size was calculated via Equation 2-1 after measuring the characteristic current-voltage (I-V) curve (blue curve in Figure 2-1) in the pH 7.0 100 mM phosphate buffer solution with 1 M KCl. After the anisotropic etching, a conically shaped nanopore was obtained with nanopore $d_{base}$ ~ 521 nm and $d_{tip}$ ~ 0.9 nm. In most of these resistive-pulse sensing measurements, we would like to fabricate the nanopore with a tip size comparable to the size of the analyte. In this study of PSS, a nanopore tip size of 10~15 nm was needed. Therefore, isotropic etching was performed and the etching process was monitored via the ion current. The current-voltage curve (red straight line in Figure 2-1) after the second step etch (isotropic etch) showed that conical nanopore $d_{tip}$ ~ 13.5 nm with assumed $d_{base}$ ~ 533 nm. We noticed that the nanopores show current rectification when the tip size is small, however, the ion current rectification disappear when the tip size gets larger, especially when the tip size is larger than 15 nm.[76]

**Characterization of Sodium Poly(styrene sulfonate)**

The hydrodynamic diameter of PSS in 100 mM pH 7.0 phosphate buffer with 100 mM KCl was measured by using dynamic light scattering (DLS). Because there is a requirement for sample volume fraction in DLS measurement, we only measured PSS at concentration of 2 μM, 20 μM and 100 μM in the solution with the same salt concentration and pH condition as our resistive pulse measurement (shown in Figure 2-2A). It is reported that the gyration radius of polyelectrolyte changes with the polymer concentration and ionic strength of the solution.[135, 136] We assume that the gyration radius follows the relationship shown in Equation 2-2 which is applied in semi-dilute region.[135] We can predict the approximate dimension of PSS in our experiment.

$$R_g \propto C^{-\frac{1}{8}} \tag{2-2}$$

where $R_g$ is the radius of gyration and C is the concentration of polyelectrolyte.

In Figure 2-2B, we plot the radius of gyration vs. the PSS concentration $C^{-1/8}$, a relationship between these two parameter is obtained. From this linear fit relation, the gyration radius at very low PSS concentration could also be calculated, for example, the $R_g$ of PSS at 10 nM is about 21.2 nm. Even though the average gyration radius of PSS is about twice of the nanopore tip size (13.3 nm), the polymer can still adopt different conformations in the solution to enter the nanopore under the effect of electrical field.

By combing the light scattering, zeta potential measurements, we can approximate the mobility of these polyelectrolytes in salt solution. The mobility and zeta potential are also obtained from the light scattering zeta potential analyzer. The mobility (μ) of PSS is $-2.09\times10^{4}$ ($\mu m^2\ V^{-1}s^{-1}$), and the negative sign means that the PSS molecules are negatively charged.

**Resistive-Pulse Measurement of Poly(styrene sulfonate)**

In the resistive-pulse measurement of poly(styrene sulfonate), we choose the nanopore tip size of 14 nm. The electrochemical cells were setup in similar to the etching setup and Ag/AgCl electrodes were used. Before measuring the PSS transport, the buffer solution in the absence of PSS (100 mM phosphate pH 7.0 with 100 mM KCl) was added to both sides of the membrane and the background steady state current was obtained. Figure 2-3A shows the background current, a smooth current in absence of any resistive pulse events.

In the following resistive-pulse measurement, we always applied positive potential on the base side of the membrane (permeation side) to electrophoretically drive negative charged PSS from tip to base in the nanopore. It was clearly observed that current pulses occurred when the buffer solution at the cathode side was replaced with the solution containing 1 nM or 10 nM PSS (Figure 2-3BC). It is also demonstrated here that the pulse frequency increased when PSS concentration was higher in the solution. To confirm that the resistive pulse events were caused by the migration of negatively charged PSS, we switched the polarity of transmembrane potential. When the anode was on the permeation side, we observed the pulse events. We then hypothesized that if the anode was on the feed side, the negatively charged PSS would migrate far away from the nanopore tip and no pulse events would be observed. The experiment results supported our hypothesis (Figure 2-3D).

**Effect of supporting electrolyte solution pH**

We also investigated the effect of solution pH value on the detection of PSS. In Figure 2-4, we demonstrate the current-time trace when PSS passed through the nanopore with solution pH at 3.0 and pH 7.0, respectively. It was easy for us to observe regular pulse events in the solution at pH 7.0. However, irregular events were observed and pulses overlapped and baseline current fluctuated when the solution was at pH 3.0.

These results suggest that the polyelectrolyte might interact with or adsorb on the nanopore when the surface carboxylate group is protonated and the possible adsorption cause the longer events duration time and baseline current fluctuation. On the contrary, the PSS polymer might have less interaction with the pore wall and migrate faster because the electrostatic repulsion between the negative charged surface and PSS reduce the adsorption. So we think that a supporting electrolyte solution at pH 7.0 is preferred for resistive-pulse measurement of PSS if considering optimizing the signal to noise ratio.

**Detection limit for resistive-pulse measuring PSS**

Different from the definition of detection limit in spectrometry, we need to define our criteria in the resistive-pulse measurement. There is no loss of signal/noise ratio even at the low concentration as long as the analyte size is comparable to the nanopore tip size. Theoretical, it is supposed to have single molecule detection capability for resistive pulse system if we can wait for long enough time to get the resistive pulse events corresponding to that single molecule translocation. Practically, however, we define the detection limit at which at least one resistive pulse current blockade can be observed in one minute time window. This time window scale combines the needs for low concentration analyte detection, time efficiency, and the cost. We studied the PSS resistive-pulse measuring in a large dynamic range, which is PSS concentration changed from 10 pM to 10 nM.

**Effect of analyte concentration on pulse frequency**

From Figure 2-3, we can easily know that the number of resistive-pulse events should increase if we raise the concentration of PSS. As Equation 2-3 shown, the electrophoretical flux $J_i(x)$ is proportional to the concentration of analyte ($C_i$),[137]

$$J_i(x) = -\frac{z_i F}{RT} D_i C_i \frac{\partial \phi(x)}{\partial x} \quad (2\text{-}3)$$

where F is faradic constant (96485.3 C $mol^{-1}$), R is the gas constant, $D_i$ is the diffusion coefficient of species i, T is the temperature and $\partial\phi(x)/\partial x$ is the electrical field strength at point x. If we multiply the Avogadro's number $N_0$ ($6.02\times10^{23}$) and area of nanopore tip and time scale, we could know the relationship between the number of events ($N_{pulse}$) in certain time window (t) with analyte concentration,

$$N_{pulse} = -\frac{Z_i F}{RT} D_i C_i \frac{\partial \phi(x)}{\partial x} N_0 \pi R_{tip}^2 t \quad (2\text{-}4)$$

where $R_{tip}$ is the radius of conical nanopore tip opening.

Figure 2-5 shows that the resistive-pulse frequency increased with PSS concentration. At lower concentration range in our experiments (10 pM to 1 nM), the pulse frequency was almost proportional to the PSS concentration, but at the 10 nM concentration of PSS, the relationship was not linear. We think such a nonlinear relationship might be because the increased analyte interactions outside of the tip at high polyelectrolyte concentration affect the detection. It seems that we could predict the number of resistive-pulse events from Equation 2-4, but it is really hard to make any prediction accurately because of the uncertainty of several parameters in the equation, such as the effective charge, real electric field strength at the tip.

**Effect of transmembrane potential on pulse frequency**

Besides the concentration dependence, we also investigated the effect of transmembrane potential on resistive-pulse event frequency.

The PSS polyelectrolyte is supposed to be negatively charged in the pH 7.0 buffer solution so that the polyanions should migrate in different directions if transmembrane potential polarity is switched. If the anode was placed at the permeate solution side, the polyanions were supposed to migrate towards the nanopore membrane and generate resistive-pulse events. On the contrary,

the polyanions were driven far away from the nanopore and no events would be observed if the anode was placed in the feed solution.

As predicted from Equation 2-4, we should observe higher resistive-pulse events frequency when the transmembrane potential increases. However, we did not observe a linear relationship between the pulse frequency and electrical field strength as described in Equation 2-4. Instead, we found that the resistive-pulse frequency had an exponential growth relationship with transmembrane potential (as shown in Figure 2-6).

Actually, the frequency of current blockade might not be proportional to the electric field strength. Because the hydrodynamic diameter of PSS in dilute solution was larger than the tip size of nanopore, the polymer chains need activation energy to overcome an activation barrier. In other words, they must pay an entropy penalty to reptate into the nanopore. It was suggested that the DNA threads through the pore rather than going though as a random coil.[134] There was literature reported that the elongation of these polyions conformation occurs under the electric field.[138] so that it is possible for PSS to change conformations and reptate into the nanopore. Similar to the transport of DNA into an nanopore, the current blockade rate R is described by Van't hoff-Arrhenius or transition-state relation.[134]

$$R = \kappa v \times \exp[-(U^{\ddagger} - \Delta U)/kT] \quad (2\text{-}5)$$

where $\kappa$ is a probability factor, ν is the frequency factor, $U^{\ddagger}$ is the activation energy or barrier height. $\Delta U$ is the reduction in the energy barrier due to the applied transmembrane potential, $k$ is the molar gas constant and T is the absolute temperature. The higher transmembrane potential leads to higher energy,

$$\Delta U = ze|E| \quad (2\text{-}6)$$

where z is the effective total number of elementary charges on the polymer and $e$ is the

magnitude of the elementary charge. The rate of blockade in a vanishing applied potential (E) is

$$R_0 = \kappa v \times \exp(-U^{\ddagger}/kT) \quad (2\text{-}7)$$

Then it gives the equation for blockade rate at different transmembrane potential,

$$R = R_0 \times \exp(ze|E|/kT) \quad (2\text{-}8)$$

and $R_0$ is independent of E. It is expected to observe the exponential growth of current blockade rate with the transmembrane potential. We can expect to have more resistive-pulse events at the same concentration of analyte if applying a high potential. We think we might be able to find a way to improve the detection limit further. The higher electric field strength which speeds up the mass transfer can lead to the higher migration flux and increase the detection efficiency as long as the mass transfer is fast enough.[81]

In summary, the polarity and magnitude of transmembrane potential have important effects on the PSS translocation through the nanopore. The polarity could change the direction of polyelectrolyte migration. The magnitude of electric field strength will affect different transport flux and provide different energy for polymers to translocate through the nanopore. Thus it might be a way to improve the detection limit by applying higher transmembrane potential, which is an important advantage of using synthetic membrane than biological nanopore system.

**Translocation time and magnitude of current blockade**

In the resistive pulsing, the translocation events duration time and amplitude of current blockade are used to identify the analyte DNA.[42] We also studied these two parameters in the experiment related with polyelectrolyte electromigration.

In this study, as an analogy to data analysis in spectrometry, we defined a current pulse as one detection event only when the amplitude of that current pulse was twice of the baseline noise. For example, the background noise of 14 nm tip conical nanopore filled with 100 mM

phosphate buffer and 100 mM KCl at applied potential 1 V was about 30 pA. In this case, only the current pulse amplitude equal to or larger than 60 pA was counted by the software as a pulse event. As we know, the background current decrease if the applied potential decrease. In such case, the signals were only counted as events when the signal/noise ratio at 2:1, but not base on the absolute value of 60 pA.

It is also known the values of ion current background and amplitude of current pulse depend on the tip size of nanopore.[53] So it is hard to compare the amplitude of pulse measured from the nanopore at different sizes. In this study, the normalized current pulse amplitude (ΔI%) was defined as the ratio of absolute value of current drop (ΔI) and average background current value ($I_0$), as shown,

$$\Delta I\% = \frac{\Delta I}{I_0} \times 100\% \quad (2\text{-}9)$$

Figure 2-7 shows the histogram of normalized PSS current pulse amplitude measured with 14 nm tip size conical nanopore membrane. It was observed that most of the current pulse amplitude is less than 15% of the background current value. Compared to the 90% current block when a single strand DNA passed through an α-Hemolysin channel, the amplitude of current pulse in this synthetic conical nanopore embedded in PET membrane is really small.

The other parameter, current pulse duration, is also important because it might include the information about the speed of analyte migrate in the pore, interactions between of analyte and pore wall or binding affinity. It seems that the duration of PSS translocate the nanopore sensing zone is really short (Figure 2-8). Most of the events are shorter than 40 ms, which might mean the PSS has little interaction with nanopore and pass through the sensing zone quickly. This might be an advantage for detection of analyte at high concentration. It is possible that pulse signal will overlap at high pulse frequency if duration is too long. But the duration of PSS at

molecule weight Mw = 127,000 still had a broad distribution, from several milliseconds to one hundred milliseconds.

Scatter plots of current pulse amplitude ($\Delta I$) versus current-pulse duration ($\tau$) were usually used to summarize resistive-pulse data. It was shown that the current pulses had large distribution for both pulse amplitude and duration. The variability of the current pulses might be because the polyelectrolyte can adopt different conformations, and thus different pulse signals.

## Conclusions

We prepared a single conical nanopore in PET membrane with good reproducibility. PET membranes contained conical nanopore at ~ 530 nm base and 14 nm tip was used for the resistive-pulse studies of polyelectrolyte translocation.

Experimental conditions for resistive pulse sensing of a prototype linear polymer analyte were investigated. Resistive pulse events of PSS translocation were observed at a large range of PSS concentrations. It was observed that the current pulse frequency increased with polyelectrolyte concentration in this range. The lowest detection limit for a one-minute measurement was 10 pM of polyelectrolyte in the solution with transmembrane potential at 1 V. It might be able to improve the limit of detection if apply much higher voltage as long as the nanopore membrane is stable.

However, the current pulse signature of this polyelectrolyte model analyte had a very broad distribution for both the pulse amplitude and pulse duration. It is very difficult to distinguish the same polyelectrolyte but at different average molecule weight. It is also important to improve the selectivity of such experiment in the future instigation.

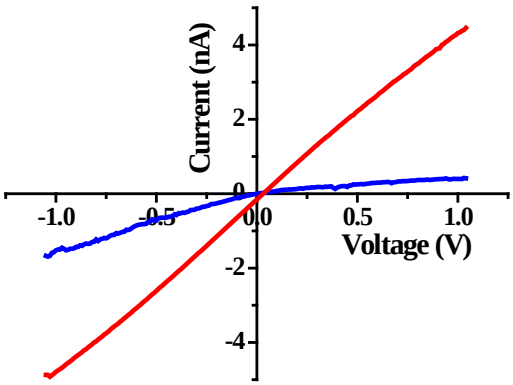


Figure 2-1. Current-voltage curves of a single conical nanopore in PET membrane. (Blue) IV curve after the first step etch. (Red) IV curve after the second step etch. Measured in pH 7.0 100 mM phosphate buffer with 1 M KCl.

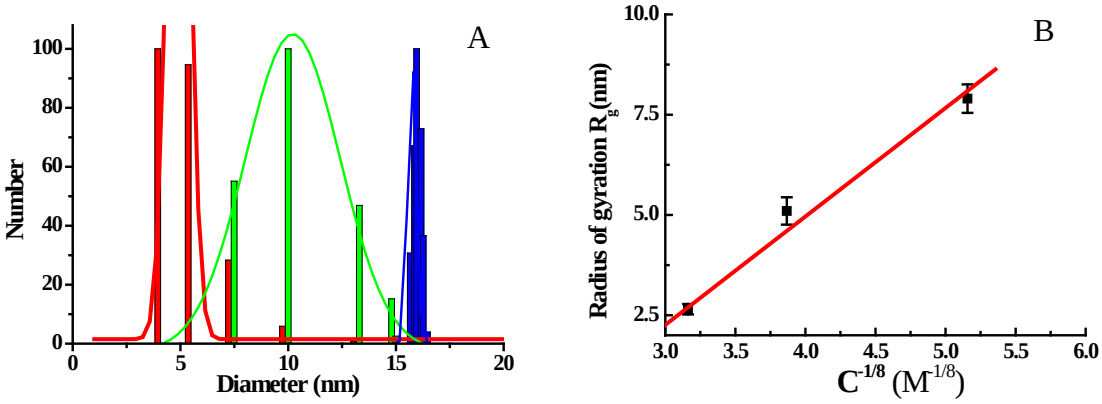


Figure 2-2. Distribution of hydrodynamic diameter of PSS at different concentrations and the relationship between the gyration radius and polyelectrolyte concentration. It was measured using dynamic light scattering. A) Distribution of PSS at different concentrations. red: 100 μM, green: 20 μM, blue:2 μM. The curves are Gaussian fit data. B) Relationship between gyration radiuses vs. PSS concentration.

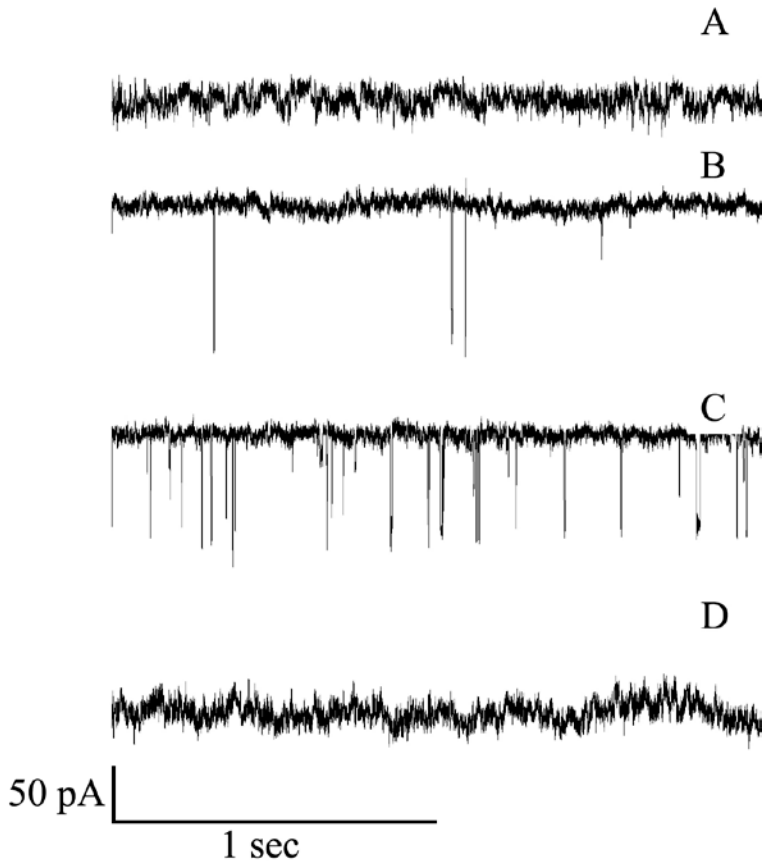


Figure 2-3. Current-time transients of resistive-pulse measuring PSS at different concentrations. A) Steady state current of buffer solution (100 mM KCl in 100 mM PBS pH 7.0). B) Resistive-pulse events with PSS concentration at 1 nM. C) Resistive-pulse events with PSS concentration at 10 nM. D) Steady state current of 10 nM PSS solution when anode is on the feed side facing tip opening of the nanopore.

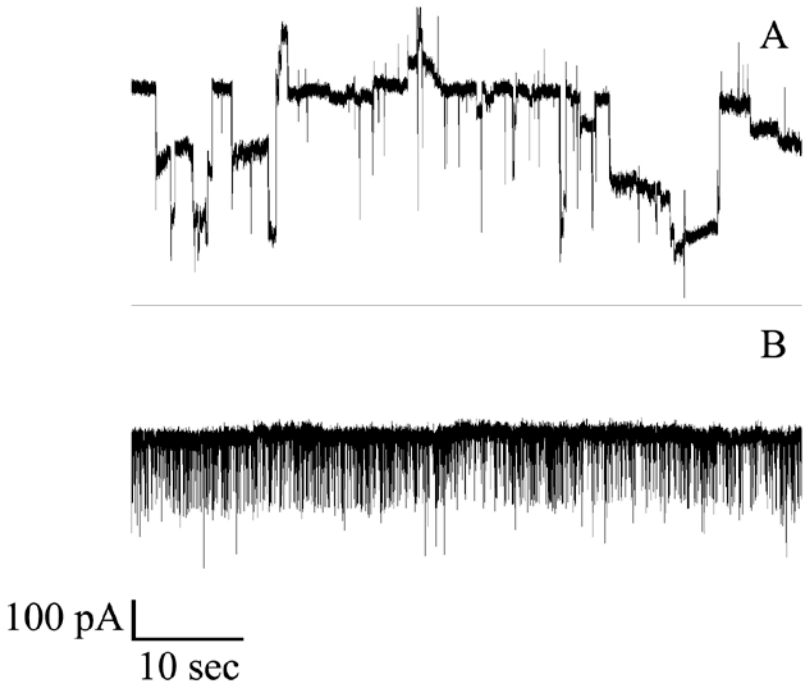


Figure 2-4. Current-time transients of resistive-pulse measuring PSS at different pH value. A) pH 3.0. B) pH 7.0. PSS concentration if 10 nM.

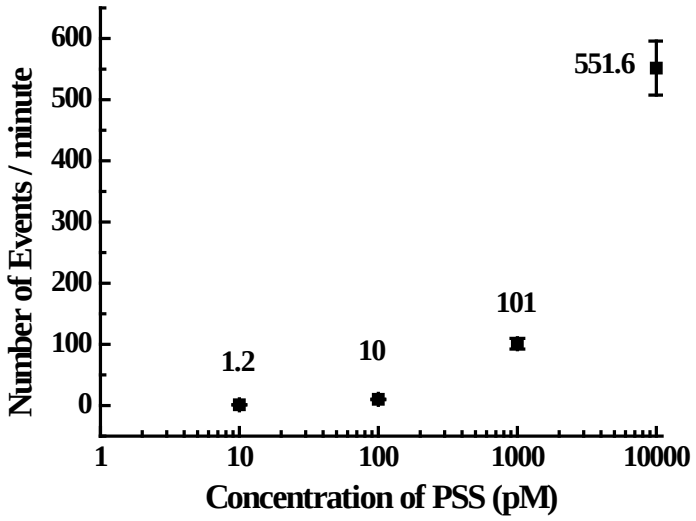


Figure 2-5. Relationship between the number of resistive-pulse events and PSS concentration. It was measured with transmembrane potential at 1000 mV.

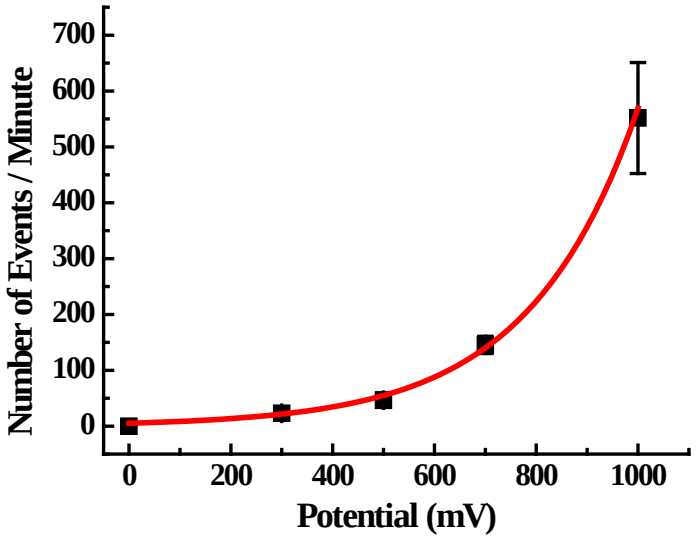


Figure 2-6. Relationship between the number of resistive-pulse events and transmembrane potential. It was measured using PSS concentration of 10 nM feed solution.

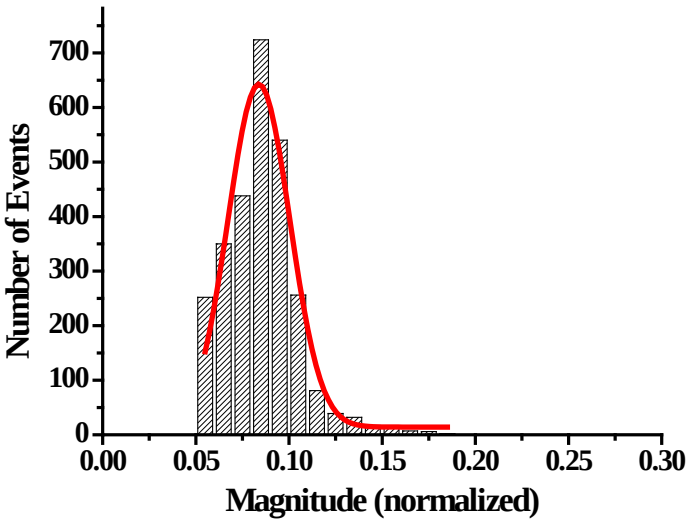


Figure 2-7. Histogram of normalized current pulse amplitude of resistive-pulse measuring PSS translocation. Nanopore tip diameter = 14 nm. PSS concentration = 10 nM. Applied transmembrane potential = 1000 mV.

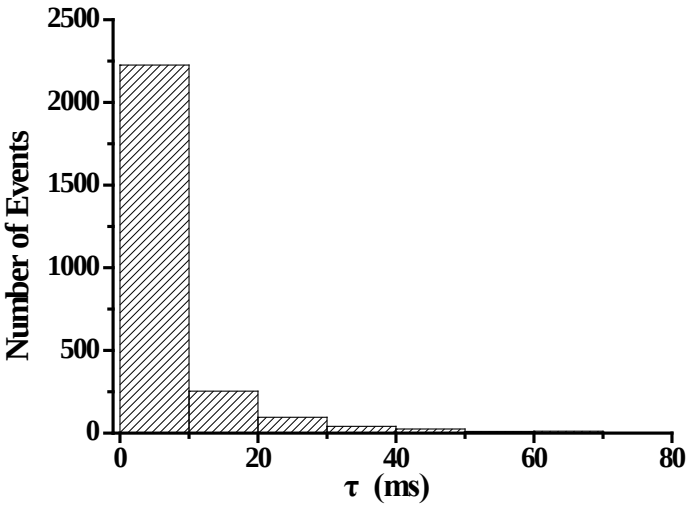


Figure 2-8. Histogram of PSS current pulse duration τ. Nanopore tip diameter = 14 nm. PSS concentration = 10 nM. Applied transmembrane potential = 1000 mV.

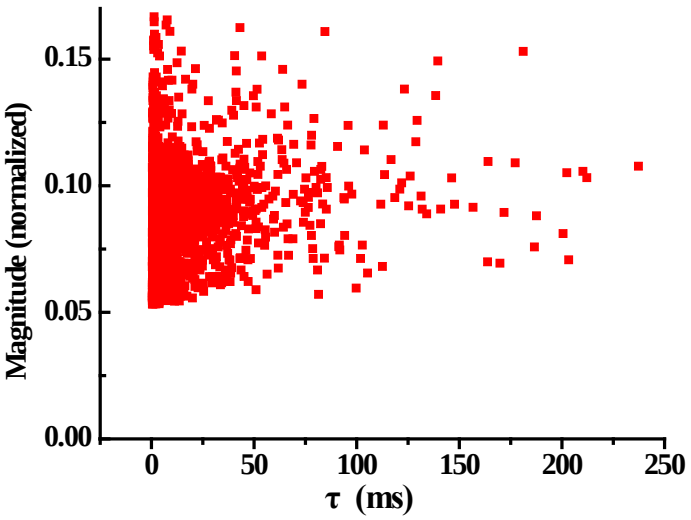


Figure 2-9. Scatter plot of normalized current-pulse amplitude versus current pulse duration τ. Nanopore tip diameter = 14 nm. PSS concentration = 10 nM. Applied transmembrane potential = 1000 mV.

# CHAPTER 3
# FABRICATION OF PYRAMIDALLY SHAPED NANOPORES IN MUSCOVITE MICA MEMBRANES

## Introduction

There is an increasing interest in developing asymmetrically shaped nanopores[16, 28, 32, 45, 47, 50, 53, 57, 61, 69, 70, 119, 139, 140] in synthetic membranes using the track-etch method for resistive-pulse[48, 133] or ion current rectification studies. However, most of these asymmetrically shaped nanopores were fabricated in polymer membranes.[53, 58, 62, 67, 119] There is also one example to prepare such conically shaped nanopores in inorganic materials, but it is in amorphous silica thin films.[24, 92]The Martin group has started exploring the fabrication of asymmetric nanopore in crystalline thin film-muscovite mica.[69] However, the fabrication process still has less control over the nanopore size and geometry, making nanopores developed in mica membranes less suitable for resistive pulse sensing studies.

In this work, we developed a multi-cycle anisotropic chemical etch method to prepare asymmetrically shaped nanopores in ion-track muscovite mica membranes. The effect of etchant concentration, transmembrane potential, and etching cycle number on nanopore size and geometry were investigated in detail. The nanopore dimensions and geometry in multipore mica were confirmed by SEM images of bare nanopore membranes and carbon replicas of the nanopores. The electrochemical measurement and calculation of the size of a single nanopore in mica were discussed as well.

The ion transport properties through a single asymmetric nanopore in mica membrane were also studied. The ionic current was highly rectified in low ionic strength electrolyte solution. We think this very strong ion current rectification is due to the highly negatively charged surface. To decrease the surface charge density, the nanopore wall can be modified with an uncharged

surface functional group. This leads to much less ion current rectification in the asymmetric nanopore.

## Experimental

### Materials

Muscovite mica ($KAl_2(AlSi_3)O_{10}(F,OH)_2$) membranes, ~10.5 μm thick and ~3 cm in diameter, were obtained from Spruce Pine Co (Spruce Pine, NC). The linear accelerator at GSI (Darmstadt, Germany) was used to ion-track the mica; $Pb^{2+}$ ions of ~8.6 MeV kinetic energy were used. Samples with a single damage track, and with $10^5$ and $10^7$ tracks per $cm^2$, were prepared. Hydrofluoric acid (~50%) was obtained from Acros Organics USA (Morris Plains, NJ). Glycidoxypropyltrimethoxysilane (GPTMS) was purchased from Gelest (Morrisville, PA). Toluene (anhydrous, 99.8%), ethanol (anhydrous, 99.5%), β-mercaptoethanol (≥99.0%) and phenol were obtained from Sigma-Aldrich (St. Louis, MO). The ethylene/helium (30% ethylene) mixture was purchased from Praxair (Danbury, CT). All other chemicals were reagent grade and used as received. Purified water, obtained by passing house-distilled water through a Barnstead, E-pure water purification system, was used to prepare all solutions.

### Asymmetric Nanopore Fabrication and Characterizations

### Fabrication of asymmetric nanopore in mica

A caliper was used to accurately measure the diameter of the membranes, and the membranes were then weighed with an analytical balance. The thickness of each membrane was calculated from the mass and the density of the mica (2.831 g $cm^{-3}$). An average value of 10.4±0.2 μm was obtained.

A multi-cycle chemical etching method was developed to fabricate pyramidally shaped nanopores in the ion-tracked muscovite mica membranes. A ~1 cm diameter hole was cut into a ~4x4 cm piece of parafilm (Alcan Inc. Neenah, WI), and the mica membrane was sandwiched

between two such films. The sandwiched membrane was placed between the two halves of the etching cell[53] described previously.

To check that there were no leaks in the parafilm seals, the half cells were filled with 1 M KCl that was 100 mM in phosphate buffer, pH = 7.0. A Ag/AgCl reference electrode was placed into each half-cell solution, and a Keithley 6487 picoammeter/voltage source (Keithley Instruments, Inc., Cleveland, Ohio) was used to apply 1 V across the membrane and measure the resulting transmembrane current. If there were no leaks a negligible current (<10 pA) was obtained. This is because the ionic conductivity of the unetched damage track is negligibly small.

After the leak check, the half-cells were emptied, rinsed, and ~3 mL of 10 M NaOH solution was pipetted into one of the cells. The membrane was exposed to this solution for 5 minutes, a Pt wire electrode was inserted into each half cell, and ~3 mL of 10 M HF was then added to the other half cell. The Keithley was used to apply a transmembrane voltage of 10 V (with the anode in the HF solution) and measure the resulting ionic current through the membrane during etching.

Because the ionic conductivity of the unetched track is essentially zero, no current flowed through the membrane at short times. However, HF etched the mica along the damage tracks to create the pores, and ultimately the pores broke through to the NaOH solution on the opposite side of the membrane. This caused a rapid rise in the transmembrane current, with the current being carried by the nascent electrolyte-filled pores. Because NaOH does not etch mica at room temperature, but instead neutralizes the HF etchant that makes its way through the pore, an asymmetrically shaped pore was obtained with the large-diameter (base) opening facing the HF solution and the small-diameter (tip) opening facing the NaOH solution.

After 10 minutes the etch was terminated by placing 1 M NaOH on both sides of the membrane and applying 10 V for 5 minutes, to ensure complete neutralization of the HF in the pores. The membrane was then rinsed with water, and water was placed in both half cells for 30 minutes to wash the NaOH from the pores. We call this procedure a 10-minute etch cycle. Membranes were etched using between one and eight of such 10-minute etch cycles.

**Scanning electron microscopy**

For the multi-track mica membranes, field-emission scanning electron microscopy (FE-SEM, JEOL 6335F) was used to measure the dimensions of the base and tip openings of the asymmetric pores. To obtain images of the tips, the mica membrane was applied with the base-side down to a piece of double-side copper tape, which was then attached to a SEM sample stub. Images of the base openings were obtained by mounting the sample with the tip side down.

Another method we have developed to image pores in multipore membrane entails depositing a material such as metal[62] or carbon[29] within the pores. This creates replicas of the pores, which can be liberated by dissolution of the template membrane and imaged.

The replicas in this case were composed of graphitic carbon, deposited within the pores by a CVD method.[29] The etched mica membrane was placed vertically into a quartz tube (diameter ~4.5 cm, length ~48 cm) with the nanopore base opening facing the gas flow. The quartz tube was then inserted into a high-temperature tube furnace (Thermolyne 21100, Aldrich) and heated to 670º C under argon flow. When the temperature stabilized, the argon gas was replaced with a 30% ethylene/helium mixture at a flow rate of 20.0 sccm (standard cubic cm per min). After 5.5 hours, the flow was changed back to argon, the furnace heater was turned off, and the tube was allowed to cool to room temperature.

The asymmetric shaped carbon replicas deposited within the pores were then exposed by dissolution of the mica template. This was accomplished by first using a methanol-wetted cotton

swab to remove the carbon surface film covering the tip side of the mica. The base side was then attached to a piece of double-side copper tape, which was attached to the bottom of a small (3 cm) plastic Petri dish.

Several drops of 50% HF solution were pipetted onto the center portion of the tip-side surface. The Petri dish was then covered with parafilm and allowed to sit for 8 hours to dissolve the portion of the mica that was covered with the HF solution. The parafilm was then removed and the HF solution allowed to evaporating to dryness. Several drops of deionized water were then applied to the same spot on the surface, and this was allowed to evaporate. The sample was then mounted on a SEM stem and sputtered with Au/Pd using a cold sputter instrument (Desk II, Denton Vacuum).

**Equivalent base and tip diameters**

Both the base and tip openings in track-etched mica are rhomboidal in shape.[141] As a result, the lengths of both the long ($a_l$) and short ($a_s$) axis of the rhomboid are required to describe the size of these openings (Figure 3-1). To simplify this situation, we define here an equivalent circular opening[141] which is a circle with the same area as the rhomboidal opening.

The area of a rhomboidal opening ($A_{rhomboid}$) and of a circular opening ($A_{circle}$) can be calculated using Equation 3-1 and Equation 3-2, respectively.

$$A_{rhomboid} = \frac{1}{2} a_l a_s \tag{3-1}$$

$$A_{circle} = \frac{1}{4} \pi d_{Eq}^2 \tag{3-2}$$

To obtain the circular area equivalent to the rhomboidal area, we set Equation 3-1 equal to Equation 3-2 and solve for the diameter of the equivalent circle, $d_{Eq}$.

$$d_{Eq} = \sqrt{\frac{2}{\pi} a_l a_s} \tag{3-3}$$

This equation can be simplified by noting that the minor angle of a rhomboidal pore in mica is approximately 60°.[71] Simple geometry shows that for such a pore the $a_l$ is equal to 1.732 $a_s$. This allows us to write

$$d_{Eq} = 0.606\, a_l \quad (3\text{-}4)$$

The $a_l$ values were obtained from the electron micrographs of the multipore mica membranes, and Equation 3-4 was used to obtain the corresponding equivalent diameters. Both of the equivalent base diameter, $d_{Eq\text{-}b}$, and the equivalent tip diameter, $d_{Eq\text{-}t}$, were determined this way for the multipore mica.

**Equivalent base and tip diameters for the single-pore mica membranes**

While the base and tip openings of nanopores in the multipore mica membranes could be easily imaged with FESEM, it is much more difficult to obtain such images for single nanopore membranes. This is especially true of the tip openings because they are so small and there is only one per sample.

As will be discussed below, for the multipore mica membranes we have obtained experimental plots of equivalent base diameter, $d_{Eq\text{-}b}$, vs. etch time. The slope of such plots provides the etch rate. As per our prior work,[53] $d_{Eq\text{-}b}$ for the single pore was calculated from the etch time and such an experimental etch rate. The equivalent diameter of the tip opening, $d_{Eq\text{-}t}$, was then measured using an electrochemical method described in detail previously.[32, 53]

Briefly, the mica membrane containing a single asymmetric nanopore was mounted between the two half-cells, and an electrolyte solution of measured conductivity was placed on either side of the membrane. In this case, the electrolyte solution was 1 M KCl that was also 100 mM in phosphate buffer at pH 7.0; the measured conductivity of this solution was ~11.8 $Sm^{-1}$. A

Ag/AgCl electrode was placed into each half-cell solution, and a current-voltage curve was obtained by scanning the potential from -1.05 V to +1.05 V at a scan rate of 1 $Vmin^{-1}$.

For single asymmetrically shaped nanopore such current-voltage curves are typically non-linear.[57] However, the portion between about +200 mV can be approximated by a straight line, and the slope of this line provides the ionic conductance of the electrolyte-filled pore, G. G is related to $d_{Eq\text{-}t}$, $d_{Eq\text{-}b}$,, and the membrane thickness, L, via,

$$G = \frac{\sigma\pi\, d_{Eq-b}\, d_{Eq-t}}{4L} \tag{3-5}$$

The $d_{Eq\text{-}t}$, values for the single nanopores were calculated from Equation 3-5.

**Electroosmotic flow measurement**

As will be discussed below, both the nanopore base and tip size increased with etch time. We wonder whether there is electroosmotic flow (EOF) in the nanopore to carry the etchant HF molecule towards the tip region during the chemical etch, an EOF experiment was performed under the similar ionic strength conditions as we etched the nanopore. EOF was investigated by measuring the flux of a probe molecule (phenol) across the membrane.

A mica membrane containing asymmetric nanopores (pore density ~$10^8$ $cm^{-2}$) was mounted between the two half-cells. A 3 mL permeate solution that was 1 M phosphoric acid was added to the cell at the tip side of the membrane. A 3 mL feed solution that was 1 M phosphoric acid containing 10 mM phenol was added to the other cell. A Pt wire electrode was placed into each half cell.

A Solartron SI 1287 electrochemical interface (Farnborough, UK) was used to apply a constant current (5.0 mA, 10.0 mA, or 15.0 mA) flowing through the multipore mica membrane. Such current is responsible for the EOF in the nanopores. The Pt wire in the feed solution will be used as working electrode and the Pt wire in the permeate solution will be used as reference and

counter electrode. The faradic reactions occurring at the Pt electrodes that support the ionic current in the nanopore were mainly the reduction and oxidation of water.

After 20 minutes, the applied current was terminated and both the permeate solution and feed solution were pipetted out of the half cells. An Agilent 8453 UV-visible spectrometry system (Waldbronn, Germany) was used to measure the UV absorbance of phenol in the permeate solution. The concentration of phenol in permeate solution was calculated from the calibration curve measured at wavelength 270 nm.[142] After the UV-visible spectrum measurement, the permeate solution was placed back into the same half cell for next 20-minute cycle translocation. A new feed solution with the same concentration of phenol was placed at the feed side for next cycle translocation. The total translocation time is 120 minutes and UV-visible spectrum of permeate solution was measured after each 20-minute translocation cycle. The diffusion of phenol across the membrane without applying current was also measured at the same time intervals.

**Acid-base neutralization in nanopores**

As will be discussed below, to study the ionic current decay we observed during the mica etch, we designed an acid-base neutralization experiment to mimic the process that might occur the same way during mica etches. In this study, to keep the HF from continuing etching and increasing the nanopore size, we replaced the HF with another weak acid - acetic acid (HAc).

A multipore (pore density ~$10^5$ $cm^{-2}$) mica membrane that etched for one 10-minute cycle was used and mounted between the two half-cells. In this experiment, a Pt wire electrode was placed on each half cell. A NaOH solution was first put into the cell facing the tip side of the membrane and a HAc solution was added into the other cell. The Keithley was used to apply a transmembrane voltage of 10 V (with the anode in the HAc solution) and measure the resulting ion current flowing through the membrane for 10 minutes. Different concentration (1 M, 2.5 M,

5 M, 10 M) of NaOH were used in a series of experiments and the corresponding ionic current was recorded.

**Nanopore Surface Modification**

Nonlinear current-voltage curves are typically observed for conically shaped nanopores that have tip diameters in one nm to tens of nm range.[31, 57] This non-linearity is an ion-current rectification phenomenon, and has been discussed in detail in the literature.[24, 56, 57, 74, 143] In order to see rectification, the pore wall must have excess surface charge, and the extent of rectification is affected by the ionic strength of the solution and the size of the nanopore tip.[57] A strong in current rectification is observed when the nanopore surface charge density is high, the tip diameter is small, and the ionic strength is low.

As will be discussed below, the asymmetric mica nanopores investigated here show greater ion-current rectification than the conical pores in polymeric membranes investigated by us and others. To confirm that the excess surface charge present on the muscovite mica[141] is responsible for rectification, we reacted silanol sites on the mica surface[144] with a neutral siloxane reagent to decrease the surface charge (Figure 3-2). The chemistry is analogous to that used to attach reagents to silicon surfaces.[145, 146]

The single-asymmetric-nanopore mica membrane was first cleaned by immersion in a highly acidic piranha solution (3:1 v/v of $H_2SO_4/H_2O_2$) for 1 hour. The mica membrane was then rinsed thoroughly with deionized water and stored in water for 1 hour followed by drying under a stream of nitrogen. The mica was then immersed for 30 minutes into 10% (v/v) glycidoxypropyltrimethoxysilane (GPTMS) dissolved in anhydrous toluene. This was done in a polyarylic box under nitrogen flow to limit GPTMS hydrolysis by atmospheric water. The membrane was then immersed into three portions of anhydrous toluene for five minutes for each

portion. It was then immersed into three portions of anhydrous ethanol for five minutes for each portion, and dried in air for 12 hours.

The surface epoxide terminal groups of the attached GPTMS were then converted to hydroxyl groups by reacting with β-mercaptoethanol (Figure 3-2).[146] This was accomplished by immersing the GPTMS functionalized mica in a solution that was 10% (v/v) β-mercaptoethanol dissolved in pH 7.4 phosphate-buffered silane for 3 hours. The mica was then rinsed with deionized water and dried under nitrogen.

Current-voltage curves were obtained for these hydroxyl-modified mica membranes using the same conductivity cell and Ag/AgCl electrodes as described above. However, a lower ionic strength electrolyte was used - 10 mM phosphate buffer (pH 7.0) that was also 10 mM in KCl.

## Results and Discussion

### Fabrication of Nanopore with Ion Track Method

#### Nanopore breakthrough in ion-track mica

We began our studies with multi-track mica membranes ($10^5$ tracks $cm^{-2}$) because it is easier to image the resulting pores in such multi-track membranes. Figure 3-3 shows plots of ion current flowing through the membrane during the first 10-minute etch cycle as a function of etch time for three identical mica membranes. Because the ionic conductivity of the unetched track is essentially zero, no current flowed through the membrane at short times. However, HF etched the mica along the track, and ultimately the resulting pores broke through to the NaOH stopping solution on the opposite of the membrane. This was signaled by the sudden jump in current observed at about 1 minute. When a lower concentration of etchant HF was used for etching, it took a longer time for nanopore to breakthrough.

**Current-time traces during anisotropic chemical etch**

As shown in Figure 3-3, after the current jump signaling nanopore breakthrough, the current initially decayed and then slowly increased with further etching. We think that such current change was related with the acid-base neutralization during the etch process. We hypothesize that this acid-base neutralization will cause a transmembrane acid concentration gradient, which is critical for fabrication of asymmetrically shaped nanopore in mica.

To investigate these questions, we designed two experiments to help us explain what is happening during the anisotropic chemical etching. The first one was to study whether there was EOF in the nanopore in the presence of applied current. The second one was to use HAc (weak acid) and NaOH (strong base) and their neutralization to mimic the reaction process between HF and NaOH in the nanopore during etch. Based on the results from these two experiments, we hope to develop a model of HF transport and its effect on nanopore etching.

**Electroosmotic flow in nanopores**

As we will discuss below, it is observed that the asymmetric nanopore tip opening size increased with the number of etch cycles. So we believe that the HF was always transported to the tip region during the whole process even though the concentration of HF might be very low. We wonder if there is any other flow, such as electroosmotic flow (EOF) to carry the neutral molecule HF towards the nanopore tip during etch.

In order to investigate whether there is electroosmotic flow (EOF) to carry the etchant HF molecule towards the tip region during the chemical etch, an EOF experiment was performed under the similar conditions. EOF was investigated by measuring the flux of a probe molecule (phenol, pKa =9.99) across the membrane (Miller and Martin 2002) in acid solution. The buffer used in such an investigation was 1 M phosphoric acid at pH ~1.08. Therefore, phenol was

neutral at this pH value and its translocation through the nanopore was only carried by diffusion and EOF.

During the chemical etch of mica, the anode was at the base side of the membrane and the cathode was at the tip side of the membrane. So HF was carried from base (anode) side towards the tip (cathode) if there was EOF during the chemical etch. In the EOF study, the electrolyte solution was 1 M phosphoric acid. Although it was different from the solution we used during nanopore etching (10 M HF). However the calculation shows that cation and anion concentration are almost similar to those in the 10 M HF. In 10 M HF, the cation $H^+$ and anion $F^-$ concentration are about 0.084 M ($Ka = 7.1\times10^{-4}$ $molL^{-1}$). In 1 M $H_3PO_4$, the cation $H^+$ and anion $H_2PO_4^-$ are about 0.083 M ($Ka_1 = 6.9\times10^{-3}$ $molL^{-1}$). Therefore, the pH of these two solutions were around 1.08 so that the nanopore surface charge condition were similar in both cases. Therefore, if we can prove that there was EOF from base to tip in the phenol experiment, then we might be able to conclude that there was also EOF carrying HF in the nanopore when we etched the mica.

Figure 3-4 shows the concentration of phenol in the permeate solution under different transport conditions. It was observed that the phenol transport rate is much higher in the presence of constant current than it is with no applied current. We think that the enhanced phenol flux was because the electroosmotic flow pumps the solvent and phenol to the permeate solution. Therefore, it is reasonable for us to assume that there was also EOF that pumped the HF towards nanopore tip even at a low flow rate, resulting in a constant etch rate at the nanopore tip.

**Acid and base neutralization in the nanopores**

We designed another experiment to mimic the acid-base neutralization during nanopore chemical etch. In this investigation, to avoid the nanopore size increasing because of HF etching, HF was replaced with another weak acid acetic acid (HAc). We assumed that the mass transfer and neutralization of HAc with NaOH are similar to that of HF. Figure 3-5A shows plots of ion

current flowing through the membrane during acid-base neutralization as a function of time for different NaOH concentrations. It was observed that the current-time traces show a similar trend to that we observed during HF etching mica, which was that the currents started to decrease after the acid and base contact. It is clear that the ion current flowing through the membrane is larger when the concentration of NaOH is higher. This is because high concentration NaOH consumes HF faster so that HF dissociates faster to provide ions to support the ion current.

Since we know that there was electroosmosis pumping the HF from base to tip and etching the tip all the time, so there was HF always in the nanopore during the chemical etch. In this similar experiment, it is assumed that electroosmosis will pump HAc to the tip and HAc will fill the nanopore. Because NaOH and HAc do not coexist, so we can assume that NaOH did not actually enter the nanopore since HAc always existed even though the concentration is lower than that of the bulk solution. Driven by the electric field, $OH^-$ moved from the bulk towards nanopore tip and HAc was pumped out of the nanopore to the external solution on the tip side.

We hypothesize that there was a region right outside the nanopore tip where NaOH and HAc contacted. In this region, the base $OH^-$ and acid HAc neutralized each other. We refer this region as a neutralization region. As shown in Figure 3-5B, $OH^-$ was driven to this region and reacted with HAc. The concentration of both $OH^-$ and HAc dropped to zero somewhere in the neutralization region. This caused the concentration of HAc at the tip also dropped to a certain value which was higher than zero but lower than the concentration of HAc on the base side. As a result, a concentration gradient of HAc was established in the nanopore. The concentration of HAc was lower at the tip and high at the base. Analogously, we can assume there was also a concentration gradient of HF in the nanopore during anisotropic etching of mica. The concentration of HF was lower at the tip, and it was higher at the base. As a result of the HF

transmembrane concentration gradient, the etch rate of mica was lower at the tip opening and higher at the base opening. Therefore, asymmetrically shaped nanopores were obtained in muscovite mica membrane.

**Track etch rate of mica**

The current-time transient observed after nanopore breakthrough for the multi-track mica membrane showed a sudden increase. If the breakthrough of ion tracks occurred one after another, ion current would increase gradually, which was usually observed when multi-track PET membranes were etched in aqueous solution. But if all the ion tracks break through at the similar time, then a very large current would rise rapidly because there were lots of pores that could support the current at the same moment. It was observed that the ion current flowing though the mica membrane was nearly zero in the first minute and dramatically increased to a peak value within a few seconds (Figure 3-3). We believe that this rapid rise in current was due to all the ion tracks on the membrane being etched at a similar track- etching rate and breaking through at almost the same time.

It was also observed that it took a comparable amount of time (55 to 60 seconds) for ion tracks to break through in different mica membranes of the same thickness that etched in the same way. In other words, good track-etching rate reproducibility was observed from different mica membranes and the average track etching rate is about 181±10 nm $sec^{-1}$ using 10 M HF.

It was observed that in the experiment of NaOH and HAc, the ion current approached a constant value at the end of neutralization. This is because the mass transfer and the acid-base neutralization achieved an equilibrium state. However, in the mica etch process, the ion current stopped decreasing and started to increase at about two to three minutes. This was because HF kept etching mica and increasing the size of nanopore tip and base openings in this case. The

resistance of the multipore membrane decreased so that the total ion current increased at the end (Figure 3-3).

Figure 3-6 shows that the current-voltage curves obtained from three identical mica membranes after the initial 10-minute anisotropic etch cycle. The similar conductance observed here showed that nanopores on the different membranes might have comparable size after one etch cycle if they were assumed to have the same number of pores from membrane to membrane. However, the nanopore size in multipore membrane was not calculated from the conductance. Taking a scanning electron microscopy image is the common method to characterize these nanopores.

**Morphology of Nanopore Openings in Muscovite Mica**

Figure 3-7ABCD shows the FESEM images of the base openings of nanopores in mica membranes that were etched under same condition but for a different number of total etch cycles. As per our prior work, the rhomboidal shape opening was characterized by the length of their long and short diagonals.[29] The minor angle θ is about 60°, which is close to the reported value.[141] Larger pores were obtained when the mica membranes were etched for more cycles. The length of diagonal of rhomboidal opening was almost proportional to the etch time under the same etch condition and the long diagonal reached ~1 μm after 8 cycles of 10-minute etch (shown in Figure 3-7D).

There was only one side of the mica membrane was exposed to the 10 M HF etchant, and HF was neutralized by 10 M NaOH on the other side. It was presumed to have a HF transmembrane concentration gradient where the concentration was lower at the tip and higher at the base. We predicted that the nanopore openings facing the NaOH solution were smaller and the openings facing the HF were larger. Figure 3-7EFGH shows the FESEM images of the tip openings of nanopores on mica membranes that were etched for a different number of total

cycles. Compare images of the base and tip openings in the mica membrane at the same etch cycle, it was found that the base openings were always much larger than those at the tip. It is clearly demonstrated that the nanopores fabricated via such a multi-cycle anisotropic etch method had an asymmetric shape. Since we found that there was EOF in the pore to carry HF to the tip, it is reasonable that we observe that the nanopore tip opening size increased with etching time.

**Asymmetric Nanopore Base and Tip Etch Rate**

The lengths of the nanopore base and tip opening long diagonals after different etch cycles were obtained from FESEM images and converted to equivalent diameter of the mica nanopore via Equation 3-4. Figure 3-8A shows the plot of nanopore base opening equivalent diameter ($d_{Eq-b}$) vs. etch time. It indicates that the base opening equivalent diameter increased almost linearly with etch time. The values are arithmetic averages with standard deviations calculated from three independently prepared mica membranes.

Because the bulk etching rates are anisotropic for different cleavage planes of mica, the radial etching rate of equivalent circular opening was used; in this case, it was about 4.0 nm $min^{-1}$ for mica etched with 10 M HF. As long as we know the etching rate, it is easier to pre-calculate how many 10-minute etch cycles are needed to make asymmetric nanopores of desired base size. Therefore, we can obtain asymmetric nanopores with different base sizes by varying the etching time. Figure 3-8B shows that the equivalent diameter of the nanopore tip also increased with etching time. This is reasonable because tip was still etched by a low concentration of HF pumped by EOF in the nanopore. The radial etching rate of tip equivalent circular opening was about 0.57 nm $min^{-1}$.

**Geometry of Asymmetric Nanopores**

The geometry of these nanopores was investigated by chemical vapor deposition of carbon into the nanopores and subsequent removal the mica template to expose carbon replicas of the nanopores.[29] Figure 3-9ABCD shows the FESEM images of nanopore replicas which reflected the pyramidal shape of the nanopores etched for different cycles. The length of the nanocones was about 10 μm, as same as the thickness of mica membrane. The width of the nanopore replica base was almost equal to the length of the long diagonal of rhomboidal base opening. These images also proved that the base opening of nanopores increased with longer etch time. The surface morphology of these carbon replicas also indicates that the entire inner surface of the nanopore was extremely smooth.

Instead of using the one-step method similar to the one we used to fabricate conical nanopores in ion-tracked polymer membranes, we would like to use this multi-cycle procedure to etch pyramidally shaped nanopores in mica membranes. In order to demonstrate that the multi-cycle anisotropic etch method is more effective in preparing asymmetrically shaped nanopores in ion-tracked mica membrane, nanopores were fabricated with the multi-cycle etch (8×10 minutes) and the one-step etch (1×80 minutes). The equivalent diameters of base and tip opening of those nanopores obtained from the one-step 80-minutes etch were around 554±10 nm and 195±42 nm, respectively. While the equivalent diameters of base and tip opening of those nanopores fabricated via multi-cycle etch were around 623±38 nm and 89±16 nm, respectively. The base size of the nanopore fabricated by the different etch procedures were not very different, but the tip size of the nanopores obtained via the multi-cycle etch was much smaller than that of the nanopore made via the one-step etch.

All the carbon replicas of these nanopores obtained from the multi-cycle etch showed uniform pyramidal geometry spanning the entire length (Figure 3-9ABCD). However, the carbon

replica of the nanopore obtained from the one-step etch did not show obvious asymmetric shape (shown in Figure 3-9E).

As we hypothesized, the NaOH-HF neutralization region was right outside of the tip and HF was pumped to this region by EOF in the nanopore. At longer etch times, this region might become less efficient at neutralizing the HF. As a result, the concentration of HF at tip increased and larger nanopore tips were obtained even though there was NaOH to stop the etching.

Another reason might be that the temperature increased at the tip region so that the etch rate increased as well. We think there might be two factors that contribute to the temperature increase at the tip region. The first reason might be the resistive heat generated at tip because we know there was a very high electric field strength focused around the tip in the asymmetric nanopore.[62] The other reason was the heat generated from acid-base neutralization reaction.

In the one-step 80-minute etch, the heat accumulated at the tip and continued increasing the temperature of local environment. As a result, the nanopore tips etch rate increased dramatically when the temperature increased. This temperature effect was extremely significant when the multiple-track mica membrane was etched, especially if the track density is very high. It was found that the solution temperature increased when we etched the mica membrane with track density at ~$10^8$ per $cm^2$. During the multi-cycle etch method, both etchant and stopping solution were replaced. The temperature of solution remained at around at 25 °C during each 10-minute etch cycle. This prevented the temperature increasing dramatically so that the etch process became more controllable.

Besides multipore membranes, the single asymmetric nanopore membranes were also prepared by using multi-cycle anisotropic etch method. In this fabrication process, mica membranes with only one track were used for chemical etch. Because the nanopore size was

small and there was only one in membrane, it was extremely hard to characterize the nanopore size by using electron microscopy. Instead, an electrochemical measurement was used as described previously.[53]

Figure 3-10 shows the current-voltage curves of such single asymmetric nanopore fabricated by using the multi-cycle method and one-step method, respectively. The overall etch time for both mica membranes were the same (80 minutes) so that we could assume the same equivalent diameter of the base openings for both membranes ($d_{Eq\text{-}b} \approx 640$ nm). From the slope of the current-voltage curves, we could calculate the equivalent diameter of tip opening using Equation 3-5. The calculations showed that the multi-cycle etch method made an asymmetric nanopore with a tip equivalent diameter of 62 nm. The one-step method gave a much larger tip equivalent diameter of 155 nm if we assumed that each has the same base equivalent diameter of 640 nm.

Both the SEM images of multi-pore membranes and current-voltage curves of single pore membranes indicated that a multi-cycle approach is more useful for preparing asymmetric nanopores in ion-tracked mica membrane. In this study, we investigated the multi-cycle anisotropic chemical etch with each cycle at 10 minutes. It was shown that the multi-cycle etch process offers better control for fabrication of asymmetric nanopore in mica than the one-step method. We wonder whether an etch cycle with shorter time window will offer even better control over nanopore geometry. However, because the nanopore etching, stopping and rinsing process is rather cumbersome, a short cycle time but with more number of cycles is impractical. Shorter cycle duration definitely requires a higher cycle count to make the nanopore base opening large enough. Considering this, the 10-minute etch cycle is desirable because both

efficiency and control of the process are optimized. In all other research about changing the parameters for mica etch, we always used 10-minute time window for one etch cycle.

Beside the duration for each etch cycle, several other parameters were investigated to optimize the etch conditions, including etchant concentration and trans-membrane potential.

**Effect of etchant concentration on nanopore geometry**

To reduce the time required for fabricating these asymmetric nanopores in ion-tracked mica membrane, a large bulk-etching rate is desirable. It is estimated that a higher concentration of etchant would produce a higher bulk-etching rate, which results in a larger base opening at the same total etching time. Different concentrations of etching solution (5 M, 10 M, 25 M) HF were evaluated when keeping the same concentration of stopping solution 10 M NaOH. As anticipated, base opening long diagonal of 487±10 nm and 1029±62 nm were observed after eight 10-minute cycles etched via 5 M HF and 10 M HF, respectively. In both cases, small nanopore tips were obtained. The SEM images of nanopore replicas demonstrate that a uniform pyramidal geometry spanned the entire replica from tip to base (Figure 3-11AB). Thus, when using 5 M and 10 M HF as etchant, 10 M NaOH could effectively stop the HF etching of mica.

However, increasing the etchant concentration even higher to 25 M HF greatly reduced the effectiveness of the 10 M NaOH stopping. It was found that carbon replica with ~1.2 μm base long diagonal and ~200 nm tip long diagonal was obtained from a nanopore chemically etched in 25 M HF for only two 10-minute cycles. It was observed that the asymmetric geometry only existed at the region a few micrometers from the tip end. The remaining nanopore appeared to have a more constant cross-sectional area (Figure 3-11C). So it is estimated that much larger tip and base will be obtained if the mica membrane is etched for eight 10-minute cycles with 25 M HF. In conclusion, at least 1:1 ratio of stopping solution to etchant concentration is required to make the nanopore have a uniform asymmetric geometry.

**Effect of applied voltage on nanopore geometry**

As per our prior work, we have shown that transmembrane potential applied during etching ion-tracked polycarbonate membrane had an effect on the size of conical nanopore base opening.[62] The effect of transmembrane potential on mica membrane etching was also investigated in this case. The ion-tracked mica membranes were etched by 10 M HF with 10 M NaOH as the stopping solution for eight 10-minute cycles, but under different potential biases (0.0 V, 2.5 V, 5.0 V, 10.0 V and 50.0 V).

The HF diffused to the tip quickly and HF would keep etching the tip openings if HF was not neutralized by NaOH immediately. Without applying electric field, $OH^-$ could only diffuse to the neutralization region, which is assumed to be located outside the tip of nanopore. Because only a very limited amount of HF is consumed to react with a few $OH^-$ that diffused to the neutralization region, the concentration of HF at tip will not be negligible. Therefore it is reasonable to obtain very large tip openings even with the presence of NaOH stopping solution.

However, mass transfer of $OH^-$ will be much faster if electrophoretical migration is applied by controlling the transmembrane potential. With larger transmembrane potential, a large amount of $OH^-$ was delivered to the neutralization region and consumed much more HF. As a result, the concentration of HF at tip was greatly decreased resulting a much slower etch rate at the tip. It also influenced the concentration gradient of HF across the membrane and the nanopore etched in various ways will have different geometries. Figure 3-12A is a scheme of showing the effect of applied electric field on the HF concentration gradient in the nanopore. If this is true, the higher potential might benefit the etch and make uniform asymmetrically shaped nanopores.

The experimental results proved this hypothesis. Figure 3-12BCDE shows the FESEM images of carbon replica from the nanopore etched at different applied voltages. The SEM images show that the long diagonal of base and tip opening etched without applying a potential

were 1256±74 nm and 649±31 nm. The tip opening was much larger than that obtained by applying +10 V transmembrane potential during etching. In Figure 3-12B, the carbon replica of nanopores obtained without applying potential showed corresponding geometry with only about 1 μm long asymmetrically shaped segment at the tip opening with the rest having a uniform cross section.

However, the segment of asymmetric shape became longer when an electric field was applied. When the applied voltage was as high as 5 V, most part of the carbon replica showed obvious asymmetric shape. The nanopore replica obtained from 10 V etch had an asymmetric shape along the entire length. It seems that the higher the electric field that was applied, the better cone shape that was obtained, at least when the voltage was lower than 10 V.

Although we demonstrated that larger base openings could be obtained by using higher potential differences in our prior research with polycarbonate membranes,[62] however, it is not always the case that better asymmetric nanopore shape could be obtained when higher potentials were employed during the etching process. In the case of an applied transmembrane potential of +50 V, the resistive heating generated from high ionic current made the etching too fast to stop. Thus, the entire mica membrane dissolved during the third 10-minute etching cycle. It is obviously that transmembrane potential needs to be well-controlled during anisotropic etching for preparing asymmetrically shaped nanopores in mica membrane.

**Fabrication of Single Pyramidal Nanopore in Muscovite Mica**

Single pyramidally shaped nanopore mica membranes were fabricated under the same experimental condition used for etching multi-track mica. After each 10-minutes etch cycle, the current-voltage curves were measured by filling the nanopore with pH 7.0 100 mM phosphate buffer solution that was 1 M KCl (Figure 3-13A). The equivalent diameter of base opening could be calculated by using the mica equivalent bulk etching rate and total etching time. The tip

equivalent diameter after each etch cycle could then be calculated from the conductance of the nanopore according to Equation 3-5.

It is observed that the current-voltage curves are not linear for these single asymmetric nanopore in mica. The non-linearity ion-current rectification phenomenon has been discussed in detail in the literature.[24, 32, 57, 74, 75] Since the surface of mica nanopore is negatively charged,[141] the electrical double layer on the nanopore could make the nanopore cation permselective and demonstrate a “on” and “off” state when a transmembrane voltage is applied.

The ionic current rectification also changes with the ionic strength of the supporting electrolyte.[32, 57] Current-voltage curves of a single asymmetric nanopore in mica membrane after different etch cycles were measured when nanopore was filled with pH 7.0 10 mM phosphate buffer solution that was 10 mM KCl (Figure 3-13B). It is interesting that a very strong ion current rectification was observed in such single asymmetric nanopore embedded in mica membrane at low ionic strength solution. The ionic current value measured when a -1 V potential was applied on the base opening increased with more etching cycles. Interestingly, the ionic current was still strongly rectified in low ionic strength solution when a +1 V potential was applied on the base side of the membrane.

We previously defined the degree of rectification as a ratio of absolute value of ion current recorded at a given negative voltage to the same absolute value at a positive voltage.[57, 119] Figure 3-13C indicates that the ion-current rectification ratio of a single asymmetrically shaped nanopore in mica increased with longer etching time (larger base opening) in pH 7.0 10 mM phosphate buffer solution that was also 10 mM KCl. It was also observed that the rectification ratio was small in the high ionic strength electrolyte solution (1 M KCl). The ion current

rectification is not significant when the electrical double layer thickness is much smaller than the pore size.

It also seems that the ion current rectification phenomenon is closely related with the pore geometry. When the base size was also very small, anions were also excluded outside of the pore so that anions could not accumulate in the tip region. As a result, the ion current was not heavily rectified. When pore base size increased, the ion current rectification became more significant as long as the tip was not too large.

We also compared the ionic current rectification of asymmetrically shaped single nanopores in mica and PET membranes with similar base (~640 nm) and tip (~60 nm) size. Current-voltage curves in Figure 3-14A indicates that the nanopore in mica membrane and the one in PET membrane had the similar tip size if calculated from the conduce of nanopore filled with 1 M KCl, pH 7.0 100 mM phosphate buffer solution. The current-voltage curve of nanopore in PET was linear and the one from mica only showed a little ion current rectification. However, a much larger ion current rectification was observed from the nanopore in mica membrane than the one in PET in a low ionic strength solution (10 mM KCl, pH 7.0 10 mM phosphate buffer). The current-voltage curve was still almost linear for nanopore in PET even in 10 mM KCl pH 7.0 10 mM phosphate buffer. However, a strong ionic current rectification was observed from the nanopore in mica at such low ionic strength. We hypothesized that the larger ionic current rectification might be due to the fact that the surface charge density of nanopore in mica (~2.1 e $nm^{-2}$)[147] is higher than that of a nanopore in PET (~1.0 e $nm^{-2}$)[148].

To test the above hypothesis and explore the reason why an asymmetrically shaped nanopore in mica has a very high ionic current rectification ratio at low ionic strength solution, surface charges were removed from the mica via modification the substrate with

glycidoxypropyltrimethoxysilane (GPTMS) followed by treating with β-mercaptoethanol to produce hydroxyl-terminated group.[145, 146] Current-voltage curves in Figure 3-15A indicate that the nanopore size had no significant change prior to and after the surface modification because the nanopore conductance were almost the same. However, the current-voltage curves in Figure 3-15B show that the ionic current was much less rectified after the surface modified with hydroxyl group. The ionic current rectification decrease was probably because some surface charges were removed because the hydroxyl group was neutral and surface charge density decreased after the modification. This result could also be used to explain why the bare nanopore in mica has stronger ionic current rectification than bare nanopore in PET because PET has lower surface charge density.

## Conclusions

In this work, we developed a multi-cycle anisotropic chemical etch method to prepare pyramidally shaped nanopores in ion-track muscovite mica membranes. The effect of etchant concentration, transmembrane potential, and etching cycle number on nanopore size and geometry were investigated in detail. The nanopore dimensions and geometry in multipore mica were confirmed by SEM images of bare nanopore membranes and carbon replicas of nanopores. The electrochemical measurement and calculation of single nanopore size in mica were discussed as well. The ion transport properties of single pyramidal nanopore in mica membrane were also studied and ionic current was highly rectified in low ionic strength electrolyte solution. We think this very strong ion current rectification is because the highly negatively charged surface caused a large difference between the transference number of cations and anions. By modifying the nanopore wall with an uncharged surface functional group, surface charge density decreased. As a result, the pyramidally shaped nanopore demonstrated much less ion current rectification.

We think this extremely high ionic current rectification properties usually not seen in nanopore on polymer membrane might be promising for exploring applications in resistive-pulse sensing or analyte separation.

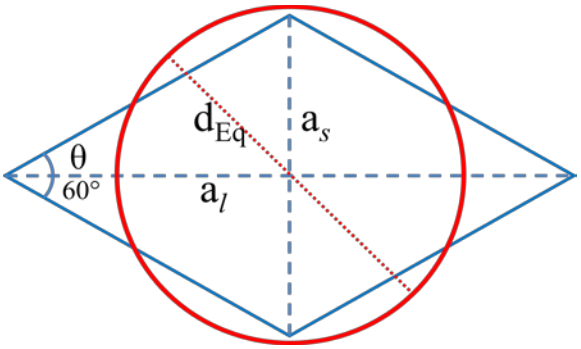


Figure 3-1. The relationship between a rhomboidal opening and an equivalent circular opening.

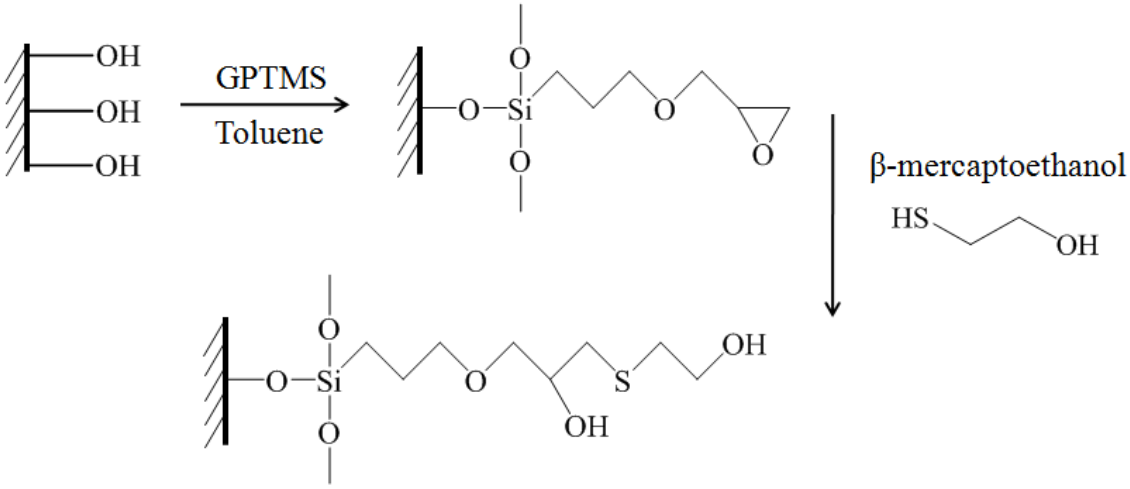


Figure 3-2. Schematic of modification GPTMS on muscovite mica to produce hydroxyl-terminated surface groups.

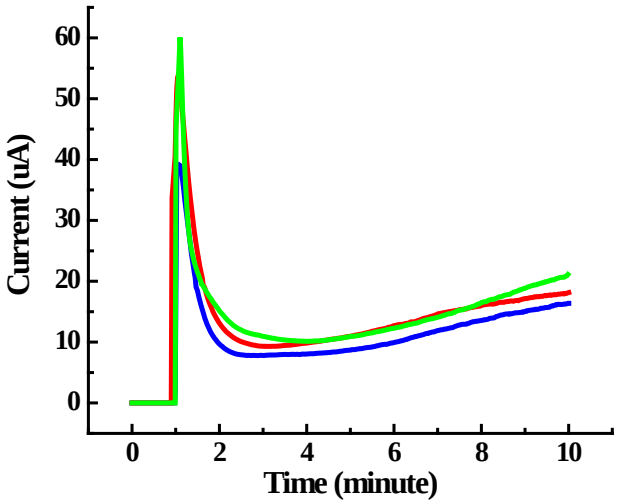


Figure 3-3. Current-time traces of the anisotropic etching of multi-track muscovite mica membranes. Etching solution was 10 M HF and stopping solution was 10 M NaOH. Data shown here were taken from the first 10-minute etch cycle, track density $10^5$ tracks per $cm^2$.

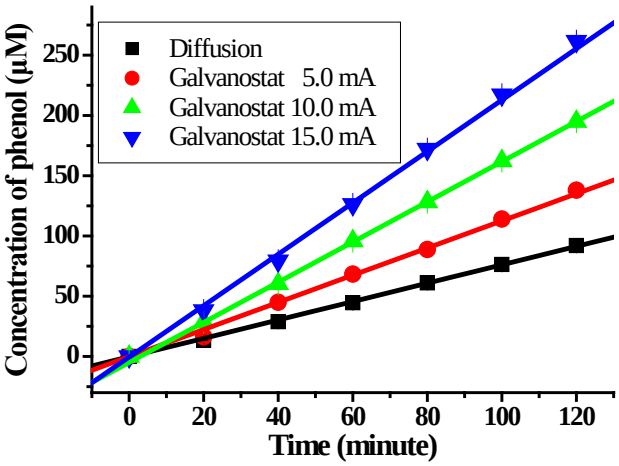


Figure 3-4. Concentration of phenol in the permeate solution at different time when it was transported from base to tip in the nanopore. There were constant current across the membrane with current of (red) 0.5 mA, (green) 1.0 mA, (blue) 1.5 mA and (black) without current.

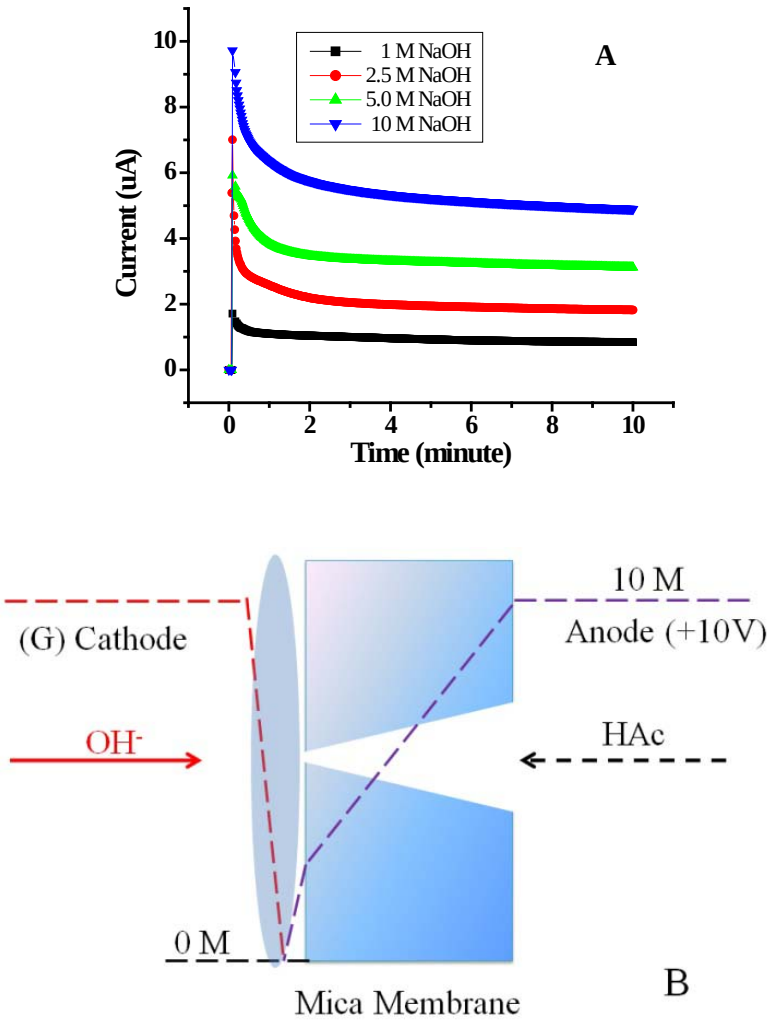


Figure 3-5. Current-time traces during the HAc and NaOH neutralization and the schematic of eletrolyte concentration profile. A) Current-time traces during HAc-NaOH neutralization in asymmetric multipore ($10^5$ $cm^{-2}$) mica membrane that was etched for one 10-minute cycle). B) Schematic of acid (HAc) and base (NaOH) concentration profile during the neutralization.

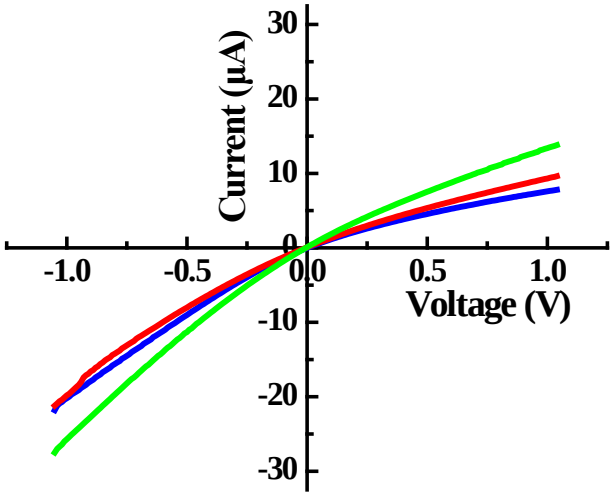


Figure 3-6. Current-voltage curves of multi-track mica membranes that were anisotropically etched for one 10-minute cycle. Track density was about $10^5$ tracks per $cm^2$ and current-voltage curves were measured in 100 mM phosphate buffer at pH 7.0 with 1 M KCl.

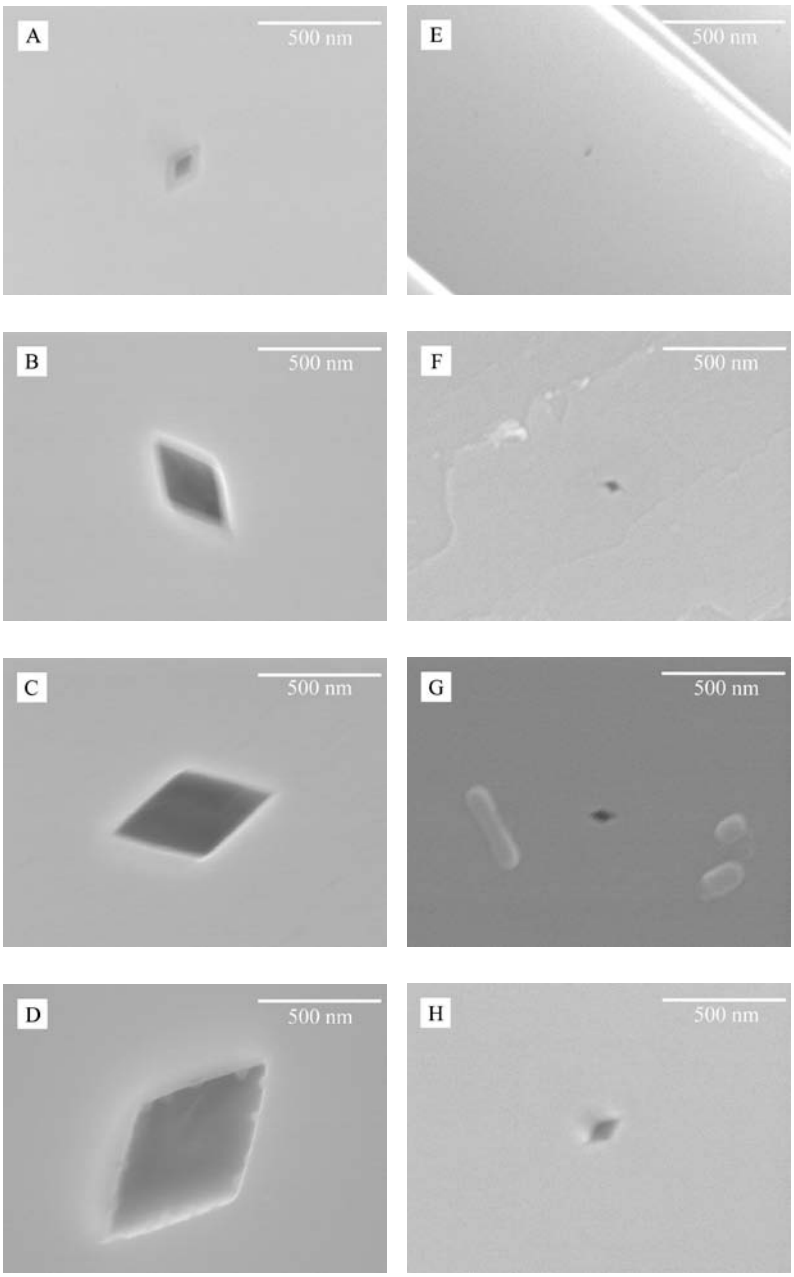


Figure 3-7. FESEM images of the base and tip openings of asymmetric nanopores in muscovite mica membranes at different etching time. ABCD) Base opening etched for 2×10, 4×10, 6×10, 8×10 minutes, respectively. EFGH) Tip opening etched for 2×10, 4×10, 6×10, 8×10 minutes, respectively.

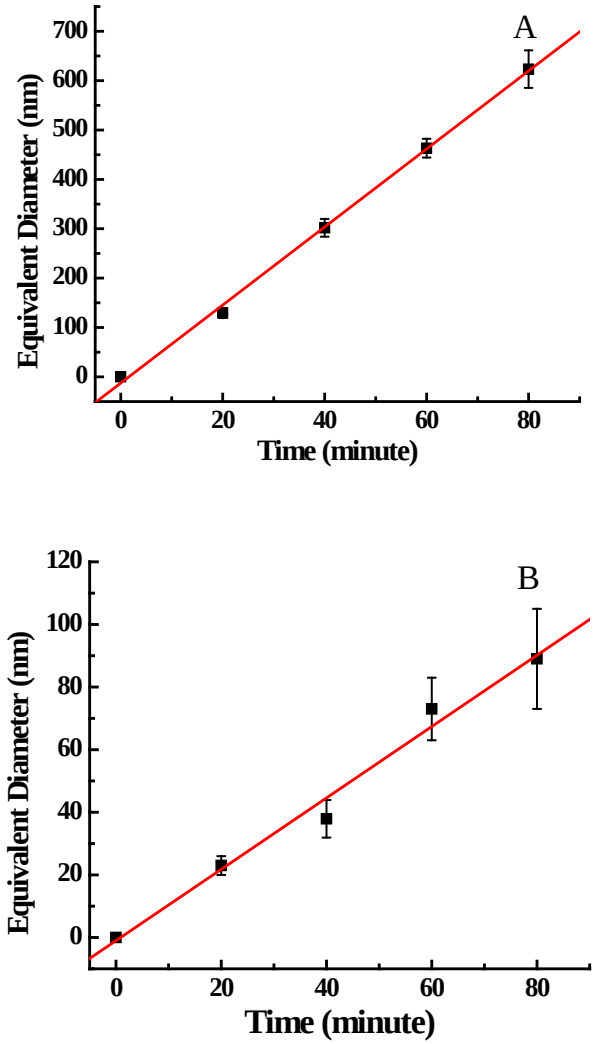


Figure 3-8. Calibration of equivalent diameters of the base and tip openings of the pyramidally shaped nanopores that were anisotropic etched for different time. A) Base openings. B) Tip openings. Equivalent diameter was calculated from the length of long diagonal obtained via FESEM images.

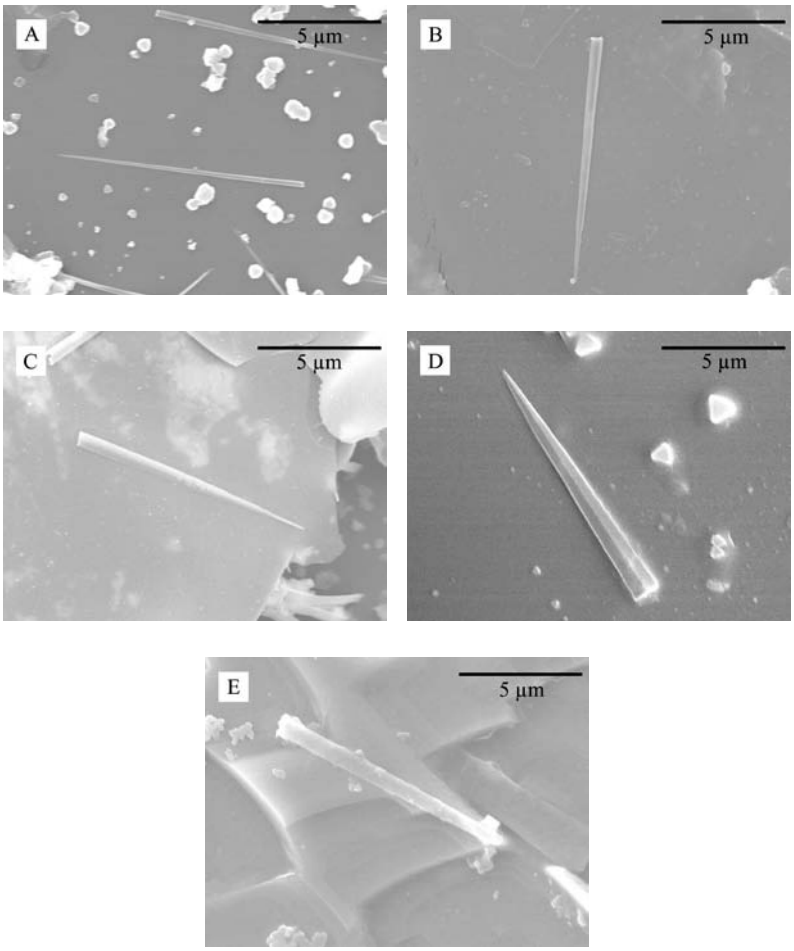


Figure 3-9. FESEM images of carbon replica of pyramidal nanopores in muscovite mica that were anisotropic etched for different time. A) 2×10 minutes. B) 4×10 minutes. C) 6×10 minutes. D) 8×10 minutes with applied transmembrane voltage at 10 V. E) 1×80 minutes without applied voltage.

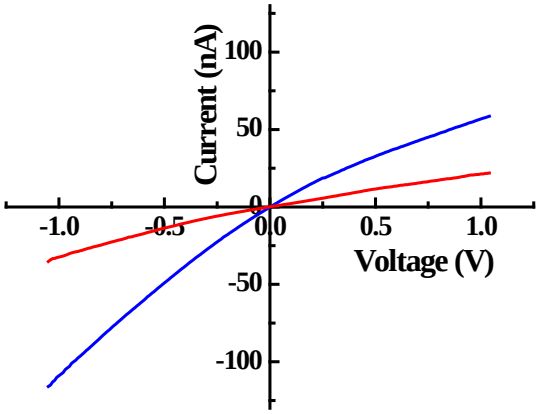


Figure 3-10. Current-voltage curves for single nanopore in mica membrane prepared by multi-cycle and one-step methods. (Red) 8×10 minutes anisotropic etching. (Blue) 1×80 minutes anisotropic etching. IV curves were measured in 1 M KCl, pH 7.0 100 mM phosphate buffer solution.

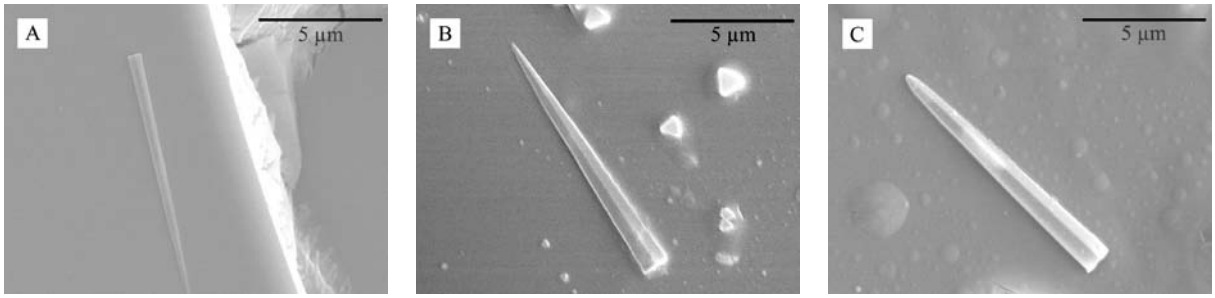


Figure 3-11. FESEM images of carbon replica of pyramidal nanopores in muscovite mica that were anisotropic etched with different concentration of HF. Transmembrane voltage was 10 V. A) 5 M HF etched for eight 10-minute cycles. B) 10 M HF etched for eight 10-minute cycles. C) 25 M HF etched for two 10-minute cycles.

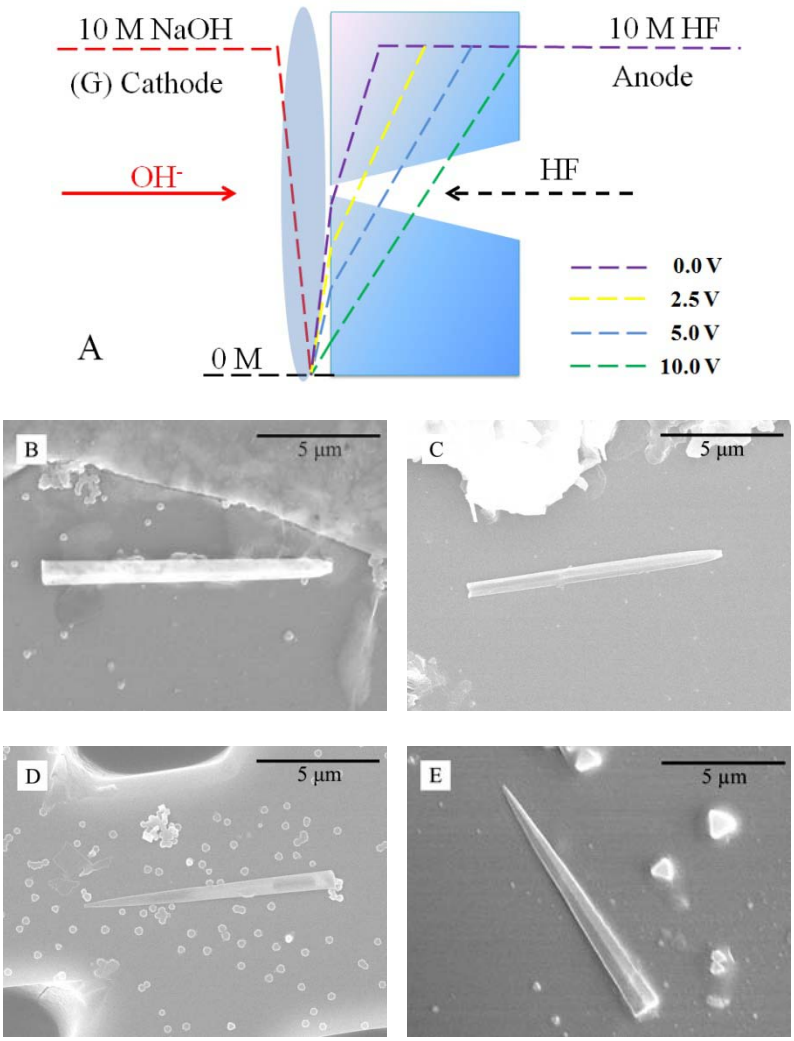


Figure 3-12. Schematic of voltage effect on HF concentration profile and FESEM images of carbon replica of asymmetric nanopores. A) Schematic of voltage effect on HF concentration profile. BCDE) FESEM images of carbon replica of asymmetric nanopores fabricated in muscovite mica via anisotropic etching with 10 M HF at different applied voltages B) 0 V. C) 2.5 V. D) 5.0 V. E) 10.0 V for eight 10-minute cycles.

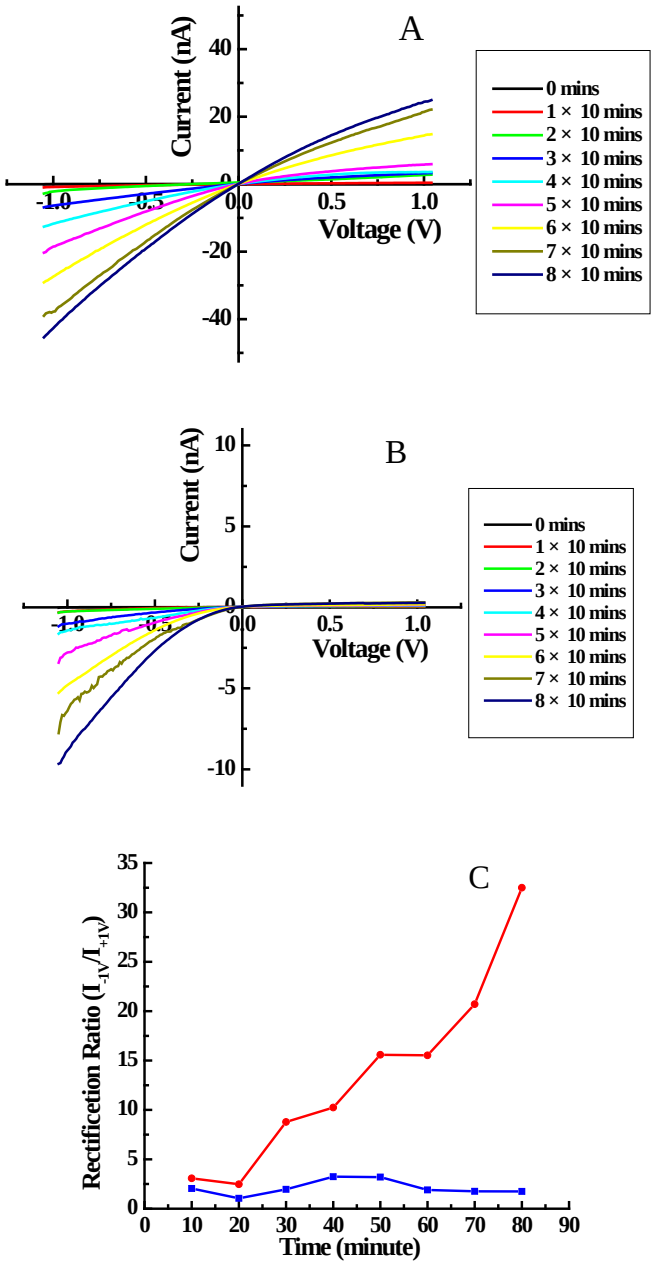


Figure 3-13. Current-voltage curves of single pyramidal nanopore in mica membrane in different salt concentration solutions and resulting ion current rectification ratio. A) IV-curves measured in pH 7.0 100 mM phosphate buffer with 1 M KCl. B) IV-curves measured in pH 7.0 10 mM phosphate buffer with 10 mM KCl. C) Ion current rectification of single pyramidal nanopore in mica membrane measured in 1 M KCl, 100 mM phosphate buffer (blue) and 10 mM KCl, 10 mM phosphate buffer (red).

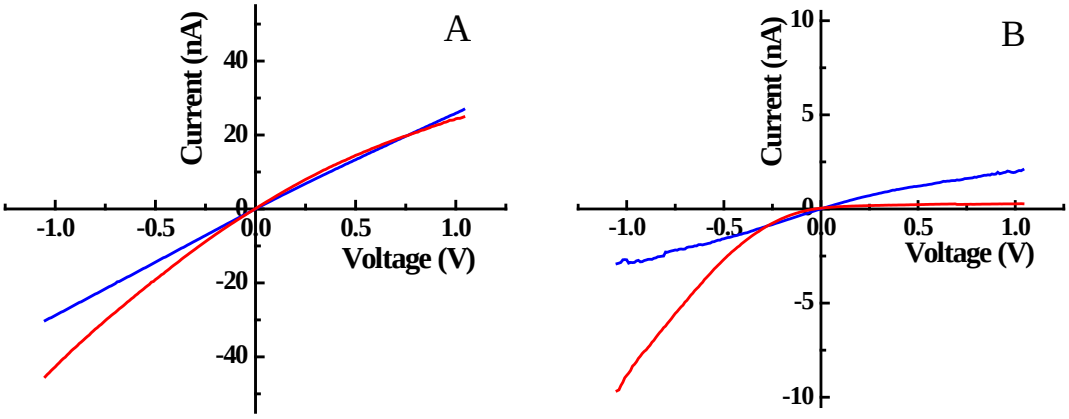


Figure 3-14. Current-voltage curves of single asymmetric nanopore in PET and mica membrane. (Blue) Nanopore in PET (Red) Nanopore in mica. IV curves were measured in A) 1 M KCl, 100 mM phosphate buffer pH 7.0, B) 10 mM KCl, 10 mM phosphate buffer pH 7.0.

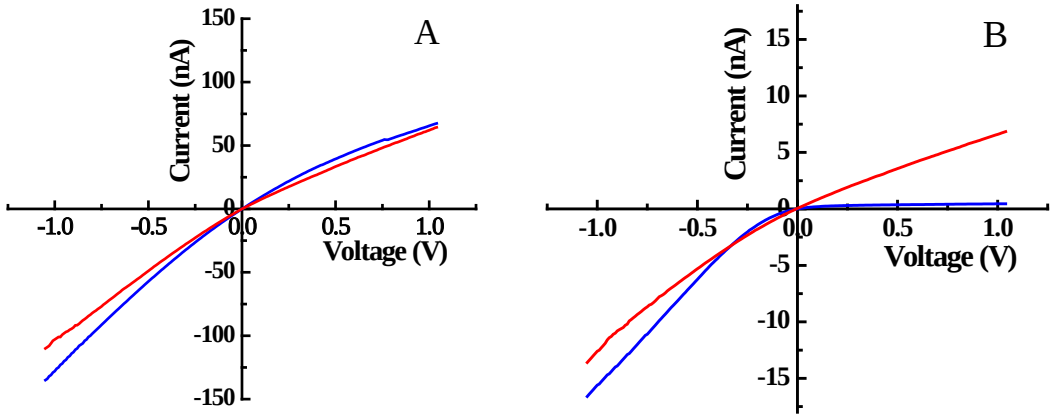


Figure 3-15. Current-Voltage curves of a single asymmetric nanopore mica membrane before and after the surface modification with hydroxyl-terminated groups. (Blue) Before and (red) after the surface modification. IV curves were measured in A) 1 M KCl, 100 mM phosphate buffer pH 7.0, B) 10 mM KCl, 10 mM phosphate buffer pH 7.0.

# CHAPTER 4
# RESISTIVE-PULSE DETECTION OF NANOPARTICLES USING A SINGLE PYRAMIDAL NANOPORE IN MICA MEMBRANES

## Introduction

Single conically shaped nanopores embedded in polymer membranes are usually used for resistive-pulse detection and ion current rectification studies. The conventional resistive-pulse signal is caused by temporary pore blocking by analyte and resulting resistance change. Recently, the ion current rectification in asymmetric nanopore has been well investigated and employed for sensing applications.[58, 119, 139, 140, 149] This type of sensing paradigm is based on the changes of the single conical nanopore wall local surface charge[150] induced by binding or adsorption of an analyte. The analyte binding was detected as a change of the ion current rectification of single conical nanopores. The quantity of the analyte in the solution can be correlated with the degree of ion current rectification.

Martin group has employed using single conical nanopore in Kapton membrane detecting drug molecules[119] and other small organic molecules.[151] The single conical nanopore demonstrated a strong ion current rectification phenomenon and ion current rectification ratio is large. After exposure of the anionic charged nanopore to the cationic drug molecules, the extent of ion current rectification changed. Such a change was due to the adsorption of cationic drug molecules on the pore wall and changing the surface charge density or even charge polarity.[119] It was found that the magnitude of the ion current rectification change was correlated with the concentration of drug molecules.

However, this type of sensing based on the ion current rectification change could only obtain the overall information of the analyte in the solution. It is difficult to measure the individual analyte interacting with the pore wall and passing through nanopore to achieve single analyte detection signal. A new resistive-pulse mechanism is proposed in this research to achieve

single analyte detection. A coating molecule is introduced to modulate the ion current rectification in single pyramidally shaped nanopore in mica. A model analyte, poly(styrene) (PS) latex nanoparticles, was driven electrophoretically through the nanopore. It is hypothesized that the nanoparticles will interact with the coating molecule resulting in a temporary surface charge inversion and generates resistive pulse events.

The local charge inversion affecting the ion current rectification in asymmetric nanopore is a well known phenomenon.[150] According to our proposed mechanism, in the 10 mM KCl and 10 mM phosphate pH 7.0 buffer solution, the current-voltage curve will have the shape as the blue curve as shown in Figure 4-1A. The steady state current flowing through the nanopore with working electrode voltage of +1 V is small, showing an "Off" state. However, if the nanopore is exposed to the coating reagent, the positively charged coating reagent will adsorb on the negatively charged mica pore wall and decrease the anionic charge density or even reverse the charge polarity. Therefore, the current-voltage curve will have the shape as the red curve as shown in Figure 4-1A. The steady state current flowing through the nanopore with working electrode voltage of +1 V is larger, showing an "On" state. The negatively charged nanoparticle at the tip side of the membrane will be electrophoretically driven into the nanopore tip. Because of the electrostatic attraction between the surface negatively charged particle and the positively charge coating reagent, the local surface charge might change momentarily. Correspondingly, the ionic current might temporarily change from the "on" state to the "off" state so that a current drop will occur. However, the local surface charge will change back to its original condition after the nanoparticle moves out of the tip region. The ionic current will recover to the "on" state. Thus a complete current pulse event will be observed when a single nanoparticle passes through the nanopore from tip to base.

## Experimental

### Materials

Bisbenzimide (Hoechst 33258) was obtained from Sigma-Aldrich (St. Louis, MO). Sulfate modified poly(styrene) latex (PS) particles were obtained from Invitrogen (Carlsbad, CA).

### Fabrication and Characterization of Single Pyramidal Shaped Nanopore in Mica

The fabrication of single pyramidal nanopore in mica is described in chapter 3. Briefly, a single tracked muscovite mica membrane was mounted between two half electrochemical cells as described before.[53] An etching solution that is 10 M HF was placed in one cell, and a stopping solution that is 10 M NaOH was added into the other cell. A Pt electrode was placed in both of the cells. A transmembrane voltage of 10 V was applied with the cathode in the stopping solution. The chemical etch was terminated at 10 minutes and the solutions in both cells were replaced with 10 M NaOH stopping solution. The membrane was etched for totally eight 10-minute etch cycles.

The current-voltage curve was measured to calculate the nanopore tip size. An electrolyte solution that was 1 M KCl and 100 mM phosphate buffer at pH 7.0 was added to both half electrochemical cells. The voltage was scanned form -1 V to +1 V at 1 $Vmin^{-1}$ with working electrode at the nanopore large opening side (base). The length of major axis of base opening was calculated with the etch rate and equivalent diameter of base was obtained from via,

$$d_{Eq-base} = 0.606\, a_l \tag{4-1}$$

The single pore small opening (tip) equivalent diameter ($d_{Eq\text{-}tip}$) can be calculated from the pore conductance via,

$$G = \frac{\pi d_{Eq-base}\, d_{Eq-tip}}{4L} \tag{4-2}$$

In this research, the pyramidal nanopore base equivalent diameter $d_{Eq\text{-}base}$ is ~ 640 nm and the tip equivalent diameter $d_{Eq\text{-}tip}$ ~85 nm.

**Characterization of Poly(styrene) Nanoparticles**

The sulfate modified poly(styrene) latex particles with diameter of 29 nm were characterized in the presence of the coating molecule, Hoechst 33258, before used as model analyte. Suspensions contained 50 nM of PS particles with different concentration of Hoechst 33258, were prepared. Brookhaven ZetaPlus was used to measure the size distribution and the zeta potential of PS particles in the suspension. Suspensions contained 50 nM of PS particles with different concentration of HATC were prepared and used for size distribution and zeta potential measurement as well.

**Current-Voltage Curves Measurement in the Presence of Coating Reagents**

A current-voltage curve of a single pyramidal nanopore in mica was first measured in the solution of 10 mM KCl and 10 mM phosphate buffer at pH 7.0 without Hoechst 33258. The current-voltage curves were also measured when the buffer contained 15 μM coating reagent, Hoechst 33258.

**Resistive-Pulse Detection of Poly(styrene) Nanoparticles**

A mica membrane contained a single pyramidal nanopore was mounted between the two half electrochemical cells. A supporting electrolyte solution was added to both sides of the membrane. In these series experiments, there were two types of supporting electrolyte solutions used. The first type of solution was a phosphate buffer solution at pH 7.0 with 10 mM KCl. The second solution was the first type solution also contained 15 μM Hoechst 33258. A Ag/AgCl electrode was placed in each solution. The ionic current flowing through the single nanopore full of electrolyte solution was measured with an Axopatch 200B current amplifier (Molecular Devices Corporation, Union City, CA) in the voltage-clamp mode with a low-pass Bessel filter at

2 kHz bandwidth. The signal was digitized using a Digidata 1233A analog-to-digital converter (Molecular Devices Corporation). Data were recorded and analyzed with pClamp 9.0 software (Molecular Devices Corporation). The current data was recorded every 10 μs and the time window was 1 minute. A background steady state current was measured without adding model analyte PS particles. At least 5 minutes of data were recorded for each experimental condition.

During the PS particles translocation experiment, the solution at one side of the membrane was replaced with the same buffer solution but also containing 50 nM PS particles. The working electrode was placed on the side facing the base opening and the reference electrode was in the solution facing the nanopore tip opening.

In the case of transporting PS particles through the nanopore from tip to base, a +1 V voltage was applied on the working electrode so that the electrode facing the tip was cathode. However, a -1 V voltage was applied on the working electrode when PS particles were transported from base to tip so that the electrode facing the base was cathode. In the control experiments, a similar approach was used. The only difference was using symmetric nanopore in mica.

## Results and Discussion

A new mechanism was proposed to increase resistive-pulse detection sensitivity and signal intensity by using a coating reagent, Hoechst 33258. Other control experiment was performed to further study the hypothesized mechanism, such as transport PS through the nanopore from different direction, changing nanopore geometry, and nanopore materials.

### Characterization of Poly(styrene) Nanoparticles

As we known, the negatively charged PS nanoparticles will interact with the positively charged coating reagent, e.g., Hoechst 33258,[119] in the suspension and result in aggregation or even precipitation of nanoparticles. Since we are trying to detect the resistive-pulse signal of

single nanoparticle translocation through the nanopore, it is extremely important to prove that the PS nanoparticles are monodispersed in the suspension with the presence of coating reagent. The dynamic light scattering measurement showed that the mean diameter of the PS nanoparticle is about 26.7 nm in the presence of 15 μM Hoechst 33258, which is close to the diameter reported by the manufacture. The size distribution of PS nanoparticle in this solution is shown in Figure 4-2. The zeta potential measurement shows that the zeta potential of PS nanoparticles surface is about -52.15 mV, which means that particle surface is still negatively charged in solution even with the presence of 15 μM of Hoechst 33258. The above studies demonstrated that the PS nanoparticles were negatively charged and monodispersed in the solution used in the resistive-pulse detection.

**Current-Voltage Curves of Nanopore in the Presence of Coating Reagents.**

The current-voltage curve of single pyramidal nanopore in mica shows strong ion current rectification in 10 mM phosphate buffer at pH 7.0 with 10 mM KCl. A larger current was observed when negative voltage is applied and a smaller current value was obtained at the positive electrode polarity (Figure 4-3). However, much less ion current rectification was observed when the coating reagent 15 μM Hoechst 33258 was in the presence (shown in Figure 4-3). The current value at positive voltage increased and the absolute current value at negative voltage decreased after nanopore was exposed to the solution contained coating reagent Hoechst 33258. In this case, it was observed that the direction of current-voltage curve reversed because the absolute current was lower at a negative voltage and the absolute current was higher at a positive voltage. This phenomenon is well known to be related with the asymmetric nanopore local charge inversion.[150] The current-voltage curve of single pyramidal nanopore in mica also showed such ion current rectification change phenomenon when positively charged coating reagent was added to the solution (shown in Figure 4-3).

**Resistive-Pulse Detection of Poly(styrene) Nanoparticles**

**Resistive-pulse detection of nanoparticles with conventional mechanism**

A conventional resistive-pulse method was used to detect the translocation of PS nanoparticles through a single pyramidal nanopore in mica membrane. The single pyramidal nanopore had a tip equivalent diameter ($d_{Eq\text{-}tip}$) ~ 85 nm and base equivalent diameter ($d_{Eq\text{-}base}$) ~ 640 nm. The steady state current of the background without the PS nanoparticles was about 380 pA when the nanopore was filled with pH 7.0 phosphate buffer with 10 mM KCl. The baseline current was also about 350 pA when the nanoparticles were present in the feed solution. Only a single event was observed and the amplitude of this event was small and comparable to the noise level (Figure 4-4). We think that there are two possibilities that might prevent large amplitude pulse events occurred. One possibility is that the negatively charged PS nanoparticle did not enter the also highly negatively charged mica[147] nanopore tip because of electrostatic repulsion. The other reason might be the charges carried by the particle, including the charges on the PS nanoparticle and the counter-ions, is almost equal to the charges in the solution which is replaced by the particle. Therefore, no current pulse was observed even though the particles did enter the nanopore tip. It seems that the conventional resistive-pulse detection is not very sensitive for detecting the nanoparticles in this case.

**Resistive-pulse detection of nanoparticles involving coating reagent**

The steady state current of the nanopore filled with 10 mM phosphate buffer at pH 7.0 with 10 mM KCl and 15 μM Hoechst at +1 V was about 1400 pA (Figure 4-5). This steady state background current value was comparable to the current value at +1 V when the current-voltage curve was measured. Because there was a dynamic equilibrium of Hoechst 33258 adsorption/desorption on the pore wall and the ion current was sensitively affected by this equilibrium process, the background current fluctuated a little.

When the nanopore was exposed to the same buffer but also contained 50 nM PS nanoparticles, the steady state current decreased to about 1000 pA. Such steady state current decrease might because the presence of nanoparticle partially decreased the concentration of free Hoechst 33258 in the solution, resulted in a baseline ion current change. More interesting, when 50 nM PS nanoparticles was present, a large amount of current pulses were observed. The current pulses amplitude were much larger than those obtained without using coating reagent.

In most of the conventional resistive-pulse experiment, the current pulses are downward signals, which mean the absolute current value decrease when such pulses occur. In the case of transporting PS nanoparticles from tip to base, similar downward current pulse signals were also observed. We hypothesize that such large current pulses were generated because of a newly proposed mechanism, instead of the conventional mechanism. An experiment of transporting PS nanoparticles from base to tip was designed to validate this mechanism.

**Validation of the hypothesized resistive-pulse detection mechanism involving coating reagent**

As discussed above, the current-voltage curves inversed after the nanopore was exposed to the coating reagent Hoechst 33258. When the negatively charged PS nanoparticles were placed on the base side of the membrane, a -1 V voltage was applied so that PS nanoparticles were driven electrophoretically from base to tip. As shown in Figure 4-1B, the steady state current is larger when the supporting electrolyte solution does not contain the coating reagent and it is defined as “on” state. However, the steady state current is much lower when nanopore is exposed to the coating reagent and this is defined as “off” state. When the nanoparticle enter the nanopore from the base, negatively charged PS particle will interact with the positively charged coating molecule, causing a nanopore surface charge change. Therefore, the ion current will temporarily increase from the “off” state to “on” state. But the ion current will change back to “off” state

when the nanoparticle move out of the sensing zone. Thus a current pulse will be observed when a nanoparticle passes through the nanopore tip. Especially, the current pulse event is a current enhance signal, instead of absolute current value drop as the conventional signal.

The experiment data confirmed our prediction about the current pulse direction, as shown in Figure 4-6. The background current was about -250 pA because of the adsorption of Hoechst 33258 on the pore wall. When the PS particles were present, the baseline current increased to -450 pA and a large amount of current pulses were observed. Interestingly, these current pulses were current enhancement signals, the same as we predicted according to the proposed mechanism. If the signal were produced according to the conventional mechanism, the current pulse signal would either only increase or decrease from the baseline current no matter which direction the analyte was driven into the nanopore. But according to our proposed mechanism, the pulse event current decrease when nanoparticle moved from tip to base and the pulse event enhanced the current when nanoparticle moved from base to tip. Importantly, our experiments proved that the hypothesis about the local charge inversion induced current pulses is correct.

**Current pulse shape**

According to the proposed mechanism, the directions of the current pulse are different when the nanoparticles are transported from the opposite directions. More interestingly, the experimental data demonstrated that the current pulse shapes were quite different in these two cases and we believe the pulse shapes were related with the nanopore pyramidal geometry.

When the PS nanoparticle was driven into the nanopore and moved from tip to base by electrical field, the nanoparticle first entered the tip region, where has the narrowest entrance and is most sensitive to the resistance change. Especially, the negatively charged nanoparticle had the greatest chance to interact with the coating reagent that adsorbs on the pore wall, causing the largest extent of local charge inversion. Thus, it was expected a large current value change when

the nanoparticle first entered the tip region (as shown Figure 4-7A). When the nanoparticle entered the pore tip region and started to move forward, the impact of particle on the local surface change decreased because the cross section of nanopore increased along the axis direction. As a result, the nanoparticle had less effect on ion current when the particles were in the pore but far from the tip. Therefore the ion current slowly recovered to the baseline value when the nanoparticle moved from the tip to base with time. As a result, the current pulse in this case had a tale at the end of each pulse.

However, the current pulses had different shapes when the negatively charged PS nanoparticles were driven into the base and moved from base to tip by electrical field. At the beginning, the cross section of nanopore base opening was large so that nanoparticle had no or less effect on the local charge inversion. When the nanoparticle moved into the sensing zone that was in close proximate to the tip, it began interacting with the coating reagent on the pore wall because of being in a confined space. This resulted in a larger extent of local charge inversion. Thus, an ion current started to change gradually corresponding to the local charge change. We think that the greatest ion current change occurred when the nanoparticle was closest to the tip where the cross section of nanopore was smallest. But because the nanoparticle moved in the direction in which nanopore narrowed down, there were increasing chances that nanoparticle collided with the pore wall. These collisions might cause the multi-time nanoparticle adsorption/desorption on the pore wall, and as a result, the current fluctuated as responses. At the end, the current recovered to the baseline value quickly when the nanoparticle left the nanopore from tip (as shown in Figure 4-7B).

**Current pulse amplitude**

One characteristic of the resistive-pulse event is the current pulse amplitude. In the conventional resistive-pulse detection, the pulse amplitudes are supposed to be the same when

analyte moves from different directions of the nanopore. The current pulse amplitude depends on how much charges in the supporting electrolyte solution were replaced by the analyte. However, in the experiments involving the coating reagent will depend on how much the local charges on the pore wall were affected. The current pulse amplitudes depend on how large the difference of steady state current value at the “on” and “off” states.

As shown in Figure 4-3, when the anode (+1 V) was on the base side of the membrane, the absolute current difference between the “on” and “off” state was only about 900 pA at +1 V, which determined the maximum current pulse amplitude. However, there was a much larger absolute current difference between the “on” and “off” states when the anode was on the tip side of the membrane. The maximum difference was about 9000 pA at -1 V, which allowed large pulse signals occurs. It is interesting that the experimental data was coincident with our prediction. The current pulse amplitude (679 ± 179 pA) was larger when the nanoparticle moved from base to tip and the pulse amplitude (302 ± 68 pA) was smaller when they moved from tip to base (as shown in Figure 4-8).

**Current pulse duration**

The other important parameter for the resistive-pulse events is the pulse duration, which might be able to reflect the information about the interaction between analyte and nanopore surface. Generally, the current pulse is longer if the analyte move slower in the sensing zone of nanopore. In our experiment, it was noticed that the average current pulse duration (789 ± 777 ms) when the nanoparticles moved from base to tip was much longer than the duration (22 ± 20 ms) when they moved from tip to base. We think the average pulses duration was short because the nanoparticles had fewer chances to interact with the pore wall and stay less time because the nanopore became wider along the axis. However, the nanoparticle might collide with the nanopore for multiple times when they moved from base to tip and stay longer time because the

nanopore became narrower along the axis. It is reasonable that the longer pulse duration is because of the multiple times collision of nanoparticle on the pore wall.

**Current pulse frequency**

In these experiments, we studied the translocation of 29 nm diameter PS nanoparticles through the asymmetric nanopore with ~85 nm tip and ~640 nm base. When the feed solution was on the tip side, the sensing zone at tip was exposed to the bulk analyte solution. When the feed solution was on the base side, however, the sensing zone was far from the base and exposed to the solution with lower analyte concentration than the bulk because partition problem. This difference might cause the pulse frequency difference when we transported analyte nanoparticles from the different directions. We did observe such difference in our resistive-pulse measurement. It was obtained about 325 ± 22 pulse events on the average when the nanoparticles were transported from tip to base and only an average 28 ± 8 counts when they were transported from the other direction. We think that the collisions between the nanoparticles themselves in the base region also might slow down nanoparticle translocation.

**Control Experiments for Studies of the Hypothesized Sensing Mechanism**

We think there is one key criterion for successful detection of the analyte according to our proposed mechanism, which is that the nanopore need to rectify the ion current and the ion current rectification has to change according to the surface charge conditions. We tried to prove such a criterion by using nanopore with different geometries and different salt concentration supporting electrolyte solution.

As we known, the ion current rectification is widely observed in asymmetric nanopore filled with electrolyte solution, especially when the ionic strength is low.[32, 57] If the sensing experiment was conducted in the solution with high salt concentration where ion current did not rectify, we are not supposed to observe the ion current rectification switch between the “on” and

"off" state after adsorption of coating reagent. However, it was found out that the PS nanoparticles and the coating reagent Hoechst 33258 easily aggregated and precipitated in 100 mM KCl or high concentration solution without adding surfactant to stabilize the monodispersed nanoparticles. Therefore, we were unable to perform such a experiment to prove the mechanism.

We tested the proposed mechanism by using a single straight nanopore, instead of the asymmetric nanopore in mica but still in a low salt concentration solution (10 mM phosphate buffer at 7.0 with 10 mM KCl). It is well known that the straight nanopore with uniform surface charge distribution will not rectify the ion current even in very low ionic strength solution. Therefore the ion current rectification switch did not occur even though the local charge inversed when the coating reagent adsorbed on the pore wall and interacted with nanoparticles. Our experiment with a straight nanopore in mica membrane (equivalent diameter ~ 75 nm) showed that no pulse event was observed. This experiment demonstrated that ion current rectification in asymmetric nanopore is important for such sensing mechanism. However, further investigations about the proposed mechanism are still necessary and the exactly process how the coating reagent interacts with the analyte and affects the current pulse signals are important.

## Conclusions

In this research, a single pyramidal nanopore in mica membrane was used to study the resistive-pulse detection of model analyte. Different from the conventional mechanism, a new signal producing mechanism was proposed. Such mechanism involves the use of a cationic coating reagent to modulate the nanopore surface local charge. The analyte interacted with the coating reagent and temporarily affected the nanopore tip surface charge condition and current pulses with large amplitude were observed. It was observed that there were differences in the current pulse shape, pulse amplitude, pulse duration and pulse frequency when the nanoparticle model analyte was transported from different direction of the nanopore. We believe that the

proposed mechanism is a first step to an alternative means of improving the detection sensitivity and increasing the signal intensity. However, further investigations are necessary to explore and prove the mechanism to improve the sensing effect.

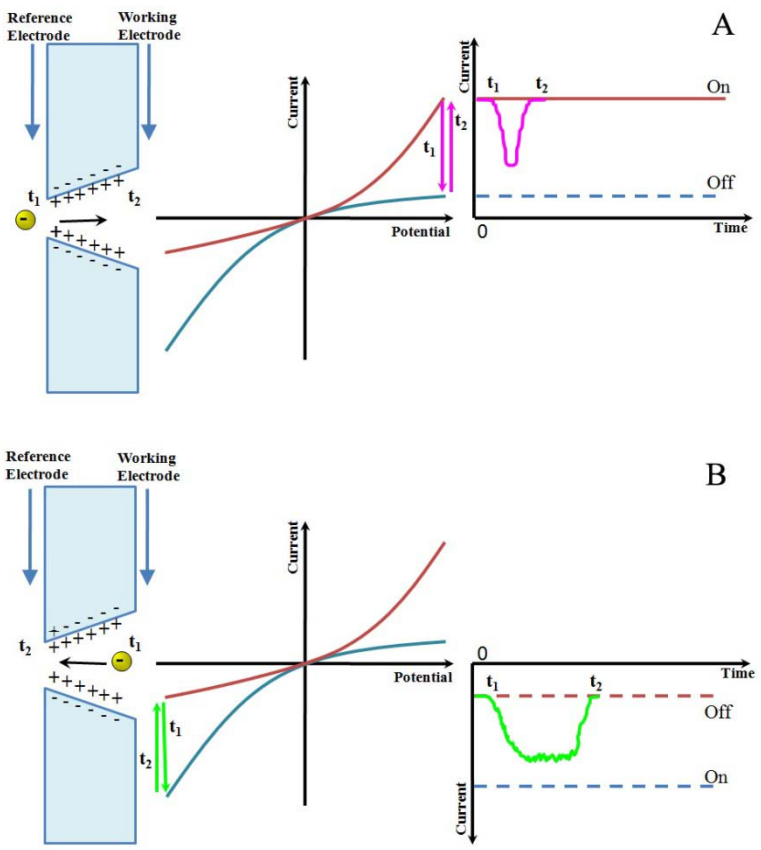


Figure 4-1. Schematic of hypothesized mechanism of resistive-pulse detection. A) PS particles are transported from tip to base. B) PS particles are transported from base to tip.

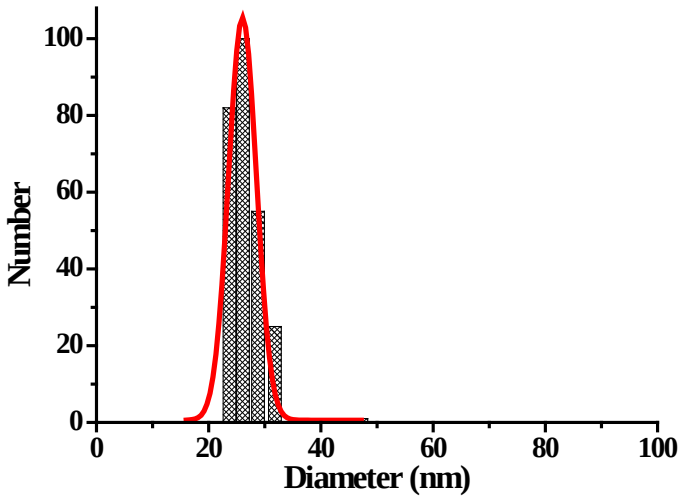


Figure 4-2. Size distribution of poly(styrene) nanoparticles in the buffer solution. It was measured using dynamic light scattering. The red curve is Gaussian fit data. The solution was a 10 mM phosphate buffer at 7.0 also contained 10 mM KCl and 15 μM Hoechst 33258. PS particle concentration was 50 nM.

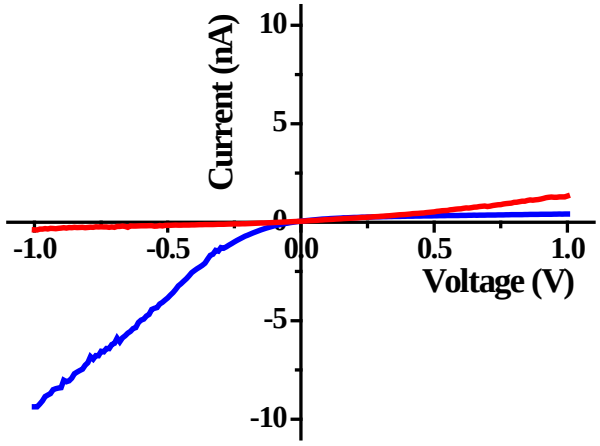


Figure 4-3. Current-voltage curves of a single pyramidal nanopore in mica measured in different supporting electrolyte solution. Blue curve: 10 mM phosphate buffer at pH 7.0 with 10 mM KCl. Red curve: 10 mM phosphate buffer at pH 7.0 with 10 mM KCl and 15 μM Hoechst 33258.

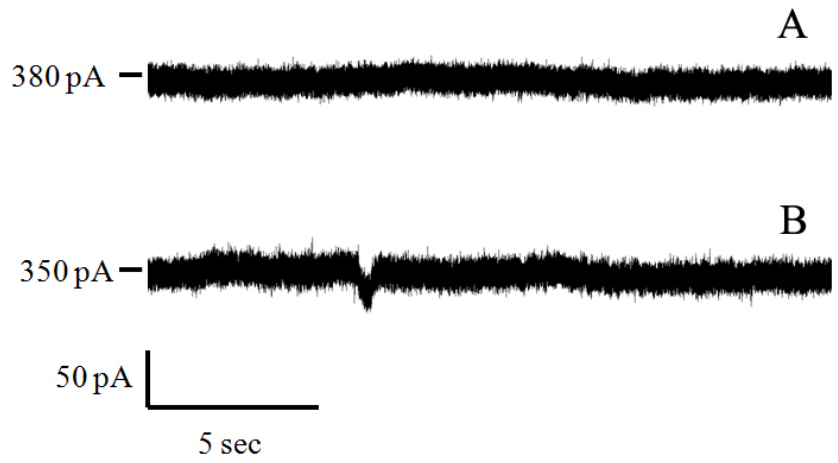


Figure 4-4. Current-time transients for conventional resistive-pulse detection of nanoparticles using a single pyramidal nanopore in mica. A) Steady state current without nanoparticles. B) A solution (10 mM phosphate buffer at pH 7.0 with 10 mM KCl) contains 50 nM PS particles with diameter at 29 nm was place at tip side of the membrane. Pyramidal nanopore $d_{Eq\text{-}tip}$ ~ 85 nm, $d_{Eq\text{-}base}$ ~ 640 nm. Transmembrane potential = 1000 mV.

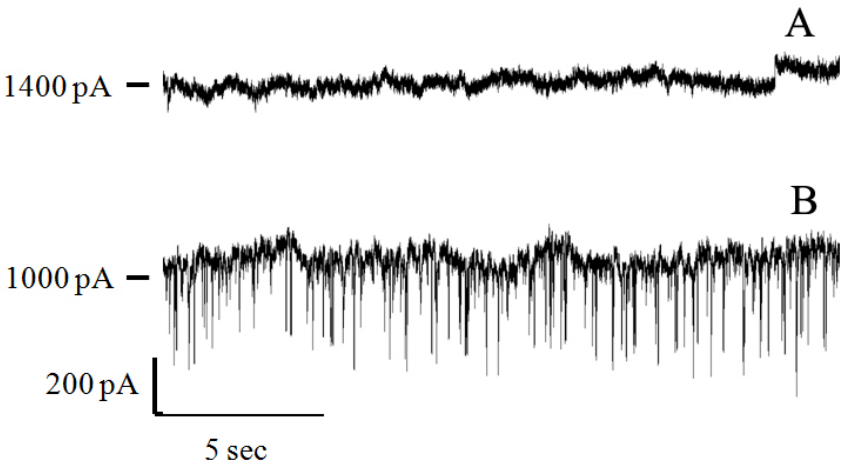


Figure 4-5. Current-time transients for coating reagent assisted resistive-pulse detection of nanoparticles using single pyramidal nanopore in mica. A) Steady state current without nanoparticles. B) A solution (10 mM phosphate buffer at pH 7.0 with 10 mM KCl and 15 μM Hoechst 33258) contains 50 nM PS particles with diameter at 29 nm was place at tip side of the membrane. Pyramidal nanopore $d_{Eq\text{-}tip}$ ~ 85 nm, $d_{Eq\text{-}base}$ ~ 640 nm. Transmembrane potential = 1000 mV.

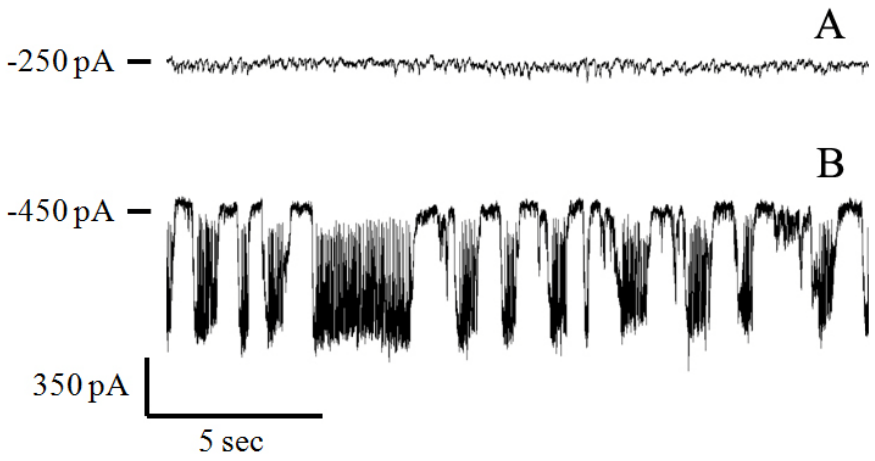


Figure 4-6. Current-time transients for coating reagent assisted resistive-pulse detection of nanoparticles using single pyramidal nanopore in mica. A) Steady state current without nanoparticles. B) A solution (10 mM phosphate buffer at pH 7.0 with 10 mM KCl and 15 μM Hoechst 33258) contains 50 nM PS particles with diameter at 29 nm was place at base side of the membrane. Pyramidal nanopore $d_{Eq\text{-}tip}$ ~ 85 nm, $d_{Eq\text{-}base}$ ~ 640 nm. Transmembrane potential = 1000mV.

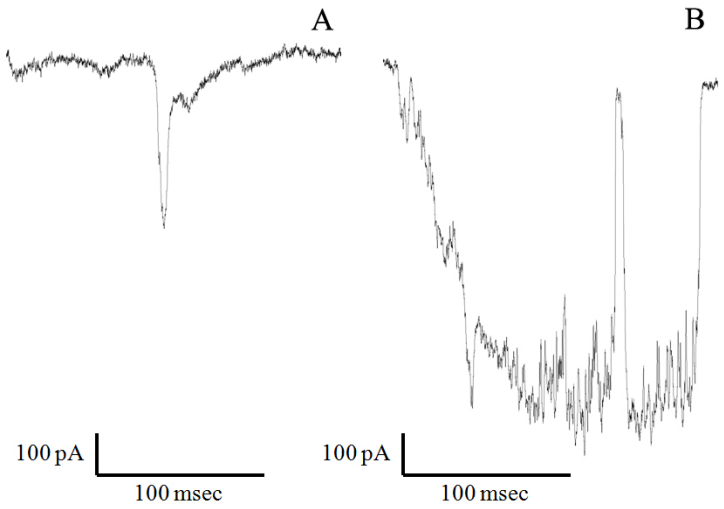


Figure 4-7. Expanded views of current pulse for nanoparticles translocation from the opposite directions. A) From tip to base, B) From base to tip. Tip diameter = 17 nm. Pyramidal nanopore $d_{Eq\text{-}tip}$ ~ 85 nm, $d_{Eq\text{-}base}$ ~ 640 nm. Transmembrane potential = 1000 mV.

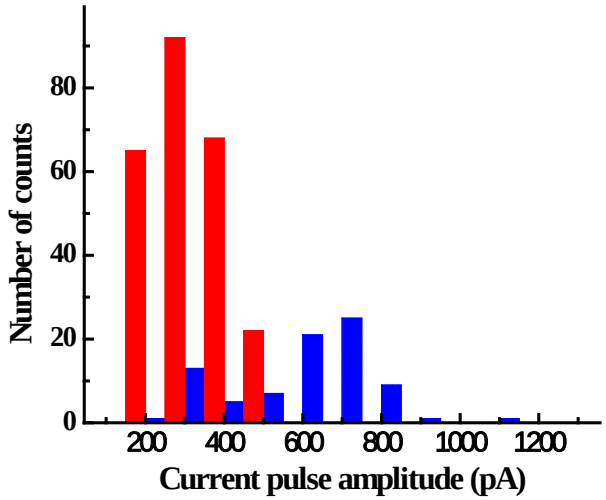


Figure 4-8. Histogram of current pulse amplitude for nanoparticles translocation from the opposite directions. (Red) Nanoparticles moved from tip to base. (Blue) Nanoparticles moved from base to tip.

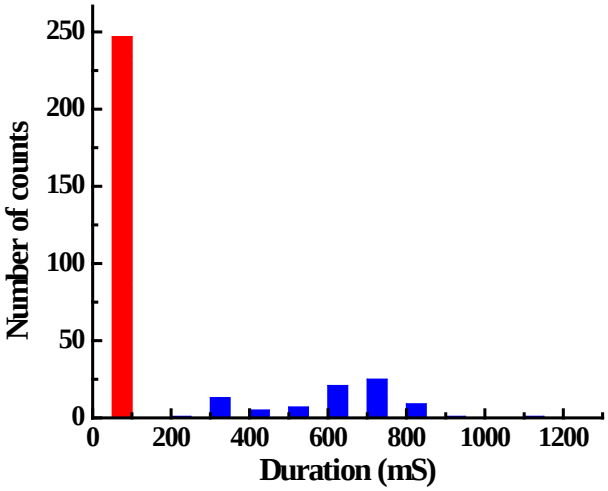


Figure 4-9. Histogram of current pulse duration for nanoparticles translocation from the opposite directions. (Red) Nanoparticles move from tip to base. (Blue) Nanoparticles move from base to tip.

# CHAPTER 5
# STUDIES OF ELECTROOSMOTIC FLOW RECTIFICATION IN PYRAMIDAL NANOPORES IN MICA MEMBRANES

## Introduction

Electroosmotic flow (EOF) is an electro-kinetic phenomenon that occurs when an ionic current is passed through a channel or porous medium that contains excess surface charge.[124-132, 142] EOF is used to pump fluids through microfluidic devices[126] and capillary electrophoresis columns[127]. While the pore and channels typically have a symmetrical shape, there is increasing interest in transport through asymmetrical pores[24, 120] and channels[143], for example conically shaped pores in polymer membranes[76].

More importantly, transport in conically shaped pores is of interest because such pores act as ion-current rectifiers; i.e., the magnitude of the current flowing through the pore depends on the polarity of the potential difference applied across the membrane.[57] It occurred to us that this ion-current rectification phenomenon might produce a corresponding rectification of the EOF rate across the membrane. If this is true, such membranes could be used as EOF rectifiers, yielding high flow rates for one polarity and low flow rates when the polarity is reversed. We report here the first demonstration of this rectified electroosmotic flow effect.

## Experimental

### Materials

Muscovite mica ($KAl_2(AlSi_3)O_{10}(F,OH)_2$) membranes, ~10.4 μm thick and 3 cm in diameter, were obtained from Spruce Pine Co (Spruce Pine, NC). The linear accelerator at GSI (Darmstadt, Germany) was used to ion track the mica; $Pb^{2+}$ ions of ~8.6 MeV kinetic energy were used. Samples with $10^5$ track $cm^{-2}$, were prepared. Hydrofluoric acid (~50%) was obtained from Acros Organics USA (Morris Plains, NJ). Phenol was obtained from Sigma-Aldrich (St. Louis, MO). All other chemicals were reagent grade and used as received. Purified water,

obtained by passing house-distilled water through a Barnstead, E-pure water purification system, was used to prepare all solutions.

**Fabrication of Pyramidally Shaped Nanopores in Muscovite Mica**

The method of fabrication and characterization of pyramidally shaped nanopores were discussed in detail in Chapter 3. Briefly, a ~1 cm diameter hole was cut into a ~4x4 cm piece of parafilm, and the multi-track mica membrane was sandwiched between two such films. The sandwiched membrane was placed between the two halves of the etching cell described previously. The total area of mica membrane exposed to solution is about 0.785 $cm^2$.

A 3 mL of 10 M NaOH solution was pipetted into one of the cells. A Pt wire electrode was inserted into each half cell, and ~3 mL of 10 M HF was then added to the other half-cell. The Keithley 6487 picoammeter/voltage source was used to apply a trans-membrane voltage of 10 V (with the anode in the HF solution) and measure the resulting ionic current flowing through the membrane during etching.

After 10 minutes the etch was terminated by placing 1 M NaOH on both sides of the membrane and applying 10 V for 5 minutes, to ensure complete neutralization of the HF in the pores. The membrane was then rinsed with water, and water was placed in both half cells for 30 minutes to wash the NaOH from the pores. We call this procedure a 10-minute etch cycle.

The same mica membrane is anisotropically etched for one to four 10-minute cycles. The current-voltage curves were measured after each cycle, and the EOF experiments were conducted at each pore size.

**Fabrication of Straight Nanopores in Muscovite Mica**

To compare the electroosmotic flow in asymmetric nanopores, straight nanopores with equal size openings on both sides of the membrane was prepared. A symmetric chemical etching method was used to prepare straight nanopores in the ion-tracked muscovite mica membranes.

Instead of using 10 M NaOH as stopping solution on one side of the membrane and 10 M HF as etching solution on the other, a ~3 mL of 5 M HF was placed on both sides of the membrane to etch mica from different directions at the same time.

After 2.5 minutes the chemical etch was terminated as the same way we did for etching asymmetric nanopores. The nanopores etched at this condition are supposed to have almost equal size openings on both sides of the membrane.[29]

The same membrane was etched for another 2.5 minutes, 5 minutes, and 10 minutes to achieve different pore sizes. The total etch time after each step were 2.5 minutes, 5 minutes, 10 minutes and 20 minutes, respectively. The current-voltage curves were measured in 10 mM phosphate buffer at pH 7.0 after each etches. The electroosmotic flow in these straight nanopores at different sizes was studied as well after each etch step.

**Nanopores Characterization**

For the multipore mica membranes, field-emission scanning electron microscopy (FE-SEM, JEOL 6335F) was used to measure the dimensions of the nanopore openings on both sides of the membranes. A straight nanopores membrane etched for 20 minutes and an asymmetric nanopores membrane etched for four 10-minute cycles were used for SEM imaging.

Even though it is not necessary to calculate the nanopore membrane conductance by using current-voltage curves, it is still useful to obtain the ion current rectification information from those curves. Briefly, the mica membrane containing nanopores was mounted between the two half cells, and an electrolyte solution of 10 mM phosphate buffer at pH 7.0 was placed on both sides of the membrane. A Ag/AgCl electrode was placed into each half-cell solution, and a current-voltage curve was obtained by scanning the potential from -10.0 V to +10.0 V at a scan rate of 10 $Vmin^{-1}$.

**Phenol Transport Measurements**

A mica membrane containing nanopores (pore density ~$10^5$ per $cm^2$) was mounted between the two half cells and a 0.785 $cm^2$ portion of the mica membrane was exposed to the electrolyte solution.

The rate of EOF was investigated by measuring the flux of a probe molecule (phenol) across the membrane and into the permeate half-cell. A 3 mL of permeate solution with 10 mM phosphate buffer pH 7.0 was added to the cell on one side of the membrane. A 3 mL feed solution that was 10 mM phosphate buffer pH 7.0 containing 10 mM phenol was added to the other. A Pt wire electrode was placed into each half cell. The Pt wire in the feed solution was the working electrode (anode) and the Pt wire in the permeate solution was the reference and counter electrode (cathode). Since the mica surface is negatively charged,[147] the EOF direction is same as the direction of cations migration (anode to cathode).

A Solartron SI 1287 electrochemical interface (Farnborough, UK) was used to apply a constant current of 100 μA through the multipore mica membrane. After 20 minutes, the ion current was terminated and both the permeate solution and feed solution were pipetted out of the two half cells. An Agilent 8453 UV-visible spectrometry system (Waldbronn, Germany) was used to measure the UV-Vis absorbance of phenol in the permeate solution. The concentration of phenol in permeate solution was calculated from the calibration curve measured at wavelength 270 nm. We called this procedure a 20-minute transport cycle.

After the UV-visible spectrum measurement, the permeate solution was placed back into the original half cell for next 20-minute cycle transport. To reduce the effect of oxidized phenol on transport and the UV-Vis spectrum, a fresh feed solution with 10 mM of phenol was placed into the cell on the original feed side. This 20-minute transport cycle was repeated for six times

and the total time we applied current was 120 minutes. The UV-visible spectrum of permeate solution was measured after each 20-minute transport cycle.

Then the permeate and feed solution were switched to the other side of the membrane and the flux from the opposite direction was measured for another 120 minutes.

The diffusion of phenol across the asymmetric nanopore membrane without applying voltage was also measured at the same 20-minute time intervals for the total 120-minutes transport. But for the straight nanopores membrane with very small openings, the diffusion flux was too small to transfer enough phenol for accurate measurement. A much longer time interval to measure the phenol concentration was necessary, so a 2-hour transport cycle was performed in this case and the total transport time was 6 hours.

EOF measurement was performed for asymmetric multipore mica membrane after each 10-minute etch cycles and straight multipore mica membrane etched for 2.5, 5, 10, 20 minutes.

## Results and Discussion

### Characterizations of Nanopore Size in Multipore Mica Membrane

To calculate the size of a nanopore opening in single pore membrane, we usually measure the nanopore conductance when it is filled with electrolyte solution. However, two reasons make it inappropriate way to characterize the average nanopore size for multipore membrane.

The first reason is the uncertainty of nanopore density in the mica membrane. Even though we can calculate the average nanopore density from the scanning electron microscopy images, it still brings the error for accurate calculation of nanopore size. Another reason is the uncertainty of voltage drop across the membrane. The electrochemical measurement and calculation require knowledge of the exact membrane conductance, which is calculated from the linear part of current-voltage curves. In single nanopore membrane, the resistance of a nanopore is tremendous so that it is reasonable to assume that the voltage drop across the membrane is equal to the

voltage applied between the electrodes. However, the multipore membrane resistance is smaller and is comparable to the solution resistance. As a result, a portion of the voltage drop will be on the solution. Therefore, it is not appropriate to assume the voltage drop across the membrane is equal to the total voltage between two electrodes. Only after making a correction for the voltage on membrane, is it possible to calculate the membrane resistance accurately.

Instead, the nanopores in multipore mica can be studied by using scanning electron microscopy (SEM). To ensure that the pore density of the membrane is the same for electroosmosis experiments, we only imaged the membrane sample after completion all the EOF measurements. It is also difficult to image the nanopores when they are too small. In these studies, we imaged the asymmetric nanopore base and tip openings after they were etched for four 10-minute cycles. We also imaged the straight nanopore openings on both sides of the membrane after they were etched for 20 minutes.

Figure 5-1AB shows the SEM images of base and tip openings of asymmetric nanopores in a mica membrane etched for four 10-minute cycles. It is obvious that the base was much larger than the tip. Figure 5-1CD illustrates that straight nanopore openings on both sides of the membrane had almost equal dimensions, which was the same as we predicted. It was also shown that the nanopore had a straight shape with equal size rhomboidal openings if the membrane was etched symmetrically from both sides.[29]

The lengths of major axis ($a_l$) of the rhomboidal openings were measured from the SEM images. The equivalent diameter ($d_{Eq}$) of nanopore openings can be calculated from the long diagonals using Equation 5-1,

$$d_{Eq} = 0.606\, a_l \tag{5-1}$$

It was assumed that the etch rate was constant for base and tip, respectively. The average size of

nanopore openings on both sides of the membrane were calculated from the etch rate on each side and the total etch time. The radial etch rate of straight nanopore using 5 M HF is about 1.3 nm $min^{-1}$, which is comparable to the literature.[29] The radial etch rate of base and tip for pyramidal nanopores were about 3.75 nm $min^{-1}$ and 0.5 nm $min^{-1}$, respectively. These values are close to the data we reported in chapter 3. The calculated equivalent diameters of openings for straight nanopores etched for different times are listed in Table 5-1. The nanopore equivalent diameters of base and tip openings for asymmetric nanopores after each etch cycle were calculated and shown in Table 5-2.

**Ion Current Rectification in Asymmetrically Shaped Multipore Mica Membrane**

Figure 5-2 shows the current-voltage curves of straight and asymmetric multipore mica membranes etched for different times. For straight nanopores, the conductance of the membrane increased when the nanopore size became larger, and there was no significant ion current rectification observed for any pore size. However, strong ion current was observed when the nanopores were asymmetrically etched for only one and two 10-minute etch cycles. At longer etch time, the ion current rectification was not significant because of the larger pore size and the multipore membrane resistance became comparable to the solution resistance. We define the ion current rectification ratio as the ratio of absolute ion current value recorded at -10 V to the current value at +10 V. The ion rectification ratio is about 1 for different pore sizes for straight nanopore membranes.

**Phenol Transport Measurements**

**Electroosmotic flow in straight multipore mica membrane**

The electroosmotic flow in the straight multipore mica membrane with different pore sizes were studied. In the experiment, a constant current of 100 μA was passed through the nanopores. When the nanopores were smaller, the membrane resistance was larger. From the Ohm's law, a

larger voltage was needed to maintain the constant current for the nanopore with larger resistance. For example, an average voltage of 9.0 V was applied to maintain the constant current during the transport experiment when the nanopore. Lower voltages were applied when the nanopores were larger and membrane resistance is lower. The applied voltage was about only 3.5 V when the average nanopore equivalent diameter was about 52 nm.

The Helmholtz-Smoluchowski equation defines the relationship between the electroosmotic velocity ($v_{eof}$) and the linear electric field gradient (E(x)) across the membrane

$$v_{eof} = -\varepsilon\zeta E(x)/\eta \tag{5-2}$$

where ε and η are the permittivity and viscosity of the solution within the nanopores, respectively. And ζ is the zeta potential of the pore wall. This relationship shows that the electroosmotic velocity $v_{eof}$ is proportional to the electric field strength E(x). A larger electroosmotic velocity will give a larger electroosmotic flux.

However, the voltage drop across the multipore membrane varied with multiple nanopore membrane resistance, it was hard to know the accurate electric field strength in the pore. Equation 5-3 that deduced from the Helmholtz-Smoluchowski equation might make the explanation easier.

$$v_{eof} = -\varepsilon\zeta J_{app}\,\rho/\eta \tag{5-3}$$

where $J_{app}$ is the constant applied current density. It is obvious that value of $J_{app}$ was the same no matter which direction the current flowed through the pore.

Figure 5-3 shows the transport rate of phenol across the straight multipore membrane with pore equivalent diameter at 7 nm. It was observed that the diffusion rate of phenol across the membrane is very small and the transport rate with applied current was much larger. It is obviously that the electroosmotic flow in these nanopores greatly enhanced the transport rate of

the neutral molecule phenol. We also observed exactly equal transport rate when phenol was transported from the opposite directions.

Equation 5-3 predicts that the electroosmotic flow velocity would be smaller if we increase the nanopore size. This is because we applied a constant current of 100 μA across the membrane and the current density $J_{app}$ decreased as the total nanopore cross-section area increased. As will be discussed below, the experiments proved this prediction.

**Calculation of electroosmotic flow velocity in nanopore membrane**

Nernst-Plank equation can be used to describe the mass transfer in a one-dimensional case as[137]

$$J_i(x) = -D_i \frac{\partial C_i(x)}{\partial x} - \frac{z_i F}{RT} D_i C_i \frac{\partial \phi(x)}{\partial x} + C_i v(x) \quad (5\text{-}4)$$

where $J_i(x)$ is the flux of species i, $D_i$ is the diffusion coefficient, $\partial C_i(x)/\partial x$ is the concentration gradient, $\partial \phi(x)/\partial x$ is the potential gradient, $z_i$ and $C_i$ are the charge and concentration of species i respectively. $v(x)$ is the velocity of a volume element. The three terms in the equation correspond to the diffusion, migration and convection of species i.

In this experiment, Phenol (pKa = 9.99) will be transported mainly by diffusion and EOF because the molecule is neutral at pH 7.0. The magnitude of electroosmotic velocity ($v_{eof}$) was determined via an analysis of the phenol flux with and without the applied transmembrane current as described previously.[128, 152] Briefly, an enhancement factor is given by

$$E = N_J \,/\, N_{diff} \quad (5)$$

i.e., the ratio of the flux in the presence of an applied current to the flux without any current. Following Srinivasan and Higuchi[152], the peclet number (Pe) can be calculated from E via

$$E = Pe \,/\, (1 - \exp(-Pe)) \quad (6)$$

Pe can then be used to calculate $v_{eof}$ using

$$v_{eof} = PeD/l \quad (7)$$

where l is the thickness of the membrane and D is the diffusion coefficient (~$8.9\times10^{-6}$ $cm^2s^{-1}$).

**Electroosmotic flow in asymmetric multipore mica membrane**

The current-voltage curves in Figure 5-2B clearly demonstrates that there was ion current rectification occurred in the asymmetric nanopore mica membrane. The current was larger when the anode was on the nanopore tip side of the membrane (on state) and current was lower at the opposite electrode polarity. Because the nanopores surface is negatively charged and the size of nanopores size is comparable to the thickness of electrical double layer, the membrane became cation permselective.[30] According to literature [24, 74] Ramírez and White et al. have demonstrated a possible explanation for this ion current rectification phenomenon in asymmetric nanopore.

As shown in Figure 5-4, when the anode is on the tip side of the nanopore, cations are transported from the tip side (anode) to the base side (cathode). Anions are electrophoretically driven from the external solution at the base side of the membrane towards the tip by the electric field. However, they cannot pass through the nanopore because of electrostatic repulsion from the negatively charged pore wall close to the tip region. As a result, anions accumulate in the nanopore. To maintain electrostatic neutrality, more cations are needed in this tip region to balance the extra anions. Therefore, the local salt concentration increases and the resistance of the pore solution ρ decreases. Thus, a higher ion current was obtained when a transmembrane potential was applied in this way. We refer to this situation as the “ion accumulation mode”. Since the mica nanopore surface is negatively charged[141], electroosmosis will proceed in the same direction as that of cations electromigration. Therefore, in this ion accumulation mode, the electroosmotic flow is from the tip opening to base opening in the nanopore.

On the contrary, when the anode is placed on the base side of the nanopore (Figure 5-4 right), cations are transported from the base opening to the tip opening of the nanopore. Anions inside the nanopore are vacated from the nanopore and into the bulk solution on the base side by the electric field. However, the anions on the tip side are less likely to enter the nanopore because of electrostatic repulsion from the anionic pore wall close to tip. As a result, the local salt concentration in the nanopore decreases, and the resistivity of pore solution increases. When a transmembrane potential was applied in this way a lower ion current was obtained. We refer to this situation as the "ion depletion mode" and the EOF direction in this mode is from base to tip in the nanopore. In other word, the nanopore solution resistivity is larger in the ion depletion mode and it is smaller in the ion accumulation mode.

When the EOF was driven from base to tip, the pore solution resistivity $\rho$ was high because it was in the ion depletion mode. We expected to observe a larger electroosmotic flow velocity in this case according to Equation 5-3. When the EOF was driven from tip to base, the pore solution resistivity $\rho$ was lower because it was in the ion accumulation mode and we were expected to observe a lower electroosmotic flow velocity. The experimental results proved these predictions. As shown in Figure 5-5, a much higher phenol transport rate was observed when the flux was from the nanopore base to tip. The calculated the electroosmotic flow velocity $v_{eof}$ was about 3.8 $mms^{-1}$ and 0.37 $mms^{-1}$ when phenol was transported from the different directions (Table 5-3). It is important to point out that because the field strength in an asymmetric pore varies with position down the length of the pore, $v_{eof}$ will also vary down the pore length. The $v_{eof}$ values reported here are the net velocities in that they were obtained from the net rate of transport of phenol from the feed solution to the permeate solution.

It was also observed that the electroosmotic flow velocity became smaller if we increased nanopore size. This is because we applied a constant current of 100 μA across the membrane and the current density $J_{app}$ decreased as the total nanopore cross-section area increased. Another reason that the EOF velocity decreased so rapidly for the transport from base to tip is because the ion depletion effect decreased so much when the nanopore size increased.

**Relationship between the ion current rectification and electroosmotic flow rectification**

It is clearly demonstrated that the rectified electroosmotic flow is the direct consequence of ion current rectification. The $v_{eof}$ values obtained are shown in Table 5-3. The extent of EOF rectification was quantified by defining a parameter called the EOF rectification ratio, $r_{eof}$, which is $v_{eof}$ for the "off" state polarity divided by $v_{eof}$ for the "on" state polarity. We see that $r_{eof}$ increases with decreasing size of the pore (Table 5-3); i.e. the extent of EOF rectification is greater in smaller pores. While we will have more to say about this point in the future, this is certainly reasonable since the chance of achieving the requisite high cation transference number is greater in a smaller pore.

The extent of ion-current rectification is quantified by the ion-current rectification ratio, $r_{ic}$, defined here as the absolute value of the current at -10 V divided by the current at +10 V. The $r_{ic}$ values (Table 5-3) show that like $r_{eof}$, ion-current rectification is greater in smaller pores. We also see that $r_{eof}$ scales with $r_{ic}$, which is reasonable since both phenomena derive from the change in pore-solution resistivity with sign of the applied transmembrane potential. The proportionality between $r_{eof}$ and $r_{ic}$ indicates that a simple measurement of $r_{ic}$ (Figure 5-2) can be used to predict whether a membrane will be a good EOF rectifier.

## Conclusions

We have shown for the first time that asymmetric nanopore mica membrane rectifies EOF. As theory predicts, and as we have shown experimentally, EOF rectification was observed in

pores that show the more familiar ion-current rectification. We demonstrate that such rectified EOF is the direct consequence of the ionic current rectification at a constant applied current. The flux is larger when the EOF direction is from the base of pyramidal nanopore to the tip side. The ratio of the EOF flux from opposite direction is related to the level of the observed ion current rectification in such asymmetric nanopore. When there is no ion-current rectification, such as in the case of straight pores, we observe no difference between the EOF fluxes from the opposite directions. It is important to point out that the extents of both ion-current and EOF rectification increase with charge density on the pore wall. As a result, mica is an especially propitious material for such rectifiers since the anionic charge density on mica[147] exceeds by a factor of ~2 of the charge density on the more commonly studied polymeric membranes.[148]

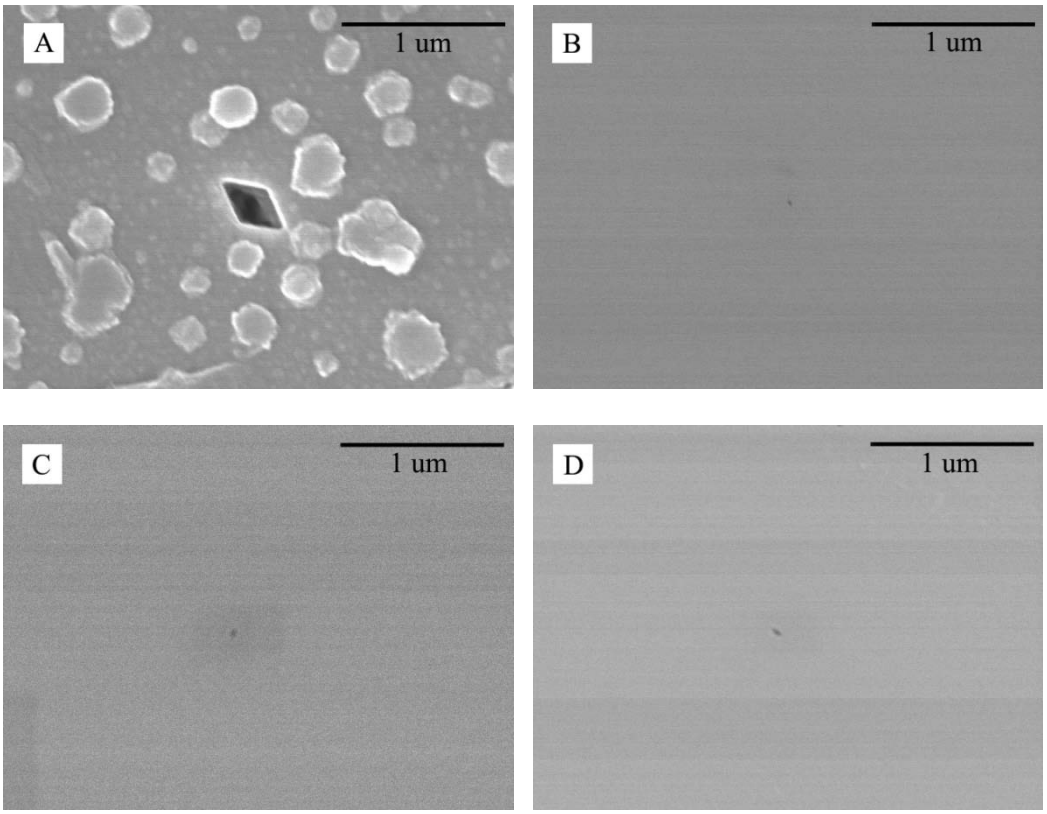


Figure 5-1. FESEM images of asymmetric nanopore and straight nanopore openings in mica membranes used in EOF experiments. A) Base openings in asymmetric nanopore membrane. B) Tip openings in asymmetric nanopore membrane. CD) Straight nanopore openings on opposite sides of the membrane.

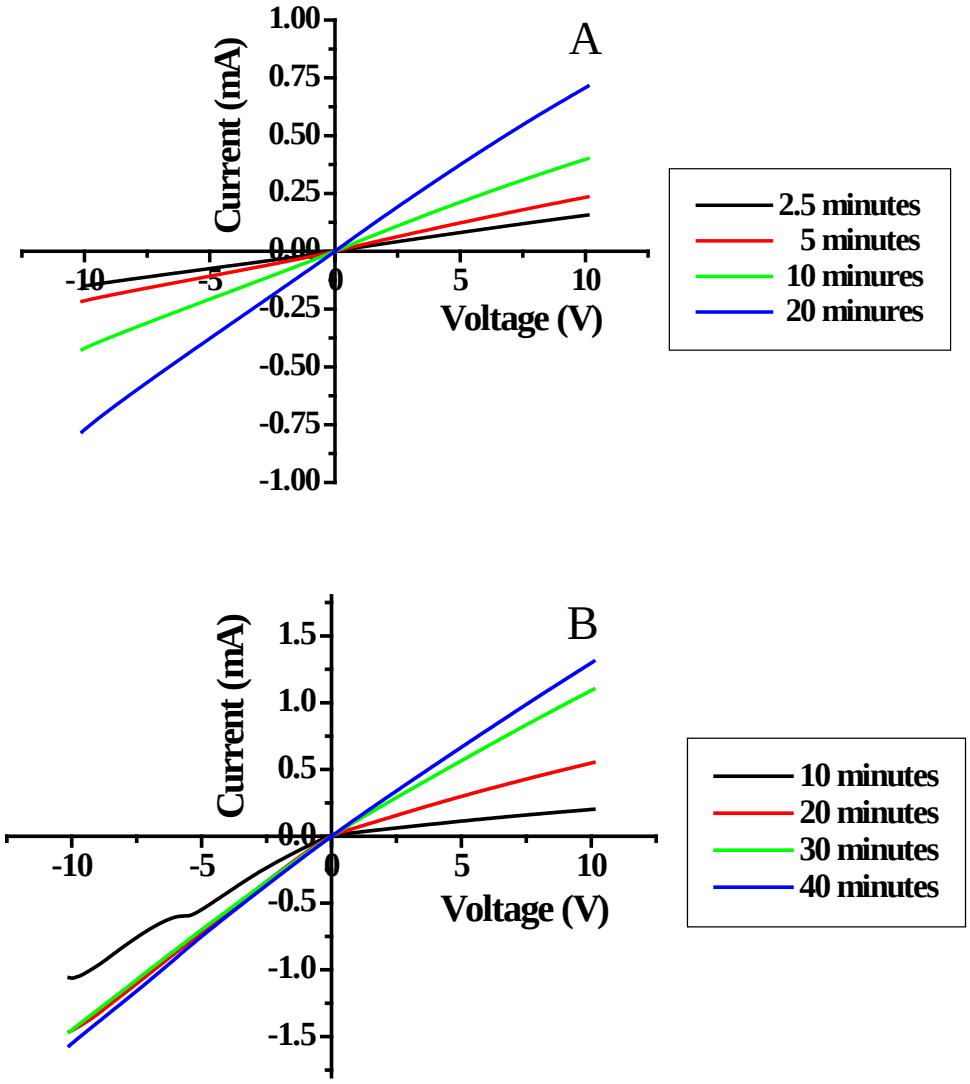


Figure 5-2. Current-voltage curves of multipore mica membrane with straight or pyramidal nanopores etched for different time. A) Straight nanopore membrane. B) Pyramidal nanopore membrane.

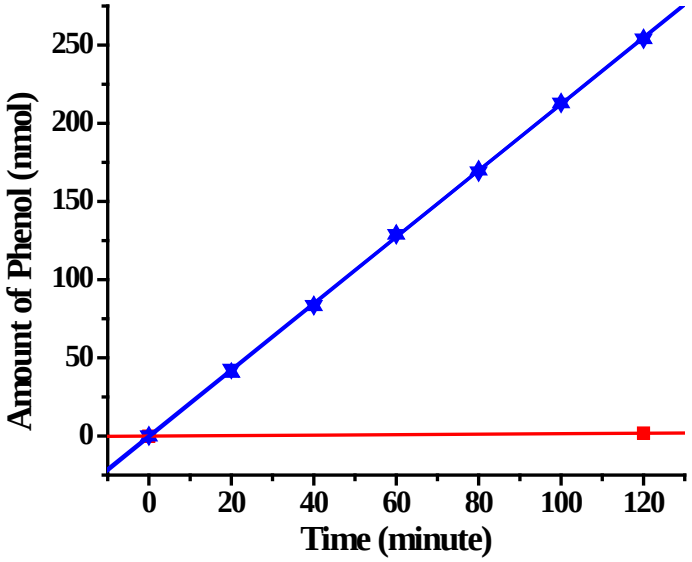


Figure 5-3. Amount of phenol transported across a straight multipore mica membrane. Equivalent diameter $d_{eq}$= 7 nm. (Blue ▲▼) Phenol transported from different directions with applying constant current of 100 μA. (Red ■) Phenol diffused across the membrane.

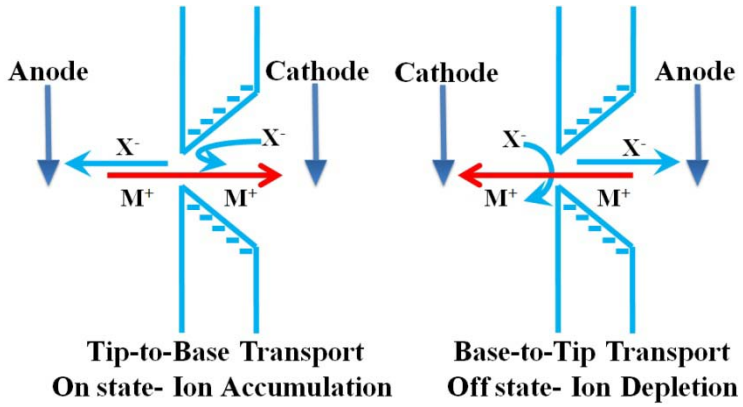


Figure 5-4. Schematic of ion accumulation and ion depletion in asymmetric nanopore and direction of corresponding electroosmotic flow.

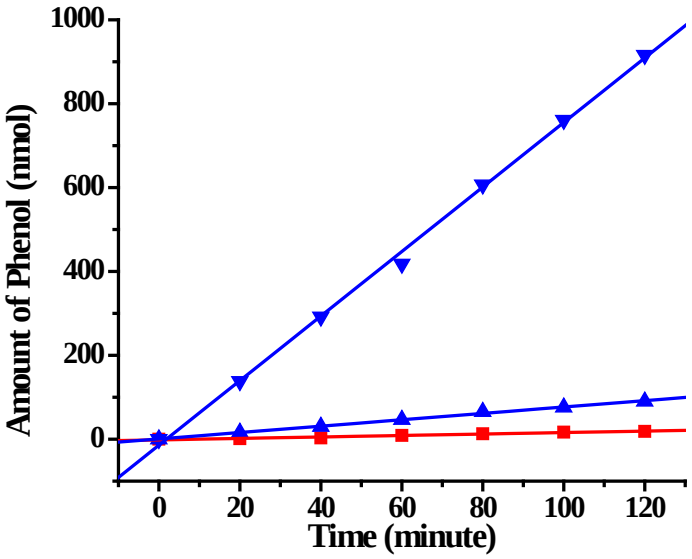


Figure 5-5. Amount of phenol transported across an asymmetric multipore mica membrane. Equivalent diameter of tip $d_{eq\text{-}T}$ = 10 nm and equivalent diameter of base $d_{eq\text{-}B}$ = 74 nm. (Blue) Phenol transported from different directions with applying constant current of 100 μA (▼ base to tip, ▲ tip to base). (Red ■) Phenol diffused across the membrane.

Table 5-1. Estimated equivalent diameters of straight nanopore openings.

| Etch time (minutes) | Average opening on both sides $d_{eq}$ (nm) |
|---|---|
| 2.5 | ~7 |
| 5 | ~13 |
| 10 | ~26 |
| 20 | 52 ± 5 (SEM) |

Table 5-2. Estimated equivalent diameters of asymmetric nanopore base and tip openings.

| Etch time (minutes) | Base $d_{Eq-B}$ (nm) | Tip $d_{Eq-T}$ (nm) |
|---|---|---|
| 10 | ~74 | ~10 |
| 20 | ~148 | ~19 |
| 30 | ~ 222 | ~29 |
| 40 | ~296 ± 7 (SEM) | ~38 ± 6 (SEM) |

Table 5-3. EOF velocities and ion-current and EOF rectification ratios for the membranes studied here.

| Tip $d_{Eq-T}$ (nm) | Base $d_{Eq-B}$ (nm) | $v_{eof}$ (mm $s^{-1}$) | | $r_{eof}$ | $r_{ic}$ |
|---|---|---|---|---|---|
| | | Base-to-Tip | Tip-to-Base | | |
| 10 | 74 | 3.8 | 0.37 | 10.3 | 5.3 |
| 19 | 148 | 1.7 | 0.35 | 4.9 | 2.7 |
| 29 | 222 | 0.55 | 0.32 | 1.7 | 1.3 |
| 38 | 296 | 0.32 | 0.23 | 1.4 | 1.2 |
| 7 | 7 | 12 | 12 | 1.0 | 1.0 |

# CHAPTER 6
# CONCLUSIONS

The goal of this research was to develop asymmetrically shaped nanopores in thin film materials and to investigate the potential applications of these devices as resistive-pulse sensors. Chapter 1 introduced and reviewed all relative background information for these studies, including the track-etch method, characterization of asymmetric nanopores, ion current rectification phenomenon in asymmetric nanopore and nano-channel, resistive-pulse sensing with biological and artificial nanopores.

In Chapter 2, polyelectrolyte sodium poly(styrene sulfonate) was used as a model analyte to study some fundamental parameters of the resistive-pulse sensing. In this work, a single conically shaped nanopore in PET membrane was fabricated by using two-step chemical etch method. It was shown that the polyelectrolyte translocation through the nanopore tip could be detected using such nanopore resistive-pulse detector. It was found that the current pulse frequency increased at high analyte concentration, and applying a higher transmembrane potential could increase the pulse frequency. These studies provide information about improving the detection limit of resistive-pulse method by using high voltage.

In Chapter 3, a multi-cycle anisotropic chemical etch method was developed to fabricate asymmetrically shaped nanopores in muscovite mica membrane. The effects of the etchant concentration, transmembrane potential and the number of etch cycle on the nanopore opening size and geometry were studied in detail and the etch condition was optimized. Asymmetric nanopores were prepared in both the multi-track and single-track mica membranes. A strong ion current rectification phenomenon was observed in the pyramidally shaped nanopore embedded in mica membrane, especially in the low ionic strength solution. We proposed that the strong ion current rectification in mica is because of the high surface charge density on mica. A much

weaker ion current rectification was obtained when the charges on the mica nanopore surface were partially removed.

In Chapter 4, a new mechanism based on the local charge inversion induced ion current rectification switch was proposed for resistive-pulse detection. This mechanism was tested by using a single asymmetric nanopore in muscovite mica membrane. A coating reagent was used to temporarily change the surface charge condition and resulted in ion current rectification change. We observed strong current pulse signals when the model analyte poly(styrene) nanoparticles were transported through the nanopore. The current pulse shape, pulse amplitude and pulse duration were greatly different when the nanoparticles were transported from the opposite directions in the nanopore. We believe that the nanopore local charge inversion is the key in this mechanism. However, the details about this proposed mechanism are still under investigation.

In Chapter 5, an interesting electro-kinetic phenomenon, electroosmotic flow rectification in asymmetric nanopore was reported. This phenomenon was studied by monitoring a probe molecule, phenol transported across asymmetric nanopores embedded in mica membrane. It was found that the transported rate of phenol across the membrane was higher from base to tip and it was lower from the opposite direction. We think this is because the electroosmotic flow velocity was different in each case. It was found that this rectified electroosmotic flow was because of the well known ion current rectification in asymmetric nanopores. The ion accumulation and ion depletion in the asymmetric nanopores affected the pore solution resistivity and caused such rectified electroosmotic flow when a constant current was passed through the asymmetric nanopore membranes. However, this rectified electroosmotic flow was not observed in the straight nanopores.

The work presented here has demonstrated that single asymmetric nanopores can be used for resistive-pulse sensing studies. Resistive-pulse sensing of different analytes using synthetic nanopore is relative new area with lots of phenomena and theories need to be investigated and proved. In this study, the successful fabrication of asymmetric nanopores in crystal materials mica membrane shows opportunities for many research based on its capability to strongly rectify the ion current flowing through the nanopore. Although, further studies will be needed to continue to exploring the applications, the work presented here may hopefully serve as a foundation for such research.

LIST OF REFERENCES


(1) Baker, L. A.; Jin, P.; Martin, C. R. *Crit. Rev. Solid State Mat. Sci*. **2005**, *30*, 183-205.

(2) Martin, C. R. *Science* **1994**, *266*, 1961-1966.

(3) Jirage, K. B.; Martin, C. R. *Trends Biotechnol*. **1999**, *17*, 197-200.

(4) Hou, S. F.; Harrell, C. C.; Trofin, L.; Kohli, P.; Martin, C. R. *J. Am. Chem. Soc.* **2004**, *126*, 5674-5675.

(5) Hou, S. F.; Wang, J. H.; Martin, C. R. *Nano Lett.* **2005**, *5*, 231-234.

(6) Gasparac, R.; Kohli, P.; Mota, M. O.; Trofin, L.; Martin, C. R. *Nano Lett.* **2004**, *4*, 513-516.

(7) Hillebrenner, H.; Buyukserin, F.; Stewart, J. D.; Martin, C. R. *Nanomedicine* **2006**, *1*, 39-50.

(8) Wade, T. L.; Wegrowe, J. E. Eur. Phys. *J.-Appl. Phys* **2005**, *29*, 3-22.

(9) Martin, C. R.; Siwy, Z. *Nat. Mater.* **2004**, *3*, 284-285.

(10) Lee, S. B.; Mitchell, D. T.; Trofin, L.; Nevanen, T. K.; Soderlund, H.; Martin, C. R. *Science* **2002**, *296*, 2198-2200.

(11) Kohli, P.; Harrell, C. C.; Cao, Z. H.; Gasparac, R.; Tan, W. H.; Martin, C. R. *Science* **2004**, *305*, 984-986.

(12) Yu, S. F.; Lee, S. B.; Martin, C. R. *Anal. Chem.* **2003**, *75*, 1239-1244.

(13) Yu, S. F.; Lee, S. B.; Kang, M.; Martin, C. R. *Nano Lett.* **2001**, *1*, 495-498.

(14) Bayley, H.; Martin, C. R. *Chem. Rev*. **2000**, *100*, 2575-2594.

(15) Choi, Y.; Baker, L. A.; Hillebrenner, H.; Martin, C. R. *Phys. Chem. Chem. Phys*. **2006**, *8*, 4976-4988.

(16) Sexton, L. T.; Horne, L. P.; Sherrill, S. A.; Bishop, G. W.; Baker, L. A.; Martin, C. R. *J. Am. Chem. Soc*. **2007**, *129*, 13144-13152.

(17) Howorka, S.; Siwy, Z. *Chem. Soc. Rev*. **2009**, *38*, 2360-2384.

(18) Trofin, L.; Lee, S. B.; Mitchell, D. T.; Martin, C. R. *J. Nanosci. Nanotechnol*. **2004**, *4*, 239-244.

(19) Harrell, C. C.; Kohli, P.; Siwy, Z.; Martin, C. R. *J. Am. Chem. Soc*. **2004**, *126*, 15646-15647.

(20) Martin, C. R.; Mitchell, D. T. *Anal. Chem.* **1998**, *70*, 322a-327a.

(21) Storm, A. J.; Chen, J. H.; Ling, X. S.; Zandbergen, H. W.; Dekker, C. *Nat. Mater.* **2003**, *2*, 537-540.

(22) Li, J.; Stein, D.; McMullan, C.; Branton, D.; Aziz, M. J.; Golovchenko, J. A. *Nature* **2001**, *412*, 166-169.

(23) Dekker, C. *Nat. Nanotechnol*. **2007**, *2*, 209-215.

(24) White, H. S.; Bund, A. *Langmuir* **2008**, *24*, 2212-2218.

(25) Ito, T.; Sun, L.; Henriquez, R. R.; Crooks, R. M. *Accounts Chem. Res*. **2004**, *37*, 937-945.

(26) Nilsson, J.; Lee, J. R. I.; Ratto, T. V.; Letant, S. E. *Adv. Mater*. **2006**, *18*, 427-431.

(27) Harrell, C. C.; Lee, S. B.; Martin, C. R. *Anal. Chem*. **2003**, *75*, 6861-6867.

(28) Li, N. C.; Yu, S. F.; Harrell, C. C.; Martin, C. R. *Anal. Chem.* **2004**, *76*, 2025-2030.

(29) Xu, F.; Wharton, J. E.; Martin, C. R. *Small* **2007**, *3*, 1718-1722.

(30) Nishizawa, M.; Menon, V. P.; Martin, C. R. *Science* **1995**, *268*, 700-702.

(31) Siwy, Z.; Kosinska, I. D.; Fulinski, A.; Martin, C. R. *Phys. Rev. Lett*. **2005**, *94*, 048102/1-048102/4.

(32) Siwy, Z.; Apel, P.; Dobrev, D.; Neumann, R.; Spohr, R.; Trautmann, C.; Voss, K. *Nucl. Instrum. Methods Phys. Res. Sect. B* **2003**, *208*, 143-148.

(33) Awasthi, K.; Kulshreshtha, V.; Tripathi, B.; Acharya, N. K.; Singh, M.; Vijay, Y. K. *Bull. Mat. Sci*. **2006**, *29*, 261-264.

(34) Jirage, K. B.; Hulteen, J. C.; Martin, C. R. *Science* **1997**, *278*, 655-658.

(35) Siwy, Z.; Trofin, L.; Kohli, P.; Baker, L. A.; Trautmann, C.; Martin, C. R. *J. Am. Chem. Soc*. **2005**, *127*, 5000-5001.

(36) Kang, M. C.; Trofin, L.; Mota, M. O.; Martin, C. R. *Anal. Chem*. **2005**, *77*, 6243-6249.

(37) Heins, E. A.; Baker, L. A.; Siwy, Z. S.; Mota, M.; Martin, C. R. *J. Phys. Chem. B* **2005**, *109*, 18400-18407.

(38) Cepak, V. M.; Martin, C. R. *Chem. Mat*. **1999**, *11*, 1363-1367.

(39) Sapp, S. A.; Lakshmi, B. B.; Martin, C. R. *Adv. Mater*. **1999**, *11*, 402-404.

(40) Che, G. L.; Lakshmi, B. B.; Fisher, E. R.; Martin, C. R. *Nature* **1998**, *393*, 346-349.

(41) Fischer, B. E.; Spohr, R. *Rev. Mod. Phys.* **1983**, *55*, 907-948.

(42) Harrell, C. C.; Choi, Y.; Horne, L. P.; Baker, L. A.; Siwy, Z. S.; Martin, C. R. *Langmuir* **2006**, *22*, 10837-10843.

(43) Clochard, M. C.; Wade, T. L.; Wegrowe, J. E.; Balanzat, E. *Nucl. Instrum. Methods Phys. Res. Sect. B* **2007**, *265*, 325-329.

(44) Zhu, Z. Y.; Duan, J. L.; Maekawa, Y.; Koshikawa, H.; Yoshida, M. *Radiat. Meas.* **2004**, *38*, 255-261.

(45) Kececi, K.; Sexton, L. T.; Buyukserin, F.; Martin, C. R. *Nanomedicine* **2008**, *3*, 787-796.

(46) Siwy, Z.; Dobrev, D.; Neumann, R.; Trautmann, C.; Voss, K. *Appl. Phys. A-Mater. Sci. Process.* **2003**, *76*, 781-785.

(47) Siwy, Z.; Apel, P.; Baur, D.; Dobrev, D. D.; Korchev, Y. E.; Neumann, R.; Spohr, R.; Trautmann, C.; Voss, K. O. *Surf. Sci.* **2003**, *532*, 1061-1066.

(48) Heins, E. A.; Siwy, Z. S.; Baker, L. A.; Martin, C. R. *Nano Lett.* **2005**, *5*, 1824-1829.

(49) Fleischer, R. L. B. P., P.; Walker, R. M., *Nuclear Tracks in Solids: principles and applications*. ed.; University of California Press: Berkeley, 1975.

(50) Sun, Y. M.; Zhu, Z. Y.; Wang, Z. G.; Liu, J.; Jin, Y. F.; Hou, M. D.; Wang, Y.; Duan, J. L. *Nucl. Instrum. Methods Phys. Res. Sect. B* **2003**, *212*, 211-215.

(51) Apel, P.; Spohr, R.; Trautmann, C.; Vutsadakis, V. *Radiat. Meas.* **1999**, *31*, 51-56.

(52) Spohr, R.; *Patent, German., DE 2 951 376 C2*, 1983.

(53) Wharton, J. E.; Jin, P.; Sexton, L. T.; Horne, L. P.; Sherrill, S. A.; Mino, W. K.; Martin, C. R. *Small* **2007**, *3*, 1424-1430.

(54) Baker, L. A.; Bird, S. P. *Nat. Nanotechnol.* **2008**, *3*, 73-74.

(55) Savariar, E. N.; Krishnamoorthy, K.; Thayumanavan, S. *Nat. Nanotechnol.* **2008**, *3*, 112-117.

(56) Apel, P. Y.; Korchev, Y. E.; Siwy, Z.; Spohr, R.; Yoshida, M. *Nucl. Instrum. Methods Phys. Res. Sect. B* **2001**, *184*, 337-346.

(57) Siwy, Z. S. *Adv. Funct. Mater.* **2006**, *16*, 735-746.

(58) Ali, M.; Yameen, B.; Neumann, R.; Ensinger, W.; Knoll, W.; Azzaroni, O. *J. Am. Chem. Soc.* **2008**, *130*, 16351-16357.

(59) Zhu, Z.; Maekawa, Y.; Liu, Q.; Yoshida, M. *Nucl. Instrum. Methods Phys. Res. Sect. B* **2005**, *236*, 61-67.

(60) Zhu, Z.; Maekawa, Y.; Koshikawa, H.; Suzuki, Y.; Yonezawa, N.; Yoshida, M. *Nucl. Instrum. Methods Phys. Res. Sect. B* **2004**, *217*, 449-456.

(61) Trautmann, C.; Bouffard, S.; Spohr, R. *Nucl. Instrum. Methods Phys. Res. Sect. B* **1996**, *116*, 429-433.

(62) Harrell, C. C.; Siwy, Z. S.; Martin, C. R. *Small* **2006**, *2*, 194-198.

(63) Sun, L.; Chien, C. L.; Searson, P. C. *J. Mater. Sci.* **2000**, *35*, 1097-1103.

(64) Crawford, W. T.; Desorbo, W.; Humphrey, J. S. *Nature* **1968**, *220*, 1313-1314.

(65) Wolf, A.; Reber, N.; Apel, P. Y.; Fischer, B. E.; Spohr, R. *Nucl. Instrum. Methods Phys. Res. Sect. B* **1995**, *105*, 291-293.

(66) Apel, P. Y. *Nucl. Tracks Rad. Meas.* **1991**, *19*, 29-34.

(67) Awasthi, K.; Kulshrestha, V.; Acharya, N. K.; Singh, M.; Vijay, Y. K. *Eur. Polym. J.* **2006**, *42*, 883-887.

(68) Aschenba.J; Fiedler, G.; Schreckk.H; Siegert, G. *Nucl. Instrum. Methods* **1974**, *116*, 389-395.

(69) Wharton, J. E. Ph.D. Dissertation, University of Florida, 2007.

(70) Trautmann, C.; Bruchle, W.; Spohr, R.; Vetter, J.; Angert, N. *Nucl. Instrum. Methods Phys. Res. Sect. B* **1996**, *111*, 70-74.

(71) Sun, L.; Searson, P. C.; Chien, C. L. *Appl. Phys. Lett.* **1999**, *74*, 2803-2805.

(72) Sexton, L. T. Ph.D. Dissertation, University of Florida, 2009.

(73) Harrell, C. C. Ph.D. Dissertation, University of Florida, 2004.

(74) Cervera, J.; Schiedt, B.; Ramirez, P. *Europhys Lett.* **2005**, *71*, 35-41.

(75) Wei, C.; Bard, A. J.; Feldberg, S. W. *Anal. Chem.* **1997**, *69*, 4627-4633.

(76) Siwy, Z.; Heins, E.; Harrell, C. C.; Kohli, P.; Martin, C. R. *J. Am. Chem. Soc.* **2004**, *126*, 10850-10851.

(77) Lee, S.; Zhang, Y. H.; White, H. S.; Harrell, C. C.; Martin, C. R., *Anal. Chem.* **2004**, *76*, 6108-6115.

(78) Bayley, H.; Cremer, P. S. *Nature* **2001**, *413*, 226-230.

(79) Bezrukov, S. M.; Vodyanoy, I.; Brutyan, R. A.; Kasianowicz, J. J. *Macromolecules* **1996**, *29*, 8517-8522.

(80) Braha, O.; Gu, L. Q.; Zhou, L.; Lu, X. F.; Cheley, S.; Bayley, H. *Nat. Biotechnol*. **2000**, *18*, 1005-1007.

(81) Braha, O.; Walker, B.; Cheley, S.; Kasianowicz, J. J.; Song, L. Z.; Gouaux, J. E.; Bayley, H. *Chem. Biol*. **1997**, *4*, 497-505.

(82) Cheley, S.; Gu, L. Q.; Bayley, H. *Chem. Biol*. **2002**, *9*, 829-838.

(83) Clarke, J.; Wu, H. C.; Jayasinghe, L.; Patel, A.; Reid, S.; Bayley, H. *Nat. Nanotechnol*. **2009**, *4*, 265-270.

(84) Gu, L. Q.; Braha, O.; Conlan, S.; Cheley, S.; Bayley, H. *Nature* **1999**, *398*, 686-690.

(85) Gu, L. Q.; Cheley, S.; Bayley, H. *Science* **2001**, *291*, 636-640.

(86) Howorka, S.; Cheley, S.; Bayley, H. *Nat. Biotechnol*. **2001**, *19*, 636-639.

(87) Howorka, S.; Movileanu, L.; Lu, X. F.; Magnon, M.; Cheley, S.; Braha, O.; Bayley, H. *J. Am. Chem. Soc*. **2000**, *122*, 2411-2416.

(88) Maglia, G.; Restrepo, M. R.; Mikhailova, E.; Bayley, H. *Proc. Natl. Acad. Sci. U. S. A.* **2008**, *105*, 19720-19725.

(89) Movileanu, L.; Howorka, S.; Braha, O.; Bayley, H. *Nat. Biotechnol*. **2000**, *18*, 1091-1095.

(90) Griffiths, J. *Anal. Chem*. **2008**, *80*, 23-27.

(91) Kang, X. F.; Cheley, S.; Guan, X. Y.; Bayley, H. *J. Am. Chem. Soc*. **2006**, *128*, 10684-10685.

(92) White, R. J.; Ervin, E. N.; Yang, T.; Chen, X.; Daniel, S.; Cremer, P. S.; White, H. S. *J. Am. Chem. Soc*. **2007**, *129*, 11766-11775.

(93) Healy, K. *Nanomedicine* **2007**, *2*, 459-481.

(94) Healy, K.; Schiedt, B.; Morrison, A. P. *Nanomedicine* **2007**, *2*, 875-897.

(95) Gershow, M.; Golovchenko, J. A. *Nat. Nanotechnol*. **2007**, *2*, 775-779.

(96) Fologea, D.; Gershow, M.; Ledden, B.; McNabb, D. S.; Golovchenko, J. A.; Li, J. L. *Nano Lett*. **2005**, *5*, 1905-1909.

(97) Li, J. L.; Gershow, M.; Stein, D.; Brandin, E.; Golovchenko, J. A. *Nat. Mater*. **2003**, *2*, 611-615.

(98) Stein, D. *Nat. Nanotechnol*. **2007**, *2*, 741-742.

(99) Yan, H.; Xu, B. Q. *Small* **2006**, *2*, 310-312.

(100) van Dorp, S.; Keyser, U. F.; Dekker, N. H.; Dekker, C.; Lemay, S. G. *Nat. Phys.* **2009**, *5*, 347-351.

(101) Skinner, G. M.; van den Hout, M.; Broekmans, O.; Dekker, C.; Dekker, N. H. *Nano Lett.* **2009**, *9*, 2953-2960.

(102) Smeets, R. M. M.; Kowalczyk, S. W.; Hall, A. R.; Dekker, N. H.; Dekker, C. *Nano Lett.* **2009**, *9*, 3089-3095.

(103) Smeets, R. M. M.; Keyser, U. F.; Krapf, D.; Wu, M. Y.; Dekker, N. H.; Dekker, C. *Nano Lett.* **2006**, *6*, 89-95.

(104) King, G. M.; Golovchenko, J. A. *Phys. Rev. Lett.* **2005**, *95*, 216103/1 – 216103/4.

(105) Sohn, L. L.; Saleh, O. A.; Facer, G. R.; Beavis, A. J.; Allan, R. S.; Notterman, D. A. *Proc. Natl. Acad. Sci. U. S. A.* **2000**, *97*, 10687-10690.

(106) Carbonaro, A.; Mohanty, S. K.; Huang, H. Y.; Godley, L. A.; Sohn, L. L. *Lab Chip* **2008**, *8*, 1478-1485.

(107) Saleh, O. A.; Sohn, L. L. *Nano Lett.***2003**, *3*, 37-38.

(108) Saleh, O. A.; Sohn, L. L. *Proc. Natl. Acad. Sci. U. S. A.* **2003**, *100*, 820-824.

(109) Carbonaro, A.; Sohn, L. L. *Lab Chip* **2005**, *5*, 1155-1160.

(110) Saleh, O. A.; Sohn, L. L. *Rev. Sci. Instrum.* **2001**, *72*, 4449-4451.

(111) Sun, L.; Crooks, R. M. *J. Am. Chem. Soc.* **2000**, *122*, 12340-12345.

(112) Ito, T.; Sun, L.; Crooks, R. M. *Anal. Chem.* **2003**, *75*, 2399-2406.

(113) Ito, T.; Sun, L.; Bevan, M. A.; Crooks, R. M. *Langmuir* **2004**, *20*, 6940-6945.

(114) Ito, T.; Sun, L.; Crooks, R. M. *Chem. Commun.* **2003**, *13*, 1482-1483.

(115) Uram, J. D.; Ke, K.; Hunt, A. J.; Mayer, M. *Angew. Chem.-Int. Edit.* **2006**, *45*, 2281-2285.

(116) Uram, J. D.; Mayer, M. *Biosens. Bioelectron.* **2007**, *22*, 1556-1560.

(117) Uram, J. D.; Ke, K.; Hunt, A. J.; Mayer, M. *Small* **2006**, *2*, 967-972.

(118) Park, S. R.; Peng, H. B.; Ling, X. S. S. *Small* **2007**, *3*, 116-119.

(119) Wang, J.; Martin, C. R. *Nanomedicine* **2008**, *3*, 13-20.

(120) Shaw, R. S.; Packard, N.; Schroter, M.; Swinney, H. L. *Proc. Natl. Acad. Sci. U. S. A.* **2007**, *104*, 9580-9584.

(121) Cheng, L. J.; Guo, L. J. *Nano Lett*. **2007**, *7*, 3165-3171.

(122) Daiguji, H.; Yang, P. D.; Majumdar, A. *Nano Lett*. **2004**, *4*, 137-142.

(123) Karnik, R.; Duan, C. H.; Castelino, K.; Daiguji, H.; Majumdar, A. *Nano Lett*. **2007**, *7*, 547-551.

(123) Probstein, R. F., *Physicochemical Hydrodynamics : An Introduction*. ed.; John Wiley & Sons, Inc.: Hoboken, Ney Jersey, 2003.

(125) Probstein, R. F.; Hicks, R. E. *Science* **1993**, *260*, 498-503.

(126) Schasfoort, R. B. M.; Schlautmann, S.; Hendrikse, L.; van den Berg, A. *Science* **1999**, *286*, 942-945.

(127) Lee, C. S.; Blanchard, W. C.; Wu, C. T. *Anal. Chem*. **1990**, *62*, 1550-1552.

(128) Miller, S. A.; Young, V. Y.; Martin, C. R. *J. Am. Chem. Soc*. **2001**, *123*, 12335-12342.

(129) Miller, S. A.; Martin, C. R. *J. Am. Chem. Soc*. **2004**, *126*, 6226-6227.

(130) Gupta, A.; Denver, H.; Hirsa, A. H.; Stenken, J. A.; Borca-Tasciuc, D. A. *Appl. Phys. Lett*. **2007**, *91*, 094101/1- 094101/3.

(131) Chen, Y. F.; Li, M. C.; Hu, Y. H.; Chang, W. J.; Wang, C. C. *Microfluid. Nanofluid*. **2008**, *5*, 235-244.

(132) Chen, L.; Conlisk, A. T. *Biomed. Microdevices* **2008**, *10*, 289-298.

(133) Iqbal, S. M.; Akin, D.; Bashir, R. *Nat. Nanotechnol*. **2007**, *2*, 243-248.

(134) Henrickson, S. E.; Misakian, M.; Robertson, B.; Kasianowicz, J. J. *Phys. Rev. Lett*. **2000**, *85*, 3057-3060.

(135) Takahashi, Y.; Matsumoto, N.; Iio, S.; Kondo, H.; Noda, I.; Imai, M.; Matsushita, Y. *Langmuir* **1999**, *15*, 4120-4122.

(136) Wang, L.; Yu, H. *Macromolecules* **1988**, *21*, 3498-3501.

(137) Bard, A. J.; Faulkner, L. R., *Electrochemical Methods : Fundamental and Applications*. 2nd ed.; Wiley: New York, 2001.

(138) Ueda, K.; Iizumi, N.; Sakomura, M. *Bull. Chem. Soc. Jpn*. **2005**, *78*, 430-434.

(139) Yameen, B.; Ali, M.; Neumann, R.; Ensinger, W.; Knoll, W.; Azzaroni, O. *J. Am. Chem. Soc*. **2009**, *131*, 2070-2071.

(140) Vlassiouk, I.; Kozel, T. R.; Siwy, Z. S. *J. Am. Chem. Soc*. **2009**, *131*, 8211-8220.

(141) Frohlich, H. P.; Woermann, D. *Colloid Polym. Sci*. **1986**, *264*, 159-166.

(142) Miller, S. A.; Martin, C. R. *J. Electroanal. Chem*. **2002**, *522*, 66-69.

(143) Miller, S. A.; Kelly, K. C.; Timperman, A. T. *Lab Chip* **2008**, *8*, 1729-1732.

(144) Saito, M. T., Y.; Tamiya, E. *Nat. Biotechnol*. **2005**, *1*, 361-368.

(145) Lee, M. H.; Brass, D. A.; Morris, R.; Composto, R. J.; Ducheyne, P. *Biomaterials* **2005**, *26*, 1721-1730.

(146) Toworfe, G. K.; Composto, R. J.; Shapiro, I. M.; Ducheyne, P. *Biomaterials* **2006**, *27*, 631-642.

(147) Eriksson, C.; Blomberg, E.; Claesson, P.; Nygren, H. *Colloid Surf. B-Biointerfaces* **1997**, *9*, 67-79.

(148) Kalman, E. B.; Sudre, O.; Vlassiouk, I.; Siwy, Z. S. *Anal. Bioanal. Chem*. **2009**, *394*, 413-419.

(149) Yameen, B.; Ali, M.; Neumann, R.; Ensinger, W.; Knoll, W.; Azzaroni, O. *Small* **2009**, *5*, 1287-1291.

(150) He, Y.; Gillespie, D.; Boda, D.; Vlassiouk, I.; Eisenberg, R. S.; Siwy, Z. S. *J. Am. Chem. Soc.* **2009**, *131*, 5194-5202.

(151) Wang, J. Ph.D. Dissertation, University of Florida, 2008.

(152) Srinivasan, V.; Higuchi, W. I. *Int. J. Pharm*. **1990**, *60*, 133-138.

# BIOGRAPHICAL SKETCH

Pu Jin was born in Kunming with his parents are chemists. Under the influence of his parents, he entered Xiamen University in Xiamen, China in 1997. He spent 4 years on undergraduate study and obtained a Bachelor of Science degree in materials chemistry in July 2001. After that, he went to University of Science and Technology of China in Hefei and started his research in the fields of functional nanomaterials synthesis under the guidance of Dr. Qianwang Chen. In August 2004, after he obtained his Master of Science degree in inorganic chemistry, Pu Jin joined Dr. Charles R. Martin research group in the Department of Chemistry at University of Florida. He continued his research in the fields of nanomaterials, especially on the fabrication of nanostructure in polymeric and inorganic thin film and their application in sensing and separation. He completed his research in December 2009, obtaining a Doctor of Philosophy degree.